

University of Memphis

University of Memphis Digital Commons

---

Electronic Theses and Dissertations

---

5-28-2013

## Comparison and Evaluation of Displacement-based Methods and Modeling Assumptions for Design of Ordinary Bridges in High Seismic Regions Using Various Computer Software

Ali Hajihashemi

Follow this and additional works at: <https://digitalcommons.memphis.edu/etd>

---

### Recommended Citation

Hajihashemi, Ali, "Comparison and Evaluation of Displacement-based Methods and Modeling Assumptions for Design of Ordinary Bridges in High Seismic Regions Using Various Computer Software" (2013). *Electronic Theses and Dissertations*. 739.  
<https://digitalcommons.memphis.edu/etd/739>

This Dissertation is brought to you for free and open access by University of Memphis Digital Commons. It has been accepted for inclusion in Electronic Theses and Dissertations by an authorized administrator of University of Memphis Digital Commons. For more information, please contact [khgerty@memphis.edu](mailto:khgerty@memphis.edu).

COMPARISON AND EVALUATION OF DISPLACEMENT-BASED  
METHODS AND MODELING ASSUMPTIONS FOR DESIGN OF  
ORDINARY BRIDGES IN HIGH SEISMIC REGIONS USING VARIOUS  
COMPUTER SOFTWARE

by

Ali Hajihashemi

A Dissertation

Submitted in Partial Fulfillment of the

Requirements for the Degree of

Doctor of Philosophy

Major: Engineering

The University of Memphis

August 2013

*To My Parents*  
&  
*My Wife Elaheh*

## **ACKNOWLEDGEMENTS**

This research project was funded by the Tennessee Department of Transportation. I would like to thank Mr. Ed. Wasserman, Mr. Wayne Seger, Mr. Tim Huff, Mr. Houston Walker, and Ms. Kathleen McLaughlin. Without help from Mr. Tim Huff and Mr. Wasserman, this project would not have been possible.

## ABSTRACT

Hajihashemi, Ali. PhD. The University of Memphis. August 2013. Comparison and Evaluation of Displacement-based Methods and modeling Assumptions for Design of Ordinary Bridges in High Seismic Regions Using Various Computer Software. Major Professor Shahram Pezeshk, PhD.

The main objective of this research is to evaluate the effectiveness of three different displacement-based methods for seismic design of ordinary standard bridges. Two bridges previously designed by the Tennessee Department of Transportation (TDOT) engineers following the American Association of State Highway and Transportation Officials (AASHTO) Guide Specifications for LRFD Seismic Bridge Design are selected and investigated in this study. Two different support conditions are considered, one employing seat-type abutments with rigid bent foundations; and the second employing stub wall abutment with flexible bent foundations (Nonlinear Spring Support Configuration). In addition to the AASHTO Specifications, the analysis methods include the capacity-demand-diagram method, as an inelastic demand Capacity Demand Method (CSM), and Federal Emergency Management Agency (FEMA) 440 Procedure C as an equivalent linearization CSM. Pushover analysis methods are used to construct the capacity diagram of the system. Furthermore, the usability of the three most widely used software programs (SAP2000, ADINA, and OpenSees) for performing the displacement-based seismic analysis is studied.

This research will provide TDOT engineers with the necessary information on which procedure is the best approach to use for design of highway bridges. Also, it provides information on how well previously designed bridges response when analyzed with the new displacement-based procedures. And finally, it will provide the TDOT engineers with information on capabilities and limitations of various software packages.

## TABLE OF CONTENTS

<b>LIST OF TABLES .....</b>	<b>vii</b>
<b>LIST OF FIGURES .....</b>	<b>viii</b>
<b>1 INTRODUCTION.....</b>	<b>1</b>
<b>2 RESEARCH OBJECTIVES .....</b>	<b>11</b>
<b>3 CASE STUDIES AND MODELING PROPERTIES.....</b>	<b>12</b>
<b>3.1. Case Studies.....</b>	<b>14</b>
3.1.1. The SR21-I69 Bridge.....	14
3.1.1 The Forrester Rd-I69 Bridge.....	21
<b>3.2. Selected Pushover Analysis Software.....</b>	<b>26</b>
3.2.1. SAP2000 .....	26
3.2.2. ADINA.....	28
3.2.3. OpenSees.....	30
<b>3.3. Modal Analysis.....</b>	<b>38</b>
<b>4 NONLINEAR STATIC (PUSHOVER) ANALYSIS .....</b>	<b>40</b>
<b>4.1. General Considerations .....</b>	<b>40</b>
<b>4.2. SAP2000 .....</b>	<b>41</b>
<b>4.3. ADINA .....</b>	<b>45</b>
<b>4.4. OpenSees.....</b>	<b>47</b>
<b>4.5. Capacity Diagrams.....</b>	<b>52</b>
<b>5 DISPLACEMENT-BASED ANALYSIS PROCEDURES.....</b>	<b>58</b>
<b>5.1. Seismic Demand .....</b>	<b>58</b>
<b>5.2. AASHTO Specifications Procedure .....</b>	<b>59</b>

5.3. FEMA-440 Procedure C.....	61
5.4. Capacity-demand-diagram Method.....	66
<b>6 DISCUSSIONS AND CONCLUSIONS.....</b>	<b>71</b>
6.1. Discussions.....	71
6.2. Conclusions.....	74
<b>REFERENCES.....</b>	<b>82</b>
<b>Appendix A.....</b>	<b>90</b>

## LIST OF TABLES

<b>Table 1.</b> Summary of Fundamental Natural Periods and the Associated Modal Mass Participating Ratios for Transverse Direction. ....	39
<b>Table 2.</b> Capacity Curve Conversion Factors.....	53
<b>Table 3.</b> Bilinear Capacity Diagram Properties. ....	57
<b>Table 4.</b> Seismic Analysis Results Based on AASHTO Procedure (Adopted from TDOT Documents).....	60
<b>Table 5.</b> Seismic Analysis Results Based on FEMA-440 Procedure C. ....	65
<b>Table 6.</b> Seismic Analysis Results Based on the Capacity-demand-diagram Method.....	70
<b>Table 7.</b> Qualitative Evaluation of Selected Software Programs. ....	74



## LIST OF FIGURES

<b>Figure 1.</b> General 3D View of the SR21-I69 Bridge. ....	15
<b>Figure 2.</b> Cross Section of the SR21-I69 Bridge. ....	15
<b>Figure 3.</b> The Computer Model of the SR21-I69 Bridge.....	16
<b>Figure 4.</b> Stress-Strain Curves for SR21-I69 Bridge’s Column Elements.....	18
<b>Figure 5.</b> Moment-Curvature Curves for SR21-I69 Bridge’s Column Elements at P = 1,050 kips.....	18
<b>Figure 6.</b> Force-Displacement Curve for Nonlinear Springs at the SR21-I69 Abutments in the Longitudinal Direction.....	19
<b>Figure 7.</b> Force-Displacement Curve for Nonlinear Springs at the SR21-I69 Abutments in the Transverse Direction.....	20
<b>Figure 8.</b> Force-Displacement Curve for Nonlinear Springs at the SR21-I69 Footings in Both Directions.....	20
<b>Figure 9.</b> Plan View of the Forrester Rd-I69 Bridge.....	21
<b>Figure 10.</b> Cross Section of the Forrester Rd-I69 Bridge. ....	22
<b>Figure 11.</b> Cross-Section Changes in Forrester Rd-I69 Bridge’s Plate Girders. ....	23
<b>Figure 12.</b> The Computer Model of the Forrester Rd-I69 Bridge.....	23
<b>Figure 13.</b> Force-Displacement Curve for Nonlinear Springs at the Forrester Rd-I69 Abutments. ....	25
<b>Figure 14.</b> Force-Displacement Curve for Nonlinear Springs at the Forrester Rd-I69 Footings in Both Directions. ....	26
<b>Figure 15.</b> Moment-Curvature Diagrams at P = 1,050 kips.....	28
<b>Figure 16.</b> Defining Nonlinear Column Elements in ADINA. ....	29
<b>Figure 17.</b> Axial Force-Axial Strain Curve for Column Elements. ....	30
<b>Figure 18.</b> Discretized Column Section for Modeling as Fiber Section in OpenSees. ....	31
<b>Figure 19.</b> The Pushover Curve with Stiffness Degradation for the SR21-I69 Bridge with the Basic Support Configuration. ....	41

<b>Figure 20.</b> The Pushover Curve with Stiffness Degradation for the SR21-I69 Bridge with the Nonlinear Springs Support Configuration. ....	42
<b>Figure 21.</b> Pushover Curves with Different Plastic hinge Properties for the SR21-I69 Bridge with the Basic Support Configuration. ....	43
<b>Figure 22.</b> Pushover Curves with Different Plastic Hinge Properties for the Forrester Rd-I69 Bridge with the Basic Support Configuration. ....	43
<b>Figure 23.</b> Pushover Curves with the User-Defined Plastic Hinge Property for the Forrester Rd-I69 Bridge with Different Support Configurations.....	44
<b>Figure 24.</b> Pushover Curves with the User-defined Plastic Hinge Property for the SR 21-I69 Bridge with Different Support Configurations and Analysis Methods....	45
<b>Figure 25.</b> Pushover Curves for the SR 21-I69 Bridge with the Basic Support Configuration Using the SAP2000 Computer Program with the User-defined Plastic Hinge Property and the ADINA Computer Program. ....	46
<b>Figure 26.</b> Pushover Curves for the Forrester Rd-I69 Bridge with the Basic Support Configuration Using the SAP2000 Computer Program with the User-defined Plastic Hinge Property and the ADINA Computer Program.....	47
<b>Figure 27.</b> Pushover Curves for the SR 21-I69 Bridge with the Basic Support Configuration Using the SAP2000 Computer Program with the User-defined Plastic Hinge Property and the OpenSees Computer Program. ....	51
<b>Figure 28.</b> Pushover Curves for the Forrester Rd-I69 Bridge with the Basic Support Configuration Using the SAP2000 Computer Program with the User-defined Plastic Hinge Property and the OpenSees Computer Program. ....	51
<b>Figure 29.</b> Actual and Bilinear Capacity Diagrams for the SR21-I69 Bridge with the Basic Support Configuration Achieved from SAP2000 Results with the User-defined Hinge.....	54
<b>Figure 30.</b> Bilinear Capacity Diagrams for the SR21-I69 Bridge with Various Modeling Properties Achieved from Different Computer Programs.....	55
<b>Figure 31.</b> Bilinear Capacity Diagrams for the Forrester Rd-I69 Bridge with Various Modeling Properties Achieved from Different Computer Programs. ....	56
<b>Figure 32.</b> Design Response Spectrum for the SR21-I69 Bridge. ....	58
<b>Figure 33.</b> Design Response Spectrum for the Forrester Rd-I69 Bridge. ....	59
<b>Figure 34.</b> Seismic Analysis of the Basic Support Configuration Model of the SR21-I69 Bridge with the SAP2000 User-Defined Hinge Property Using FEMA-440 Procedure C. ....	63

<b>Figure 35.</b> Seismic Analysis of the Basic Support Model of the Forrester Rd-I69 Bridge with the SAP2000 User-Defined Hinge Property Using FEMA-440 Procedure C.....	64
<b>Figure 36.</b> Seismic Analysis of the Basic Support Model of the SR21-I69 Bridge with the SAP2000 User-defined Hinge Property Using the Capacity-Demand-Diagram Method.....	67
<b>Figure 37.</b> Seismic Analysis of the Basic Support Model of the Forrester-I69 Bridge with the SAP2000 User-Defined Hinge Property Using the Capacity-Demand-Diagram Method.....	69
<b>Figure 38.</b> Seismic Response of the Bridges with the Basic Support Configuration and the User-Defined Hinge Property Using Different Displacement-based Methods.....	75
<b>Figure 39.</b> Seismic Displacement Demand of the Forrester Rd-I69 Bridge with Different Support Models and Using Various Analysis Methods.....	76
<b>Figure 40.</b> Displacement Ductility of the Forrester Rd-I69 Bridge with Different Support Models and Using Various Analysis Methods.....	77
<b>Figure 41.</b> Seismic Displacement Demand of the SR21-I69 Bridge with Different Support Models and Using Various Analysis Methods.....	77
<b>Figure 42.</b> Displacement Ductility of the SR21-I69 Bridge with Different Support Models and Using Various Analysis Methods.....	78
<b>Figure 43.</b> Seismic Response of the Bridges with the Basic Support Configuration and Different Hinge Properties Using the Capacity-Demand-Diagram Method. .	79
<b>Figure 44.</b> Seismic Response of the Bridges with the Basic Support Configuration Using Different Computer Programs.....	80
<b>Figure 45.</b> General 3D View of the Computer Model of the SR21-I69 Bridge with Basic Support Configuration in SAP2000.....	90
<b>Figure 46.</b> Joint Spring Element Properties Used for Modeling the Linear Springs at Abutments in the Basic Support Configuration.....	91
<b>Figure 47.</b> Link/Support Element Properties Used for Modeling the Nonlinear Springs in the Nonlinear Springs Support Configuration.....	92
<b>Figure 48.</b> Directional Properties of the Link/Support Elements.....	93
<b>Figure 49.</b> Mode One Deformed Shape of the Nonlinear Springs Model.....	94
<b>Figure 50.</b> User-Defined hinge Properties Data Window.....	95

<b>Figure 51.</b> Moment-Curvature Curve Data Window Corresponding to $P = 1,050$ kips. ...	96
<b>Figure 52.</b> Assigning User-Defined Plastic Hinges to the Both Ends of the Columns.....	97
<b>Figure 53.</b> SAP2000 Auto Hinge Property Based on the FEMA-356 Tables.....	98
<b>Figure 54.</b> SAP2000 Auto hinge Property Based on the Caltrans Tables.....	99
<b>Figure 55.</b> SD Section Data Window.....	100
<b>Figure 56.</b> Caltrans Square Section.....	101
<b>Figure 57.</b> Caltrans Section Properties Window.....	102
<b>Figure 58.</b> Changing the Analysis Type to Nonlinear for the Dead Load Case. ....	103
<b>Figure 59.</b> Defining the Pushover Load Case. ....	104
<b>Figure 60.</b> Pushover Analysis Load Application Control Window. ....	105
<b>Figure 61.</b> Pushover Curve of the SR21-I69 Bridge with the Basic Support Configuration Using Caltrans Hinge Properties. ....	106

## 1 INTRODUCTION

The first implementation of a displacement-based method for seismic design of bridges goes back to Kowalsky, Priestley, and Macrae (1995) for single-degree-of-freedom bridge columns, and Calvi and Kingsley (1995) for multi-degree-of-freedom bridge structures. Kowalsky and Priestley (1995) also used the methodology of Kowalsky et al. (1995) but included the P-delta effects. Today, the shift in interest toward displacement-based seismic analysis is seen in both research and official regulations.

The American Association of State Highway and Transportation Officials (AASHTO) Guide Specifications for LRFD Seismic Bridge Design (2009), herein referred to as the AASHTO Specifications, presents a displacement-based design method for seismic design of bridges in different Seismic Design Categories (SDCs). The AASHTO Specifications consider the design and construction of non-critical and non-essential bridges to perform within the life safety level regarding a seismic hazard corresponding to a seven percent probability of exceedance in 75 years. The life safety performance objective is defined as a low probability of collapse but possible significant damage and significant disruption of service. The life safety seismic performance level was previously described by the Applied Technology Council (ATC-18, 1997) which was designated as the collapse prevention level.

If a site-specific hazard analysis is not required, design response spectra could be constructed based on the site location using the United States Geological Survey (USGS) national ground motion maps. Seismic design parameters could be simply obtained from the AASHTO GM computer software, which was developed by Leyendecker, Frankel,

and Rukstales (2009) using either latitude/longitude or the zip code of the site. According to the AASHTO Specifications, each bridge is assigned to one of the four SDCs based on the one-second period design spectral acceleration,  $S_{D1}$ . The seismic demand analysis procedure is selected based on both the SDC and the regularity of the bridge. General analytical considerations and modeling characteristics are discussed in Section 5 of the AASHTO Specifications.

Two displacement modifications must be applied to the displacement demand ( $\Delta_D$ ): (1)  $R_D$  for structures other than 5% damped; and (2)  $R_d$  for short-period structures. For bridges in SDCs B and C, the AASHTO Specifications provides explicit formulas for displacement capacity,  $\Delta_C$ . For SDC D bridges, a more detailed nonlinear static procedure, commonly referred to as “Pushover” analysis, is required. The displacement capacity,  $\Delta_C$ , is determined as the bridge structure or the bent frame reaches its limit of structural stability.

The California Seismic Design Criteria SDC-2010 (Caltrans, 2010) allows equivalent static analysis and linear elastic dynamic analysis for estimating the displacement demands, and pushover analysis for establishing the displacement capacities for “Ordinary Standard” bridges. For a bridge to be considered as an “Ordinary Standard” bridge, (1) the span length should be less than 90 m (300ft); (2) the bridge should be constructed with normal weight concrete; (3) horizontal members should be either rigidly connected, pin connected, or supported on conventional bearings, where isolation bearings and dampers are considered nonstandard components; (4) foundations must be supported on spread footings, pile caps with piles or pile shafts; (5) the soil is not susceptible to liquefaction or lateral spreading during strong shaking; and (6) the fundamental period of the bridge should be greater than or equal to 0.7 seconds in the transverse and longitudinal directions (Caltrans, 2010). The seis-

mic demand on the structural system is represented using an elastic 5% damped response spectrum. Either USGS hazard maps or the Caltrans ARS program could be used to construct the design spectrum. A reduction factor,  $R_D$ , should be applied on the seismic displacement demand for more than 5% damped structures. Equivalent Static Analysis (ESA) can be used to determine the global displacement demand,  $\Delta_D$ , if a dynamic analysis will not add significantly more insight into behavior, and the bridge system has the following characteristics: (1) response primarily captured by the fundamental mode of vibration with uniform translation; (2) simply defined lateral force distribution; and (3) low skew (Caltrans, 2010). Elastic Dynamic Analysis (EDA) must be used to determine  $\Delta_D$  for all other ordinary standard bridges. The bridge displacement capacity,  $\Delta_C$ , is determined when the first ultimate capacity is reached by any plastic hinge during the pushover analysis (Caltrans, 2010).

Due to the inelastic behavior of reinforced concrete frames (Chandler & Mendis, 2000), nonlinear analysis is typically used in all of the seismic bridge design methods. Nonlinear time history analysis is the ideal approach to evaluate structural behavior when subjected to earthquake loadings. However, the difficulties in both ground motion selection and computational process make it the least popular in the seismic design practice. In this regard, the nonlinear static pushover analysis, as described by Kim and D'Amore (1999), is mostly used because it offers a compromise between the simplification of the linear analysis and the accuracy of the nonlinear dynamic analysis (Gencturk & Elnashai, 2008; Shattarat, Syman, McLean, & Cofer, 2008). Pushover analysis also provides good insight into identifying the critical inelastic regions, predicting the sequence of yielding/failure in structural components, and thus constructing the overall capacity curve of the structure (e.g., Krawinkler & Seneviratna, 1998).

Conventional pushover analysis, such as presented in Federal Emergency Management Agency (FEMA) 356 (2000), requires the application of an increasing, but invariant, lateral load pattern on the structural system. This horizontal forces vector could be defined as either proportional to the fundamental mode shape or uniform and remains unchanged throughout the analysis. Two major limitations of the conventional pushover method occur (e.g., FEMA-440, 2005): (1) when higher modes are important, i.e., the fundamental mode does not capture 90 % or more of the total modal participating mass, and (2) if the stiffness degradation is important, which happens by pushing the structure highly into its post-yielding range. Several multi-modal pushover (MMP) procedures have been proposed to take the effects of all significant modes into account. Generally, MMPs first estimate the pushover result for a predetermined number of modes using the appropriate modal shape proportional load patterns. Paret, Sasaki, Eilbeck, and Freeman (1996) and Sasaki, Freeman, and Paret (1998) proposed to combine converted pushover curves in the Acceleration-Displacement Response Spectrum (ADRS) format; Moghadam and Tso (2002) presented the Pushover Results Combination (PRC) method as a weighted summation of individual pushover results; and Chopra and Goel (2002) suggested the Modal Pushover Analysis (MPA) method in which the SRSS rule is used to combine idealized bilinear pushover curves, which Hernandez-Montes, Kwon, and Aschheim (2004) have then adapted into an Energy-based Pushover formulation.

The above MMP procedures have shown much more accurate results for structures with significant higher modes when compared to conventional pushover analysis. However, since all of them are based on undamaged mode shape characteristics, they cannot overcome the second shortcoming of conventional pushover analysis, which is the



gradual softening in the structure. Recently, many so-called *adaptive pushover* methods have been introduced to consider the progressive stiffness degradation of the structure through updating the lateral forces vector at each step of analysis. Bracci, Kunnath, and Reinhorn (1997) presented the first fully adaptive pushover method in which a triangular initial load pattern is updated at each step by imposing the additional loads calculated from the base shear and resistance of the previous step. Gupta and Kunnath (2000) and Requena and Ayala (2000) suggested using a site-specific spectrum in defining the lateral load pattern, which is constantly updated based on the instantaneous dynamic characteristics of the structure. An Adaptive Energy-based Pushover Analysis (AEPOA) was proposed by Albanesi, Biondi, and Petrangeli (2002) in which the lateral loading is updated at each step based on both structural properties and kinetic energy. Elnashai (2001), followed by Antoniou and Pinho (2004a), developed a fiber analysis framework for a continuous, rather than discrete, updating of the force distribution. Aydinoglu (2003) extended the conventional response spectrum analysis into an adaptive multi-modal pushover method called Incremental Response Spectrum Analysis (IRSA) in which an implementation of RSA is used at each incremental step. The aforementioned forced-based adaptive procedures have provided good agreement between static and dynamic analysis results due to the consideration of spectrum scaling, higher mode contributions, and instantaneous load updating (Pinho, Antoniou, Casarotti & Lopez, 2005). However, their improvement is not significant in the case of predicting deformation patterns, when compared to non-adaptive MMPs (Antoniou & Pinho, 2004a). This deficiency is mainly due to the use of quadratic modal combination rules (SRSS and CQC) in computing the adaptive load updating (Kunnath, 2004), which results in monotonically increasing load vec-

tors and ignoring possible sign changes after developing an inelastic mechanism. Kunnath (2004) proposed an alternative modal combination, consisting of weighted Direct Vectorial Addition (DVA), which cannot yet be considered as valid for general applications. Antoniou and Pinho (2004b) proposed the innovative concept of Displacement-Based Adaptive Pushover (DAP) as a new solution, in which their displacement vectors represent different contributing modes, and reversal of story shear distribution is feasible even if a quadratic combination rule is used. Taking the results of the Incremental Dynamic Analysis procedure (IDA) (e.g., Vamvatsikos & Cornell, 2002) as “true,” Antoniou and Pinho (2009) performed comprehensive parametric studies that showed that for RC frames, steel frames, and long continuous-span bridges, which have a total length of 800m, the DAP results provide the best match with true results when compared with the results of forced-based adaptive pushover (FAD), conventional pushover with fundamental mode proportional load pattern (FCPm), and conventional pushover with uniform load pattern (FCPu). However, for short continuous-span bridges, which have a total length of less than 200m, the employment of any of the available pushover procedures (DAP, FAD, FCPm, or FCPu) gives almost the same level of agreement with the true (IDA) results.

The best-known utilization of pushover analysis is Capacity Spectrum Methods (CSMs), in which the force-displacement (pushover) curve is converted into the ADRS format to represent the capacity of the system. The CSM, originally developed by Freeman, Nicoletti, and Tyrell (1975), results in graphical assessment of the force-displacement relationship (Yu, Symans, McLean & Cofer, 1999) and provides insight into the potential failure mechanism, ductility demand, and stability under large drift.

The CSMs have also appeared in national codes such as ATC-40 (1996) and FEMA-356 (2000). Original CSM methods, such as the one used in ATC-40 (1996), define the seismic demand on a structure by the elastic response spectra with equivalent viscous damping ratios then graphically estimate the inelastic maximum displacement as the intersection of the capacity spectrum and the demand spectrum. In other words, the earthquake response of an inelastic system is estimated by replacing it with an “equivalent” linear system (Chopra & Goel, 2001). The accuracy of the capacity spectrum method used in ATC-40 depends on: (1) choosing the acceleration response spectrum to form the demand spectrum; and (2) adopting the equivalent viscous damping model. There is no stable relationship between the hysteretic energy dissipation associated with the maximum excursion and the equivalent viscous damping, which makes it very difficult to determine a suitable value for the equivalent damping ratio (Krawinkler, 1995). This inaccuracy in equivalent viscous damping relationships led to several modified CSMs. Bertero (1995) recommended using smoothed inelastic response spectra in the classical acceleration-period format. Reinhorn (1997) proposed an alternative CSM method to combine the advantage of visual representation in ADRS format and the superior physical bases of inelastic demand spectra, followed by Fajfar (1999) who formulated the so-called N2 method. The N2 method utilizes the ductility reduction factor,  $R_\mu$ , proposed by Vidic, Fajfar, and Fischinger (1994) to reduce the elastic response spectrum into inelastic demand curves. The pushover curve of the MDOF system is converted to the capacity curve of the equivalent SDOF system then replaced by its bilinear representation. The ductility demand is determined through an iterative process, and the displacement demand coincides with the intersection point of the bilinear capacity spectrum and the corresponding

reduced demand spectrum. Chopra and Goel (1999) developed the capacity-demand-diagram method, a non-iterative method that utilizes a constant-ductility inelastic design spectrum for the demand diagram. They suggested obtaining inelastic demand diagrams from their elastic counterparts by using reduction factors. The yielding branch of the capacity diagram intersects the demand diagrams for several ductility values. At one of these intersection points, the ductility factor calculated from the capacity diagram matches the ductility value associated with the intersecting demand curve, which provides the displacement demand. Chopra and Goel (1999) used three different  $R_\mu$  equations (Krawinkler & Nassar, 1992; Newmark & Hall, 1982; Vidic et al., 1994) and showed that they all provide similar results. Chopra and Goel (1999) recommended that since the term “spectrum” has traditionally implied a function of period or frequency, the terminology “diagram” should be used to address either capacity or demand curves in Acceleration-Displacement (AD) format. The capacity-demand-diagram method produces up to 50% more accurate results than those obtained from equivalent elastic procedures (Chopra & Goel, 1999, 2000). The only limitation on CSMs with reduced inelastic demand diagrams is that the reduction factors are derived for Elasto-Plastic (EP) systems with small strain hardening values. However, Rahnam and Krawinkler (1993) showed that moderate strain hardening does not have a significant influence on  $R_\mu$ , while strain softening increases the maximum displacements.

FEMA-356 (2000) presented the Displacement Coefficient Method (DCM), in which the demand is represented by inelastic displacement spectra that are obtained from the elastic displacement spectra using correction factors based on statistical analyses. This method produces almost the same level of dispersion of results when compared with

the ATC-40 (1996) capacity spectrum procedures (Lin, Chang & Wang, 2004). Lin and Chang (2003), Lin et al. (2004), and Kim et al. (2005) suggested modified equivalent viscous damping models to improve the ATC-40 CSM method. Although Lin and Chang (2003) had demonstrated that real absolute acceleration response spectra ( $S_a$ ) should be used instead of pseudo-acceleration response spectra ( $PS_a$ ) in order to improve the accuracy of the original CSM, Kim, Min, Chung, Park, and Lee (2005) argued that the effectiveness of using the peak absolute acceleration for constructing the demand spectra should be verified through additional analyses. Lin and Miranda (2004) eliminated the need for iterations in CSM, for systems with no strain hardening and known strength ratio, by deriving an equivalent damping model that is a function of the strength ratio rather than the ductility ratio. Akkar and Miranda (2005) evaluated the accuracy of five approximate methods and concluded that users of nonlinear static procedures in which target displacements are computed using equivalent linear methods or displacement modification factors should be aware of the limited accuracy offered by these approximate methods.

Due to the previously outlined problems associated with the CSM approach in the ATC-40, FEMA conducted the ATC-55 Project, released as FEMA-440 (2005). The objective of the ATC-55 Project was to evaluate the accuracy of the CSM approach in ATC-40 and the DCM approach in FEMA 356. FEMA-440 (2005) proposed modifications for both the coefficient method and the equivalent linearization procedure. Empirical equations for equivalent linear parameters, effective damping, and period are developed by minimizing the error between the maximum responses obtained from analysis of inelastic and equivalent elastic systems. An expression for the spectral reduction factor is

provided to allow displacement predictions using the demand spectra. Among all modified procedures presented in FEMA-440 (2005), Procedure C is more attractive for practice purposes. This non-iterative procedure determines the maximum seismic displacement as the intersection point of the actual (not bilinear) capacity curve and the loci of possible performance points on different demand diagrams, obtained from modified equivalent viscous damping relationships.

In a displacement-based seismic analysis, the performance of the structure is directly related to its inelastic displacement capacity. Therefore, the ability to perform nonlinear analysis and to obtain reasonably accurate displacement capacity is very important. A variety of software programs are available for performing practical seismic analysis of structures. A survey of bridge engineering consulting firms and state DOTs showed that SAP2000 (2011) and ADINA (2010) are the most popular software programs for performing nonlinear analysis (Shattarat et al., 2008). In the case of frame elements, SAP2000 takes the material nonlinearity into account by assigning either code-based built-in or user-defined plastic hinges. The element cross-section could be modeled using the moment-curvature material model in ADINA, which distributes plasticity through the member cross section and along its length. In recent years, OpenSees (2011), an open source finite element platform for earthquake engineering simulations, has been increasingly drawing attention for both research and practice (e.g., Kalkan & Kwong, 2010). Fiber-discretized, nonlinear beam-column elements can be used to model plastically designed members in OpenSees.

## 2 RESEARCH OBJECTIVES

The main objective of this research is to evaluate the effectiveness of three different displacement-based methods for seismic design of ordinary standard bridges. Two case studies have been selected: a two-span continuous bridge with prestressed bulb-T girders and a four-column bent frame and a two-span continuous bridge with steel plate girders and a two-column bent frame. The bridges were previously designed by Tennessee Department of Transportation (TDOT) engineers following the AASHTO Specifications. Two different support conditions are considered, one employing seat-type abutments with rigid bent foundations (Basic Support Configuration) and the second employing stub wall abutment with flexible bent foundations (Nonlinear Spring Support Configuration). In addition to the AASHTO Specifications procedure, the analysis methods include the capacity-demand-diagram method (Chopra & Goel, 2000), as an inelastic demand CSM, and FEMA-440 Procedure C (2005) as an equivalent linearization CSM. The elastic demand diagram for all mentioned methods is selected as the 5% damped elastic design spectrum obtained from USGS national hazard maps. In order to construct the capacity diagram of the system, two pushover analysis methods are used: the conventional method and the modal method (Chopra & Goel, 2002), both with the dominant mode shape proportional loading. Also, the usability of the three most widely used software programs (SAP2000, ADINA, and OpenSees) for performing the displacement-based seismic analysis is to be studied.

### 3 CASE STUDIES AND MODELING PROPERTIES

Two actual bridges are investigated in this research: the State Route 21 over Interstate 69 Bridge and the Forrester Road over Interstate 69 Bridge. Both bridges are located in Obion County in northwest Tennessee and have been designed by TDOT engineers according to the AASHTO Specifications.

For seismic design purposes, TDOT engineers modeled the entire superstructure by an equivalent element that passes through the cross-sectional centroid of the superstructure, and has equivalent section area and rigidities. They used the USGS national hazard maps to construct design response spectra for each site and utilized the computer program WinSEISAB (Imbsen, 2002) to run both the modal and the response spectrum analysis. The latter determines the seismic displacement demand for each bridge as allowed by the AASHTO Specifications (2009). The TDOT Structures Division team has developed an in-house spreadsheet that follows the AASHTO Specifications' *Capacity Design* concept to determine the displacement capacity of the bent frame. Furthermore, the computer program CONSEC (Matthews, 2005) has been used to perform moment-curvature analysis for column elements.

The column footings were fixed against both translation and rotation in all directions (hereafter, this will be referred to as the "Basic" support configuration), and the abutments were assumed to provide fixed support for rotation in all directions and vertical translation. The longitudinal and transverse translations in the abutments were modeled by linear springs, the stiffness of which was calculated following the Caltrans Bridge Design Specifications (2004).



In this research, the idealized mathematical model is used. The superstructure is represented by a single line of multiple three-dimensional frame elements that passes through the cross-sectional centroid of the superstructure. Each of the columns and the cap beam are represented by single three-dimensional frame elements that pass through the geometric center and mid-depth, respectively. A constraint was used to tie the superstructure center joint to the mid-point of the cap beam. All active superstructure masses plus two lanes of HL-93 lane load were applied to the model as uniform loadings and the superstructure material was modeled as massless. Furthermore, to model the weight of the abutments, two concentrated loads were assigned to the superstructure end joints. A rigid end zone was assigned to each end of all column elements to account for the offset between the clear height of the columns and the centerline of the cap beam at the top, and the centerline of the footing at the bottom. TDOT's moment-curvature analysis results have been used to model nonlinearity and to determine the effective moment of inertia,  $I_{\text{eff}}$ . The effective torsional moment of inertia,  $J_{\text{eff}}$ , was selected as  $0.2J_g$ , based on the AASHTO Specifications (2009). Shear and axial stiffnesses were based on the gross cross-sectional properties (Abeysinghe, Gavaice, Rosignoli & Tzaveas, 2002).

The seismic behavior of both bridges was evaluated in the transverse direction only and the design response spectra were obtained from the AASHTO GM (Leyendecker et al., 2009) computer program based on each bridge location's latitude and longitude. Since the 1-second period design spectral acceleration,  $S_{D1}$ , for both bridges was larger than 0.5g, the bridges were assigned to seismic design category (SDC) D (AASHTO, 2009). The earthquake resisting system (ERS) of both bridges was Type 1 (AASHTO, 2009), which requires the expected behavior of essentially elastic superstructure and duc-

tile substructure. This type of ERS forced the nonlinear behavior to occur within the inspectable locations of the columns.

In addition to the Basic support configuration, a more realistic *Nonlinear Springs* support configuration has been used in the current study. In a joint research project with the University of Tennessee at Knoxville, the actual properties of the support systems (abutments, piles, soil, etc.) were modeled, and their behavior was presented through nonlinear translation springs in the longitudinal and transverse directions. Again, the column footings and the abutments were assumed to be fixed against vertical translation and rotation in all directions (Vasheghani-Farahani, Zhao & Burdette, 2010).

Three different computer programs, SAP2000 (CSI, 2011), ADINA (ADINA R&D, 2010), and OpenSees (PEER Center, 2011) have been used in this study to perform the nonlinear static (pushover) analysis, while the modal analysis was performed by the SAP2000 software program only.

### **3.1 Case Studies**

#### **3.1.1 The SR21-I69 Bridge**

The SR21-I69 Bridge consists of two-span continuous 72-inch bulb-T girders. Each span length is 148 ft. The only bent frame includes four 3.5 ft square columns and a cap beam. All columns have 1.0% longitudinal reinforcement in a circular configuration and are designed to preclude shear failure. Each column is supported by a separate pile cap. Figure 1 shows the general 3D view of the bridge. Figure 2 shows a typical cross-section of the SR21-I69 Bridge.

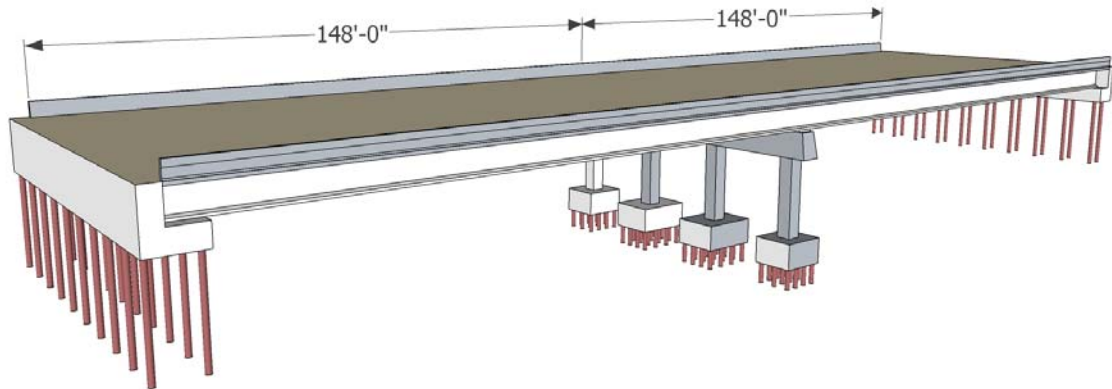


Figure 1. General 3D View of the SR21-I69 Bridge.

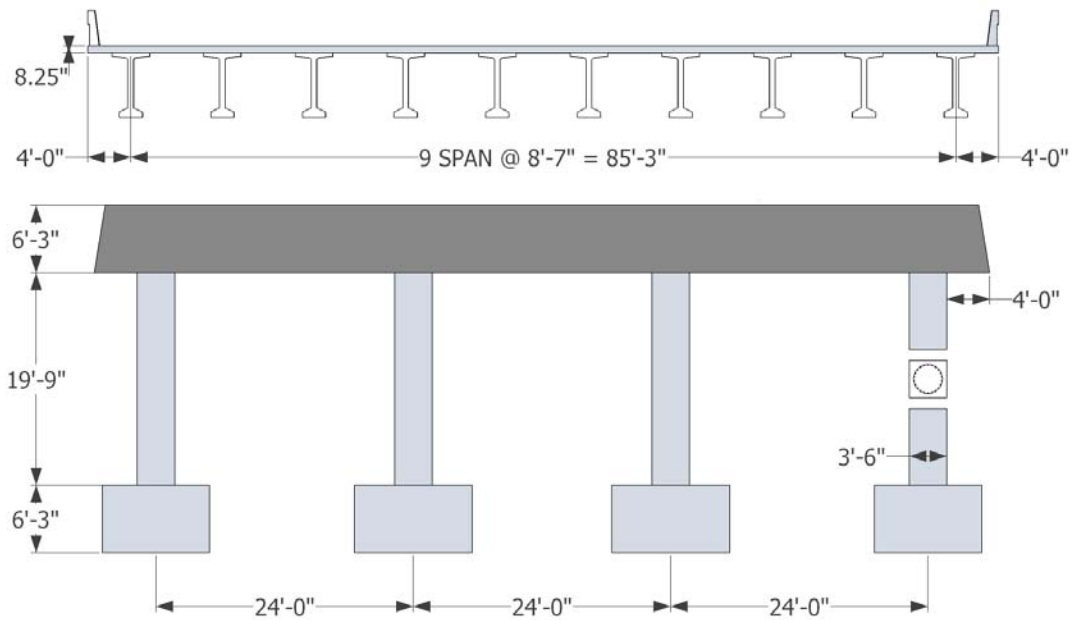


Figure 2. Cross Section of the SR21-I69 Bridge.

The idealized mathematical model of the bridge is shown in Figure 3 for the Non-linear Spring support configuration. Since the cross-section of the superstructure is uniform, it was deemed sufficient to locate the nodes at the fifth points of each span.

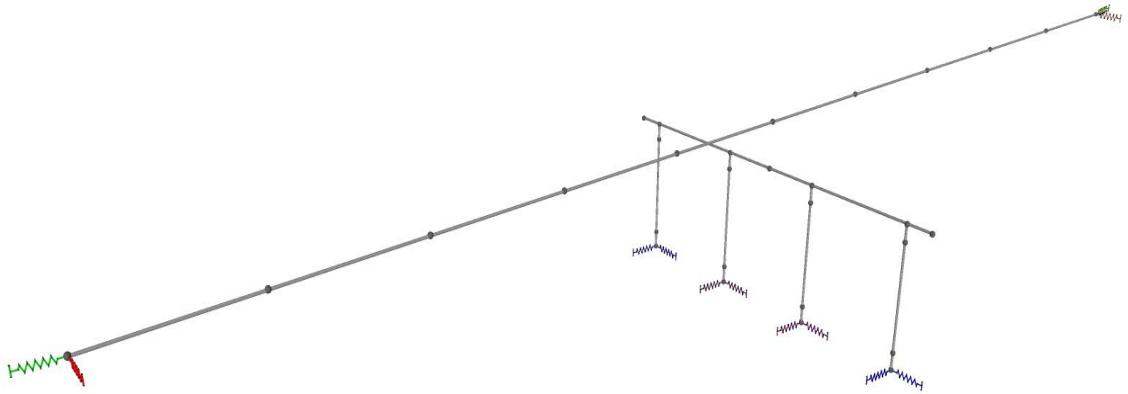


Figure 3. The Computer Model of the SR21-I69 Bridge.

The superstructure cross-sectional area is  $95.7 \text{ ft}^2$  and the moment of inertia about the strong and weak axes are  $58,128 \text{ ft}^4$  and  $540 \text{ ft}^4$ , respectively. The mass was applied to the model as a  $22.44 \text{ kips/ft}$  uniform load with half the member mass being subsequently assigned to each node. Furthermore, to model the weight of the abutments, two  $467 \text{ kips}$  concentrated loads were assigned to the superstructure end joints. The modulus of elasticity for the prestressed concrete superstructure elements was assumed to be  $828,770 \text{ ksf}$ . The cap beam cross-sectional area is  $25.2 \text{ ft}^2$  and the moment of inertia about the strong axis and torsional rigidity are  $83.3 \text{ ft}^4$  and  $81.4 \text{ ft}^4$ , respectively. The columns were modeled as a  $3.5 \text{ ft}$  square resulting in a cross-sectional area of  $12.25 \text{ ft}^2$ , gross moment of inertia of  $12.5 \text{ ft}^4$  for both axes, and gross torsional rigidity of  $21.1 \text{ ft}^4$ . The moment-curvature analyses showed that for the expected axial loads in the columns,

the effective moment of inertia,  $I_{\text{eff}}$ , would be 0.19-0.45 times the gross moment of inertia,  $I_g$ , for the minimum and maximum loads, respectively. An average value of  $0.25I_g$  was selected. The effective torsional moment of inertia,  $J_{\text{eff}}$ , was selected as  $0.2J_g$ , based on the AASHTO Specifications. Each column is reinforced by 22 #8 longitudinal bars and #5 transverse spirals with 2.0 in. clear cover and 4.0 in. spacing. A rigid end zone, 3.125 ft long, was assigned to both ends of each column element.

The concrete used in the cap beam and the columns had the normal weight of 0.15 kips per cubic foot, and was assumed to have a nominal 28-day compressive strength of 576 ksf and a modulus of elasticity of 453,936 ksf. The nominal yield strength of the longitudinal and transverse reinforcements was assumed as 8,640 ksf. The expected concrete compressive strength,  $f'_{ce}$ , and the expected reinforcement yield strength,  $f_{ye}$ , were chosen as 745 ksf and 9,792 ksf, respectively, following the AASHTO Specifications (2009). Mander's stress-strain model was used for determining the confined concrete properties. Figure 4 shows stress-strain curves for both confined and unconfined concrete materials based on the reinforcing details.

The maximum expected axial load for the column elements was assumed to be 1,500 kips. For 20 different axial load cases equally spaced within the expected range of 0.0 to 1,500 kips, the computer program CONSEC was used to obtain the  $M-\phi$  curve for each load case. Figure 5 displays the  $M-\phi$  analysis result obtained when subjected to 1,050 kips axial load. Based on the AASHTO Specifications (2009), the actual  $M-\phi$  curve could be replaced by a bilinear idealized curve. The elastic portion of the idealized curve should pass through the point marking the first reinforcing bar yield. The plastic branch is then obtained by equating the areas between the actual and the idealized curves

beyond the first yield point. The values of the idealized plastic moment,  $M_p$ , the idealized yield curvature,  $\phi_{yi}$ , and the ultimate curvature,  $\phi_u$ , were used for defining the properties of the plastic hinges in the nonlinear analysis.

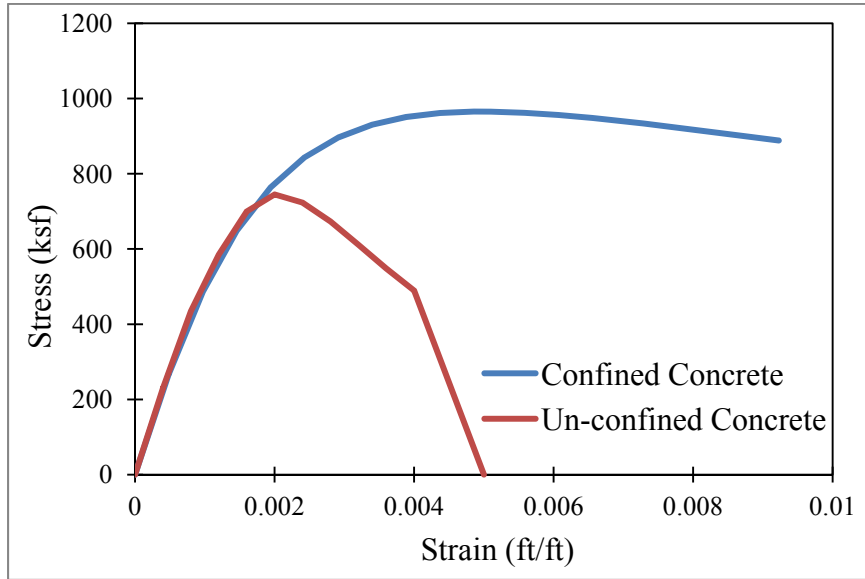


Figure 4. Stress-Strain Curves for SR21-I69 Bridge's Column Elements.

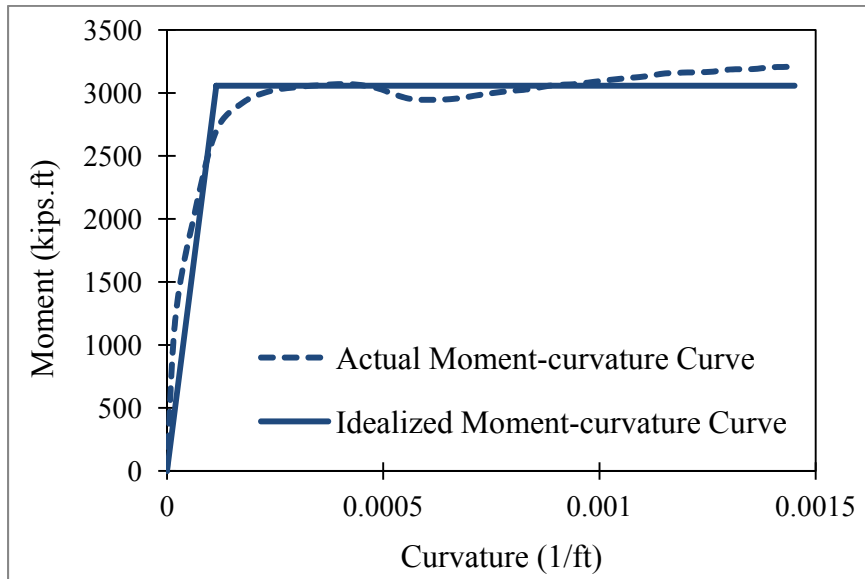


Figure 5. Moment-Curvature Curves for SR21-I69 Bridge's Column Elements at  $P = 1,050$  kips.

In the case of Basic support configuration, the stiffness value of 4,080 kips/ft was adopted for the linear springs in the longitudinal and transverse directions of the abutments based on the TDOT analysis. For the Nonlinear Springs support configuration, the nonlinear spring behavior curves from the UT/UM joint study are used. Figures 6 to 8 illustrate the nonlinear spring force-displacement diagrams for abutments and column footings.

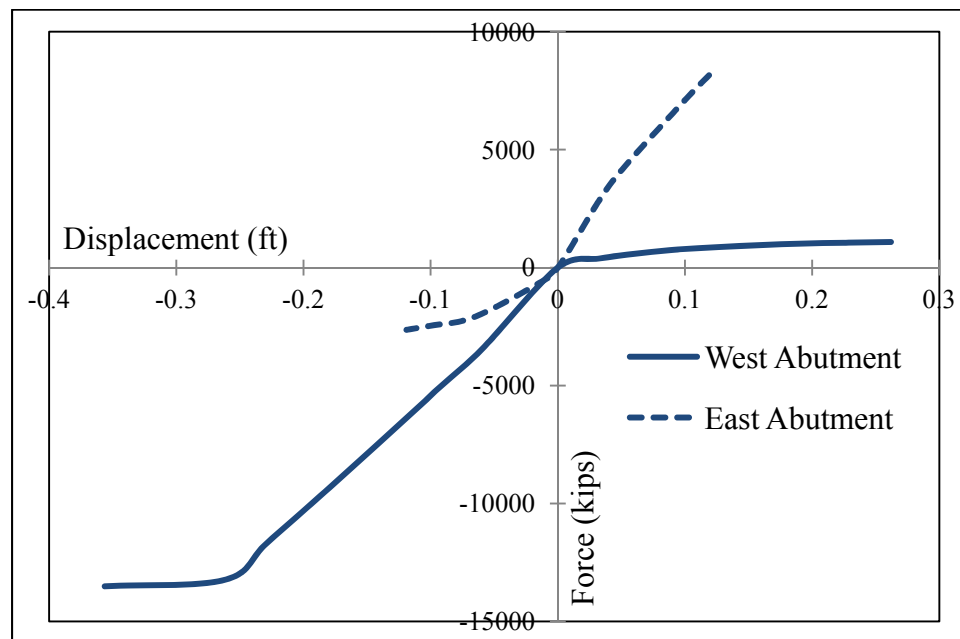


Figure 6. Force-Displacement Curve for Nonlinear Springs at the SR21-I69 Abutments in the Longitudinal Direction.

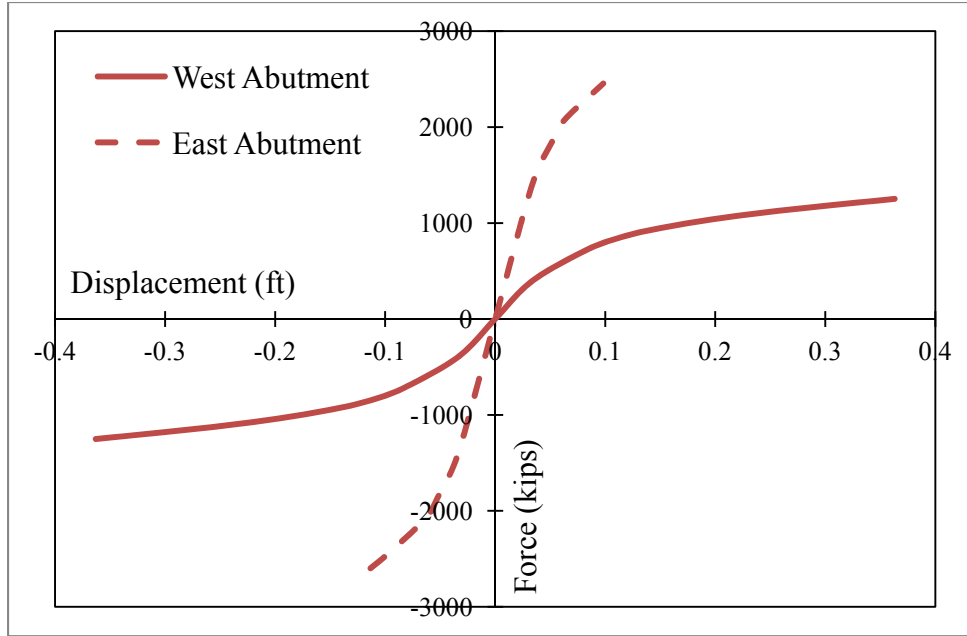


Figure 7. Force-Displacement Curve for Nonlinear Springs at the SR21-I69 Abutments in the Transverse Direction.

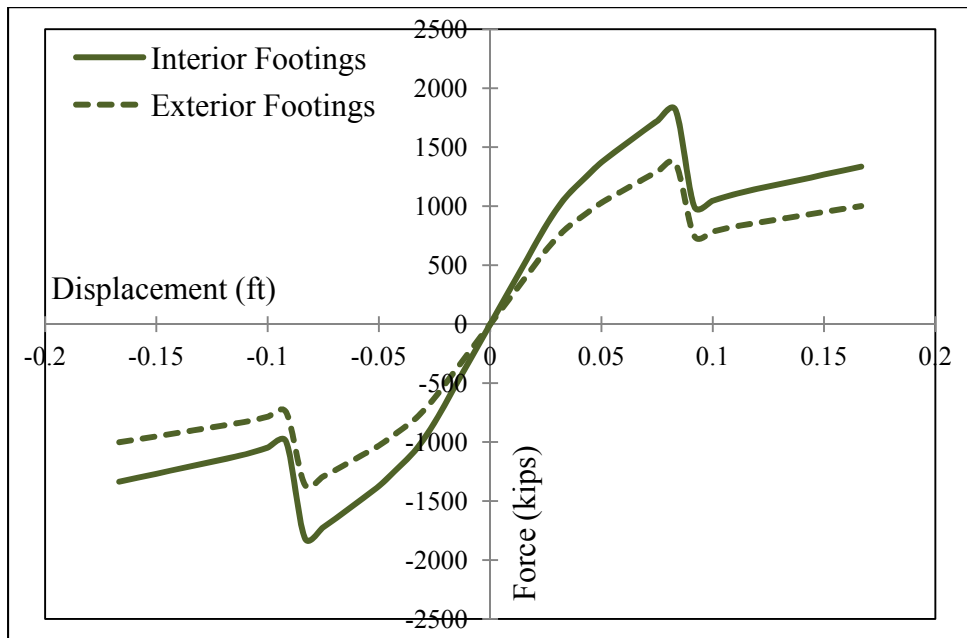
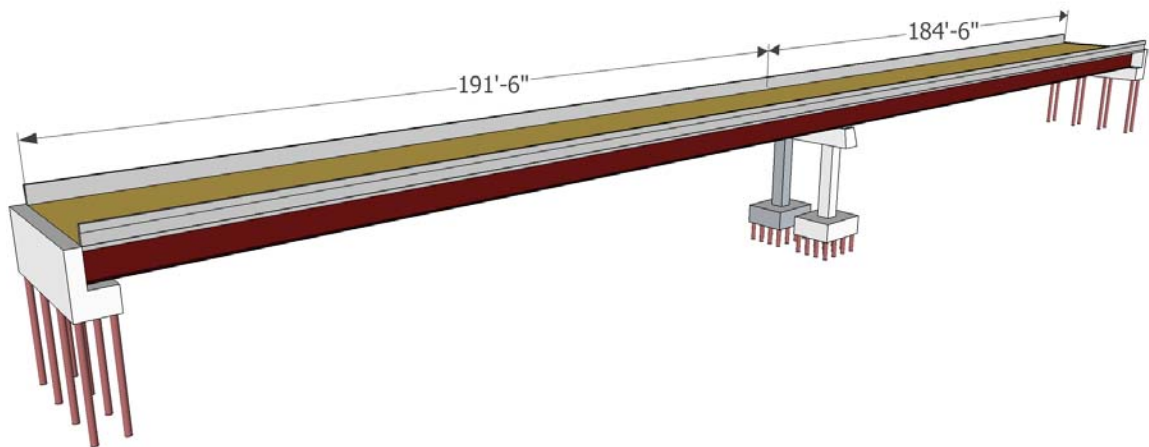


Figure 8. Force-Displacement Curve for Nonlinear Springs at the SR21-I69 Footings in Both Directions.



### 3.1.2 The Forrester Rd-I69 Bridge

The second bridge investigated in this study is a two-span continuous bridge that consists of steel plate girders with a column integral bent and spread footings. Its only bent frame consists of two 3.5 ft square columns and the cap beam. The columns have 1.0% longitudinal reinforcement in a circular configuration and were designed to preclude shear failure. Each column is supported by a separate pile cap. Figure 9 shows the general 3D view of the bridge. Figure 10 shows a typical cross section of the bridge.



*Figure 9.* General 3D View of the Forrester Rd-I69 Bridge.

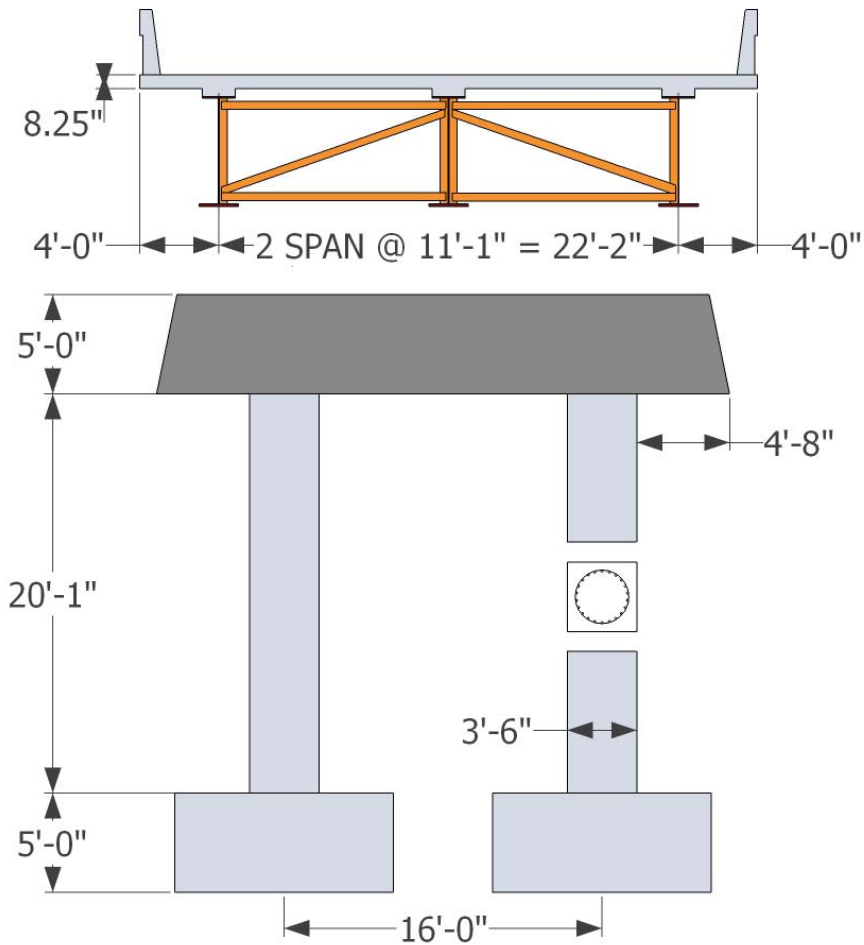
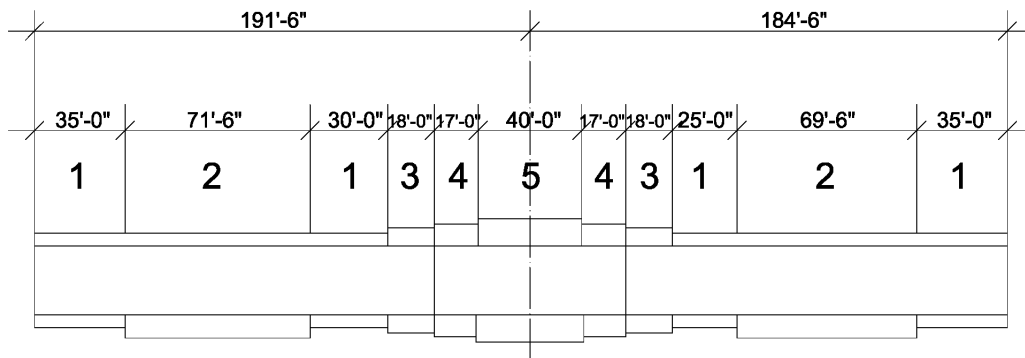


Figure 10. Cross Section of the Forrester Rd-I69 Bridge.

The idealized mathematical model of the bridge follows the same concept used in modeling the SR21-I69 Bridge, except for the Forrester Rd-I69 Bridge, the number of superstructure elements was chosen based on the steel plate girders' section variation. Figure 11 shows the changes in the girders' cross-section which determines the location of the superstructure nodes. The idealized mathematical model of the bridge is shown in Figure 12 for the Nonlinear Spring support configuration.



Section	Web	Top Flange	Bottom Flange
1	64 x 9/16	20 x 1-1/8	24 x 1-1/8
2	64 x 9/16	20 x 1-1/8	24 x 2-1/8
3	64 x 9/16	28 x 1-1/4	30 x 1-1/4
4	64 x 5/8	28 x 1-3/4	30 x 1-3/4
5	64 x 5/8	28 x 3-1/4	30 x 3-1/4

Figure 11. Cross-Section Changes in Forrester Rd-I69 Bridge's Plate Girders.

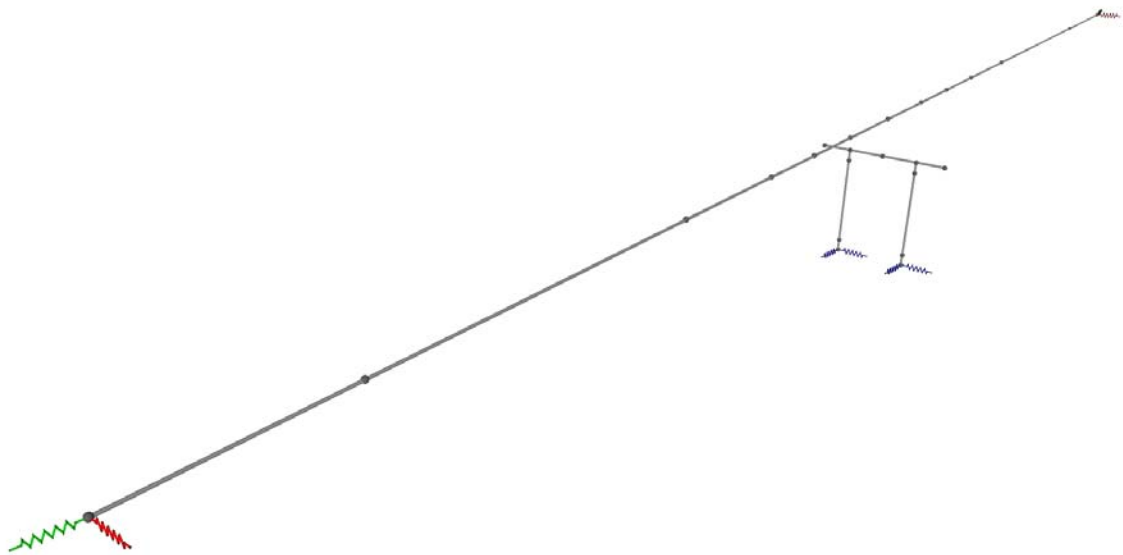


Figure 12. The Computer Model of the Forrester Rd-I69 Bridge.

Average sectional properties were used for all 12 superstructure elements. The superstructure cross-sectional area is  $5.3 \text{ ft}^2$  and the moments of inertia about the strong and weak axes are  $466 \text{ ft}^4$  and  $52 \text{ ft}^4$ , respectively. The uniform mass load applied to the superstructure elements varies from 6.87 to 8.44 kips/ft with half the member mass subsequently assigned to each node. Furthermore, to model the weight of the abutments, two 120-kip concentrated loads were assigned to the superstructure end joints. The modulus of elasticity for the steel superstructure elements was assumed to be 4,176,000 ksf. The cap beam cross-sectional area is  $22.5 \text{ ft}^2$  and the moment of inertia about the strong axis and torsional rigidity are  $46.9 \text{ ft}^4$  and  $70.5 \text{ ft}^4$ , respectively. Columns were modeled as a 3.5-ft square resulting in a cross-sectional area of  $12.25 \text{ ft}^2$ , a gross moment of inertia of  $12.5 \text{ ft}^4$  for both axes, and a gross torsional rigidity of  $21.1 \text{ ft}^4$ . An average value of  $0.25I_g$  was selected as the effective moment of inertia,  $I_{\text{eff}}$ , based on the moment-curvature analysis results. The effective torsional moment of inertia,  $J_{\text{eff}}$ , was selected as  $0.2J_g$ , based on the AASHTO Specifications (2009). Each column is reinforced by 22 #8 longitudinal bars and #5 transverse spirals with 2.0 in. clear cover and 4.0 in spacing. A rigid end zone, 2.5 ft long, was assigned to both ends of each column element.

The same material properties and stress-strain model as used in the first case study were chosen for the concrete material used in the cap beam and the columns. The maximum expected axial load for the column elements was assumed to be 2,200 kips, and the computer program CONSEC was used to obtain the  $M-\phi$  curve for thirty different axial load cases equally-spaced within the expected range of -500 to 2,200 kips. Again, the actual  $M-\phi$  curves were replaced by their bilinear idealized representatives. In the case of the Basic support configuration, the stiffness value of 1,680 kips/ft for the linear

springs in the longitudinal and transverse directions of the abutments was adopted from TDOT documents, and the results of the UT/UM joint study, as shown on Figures 13 and 14, were used to model the Nonlinear Springs support configuration.

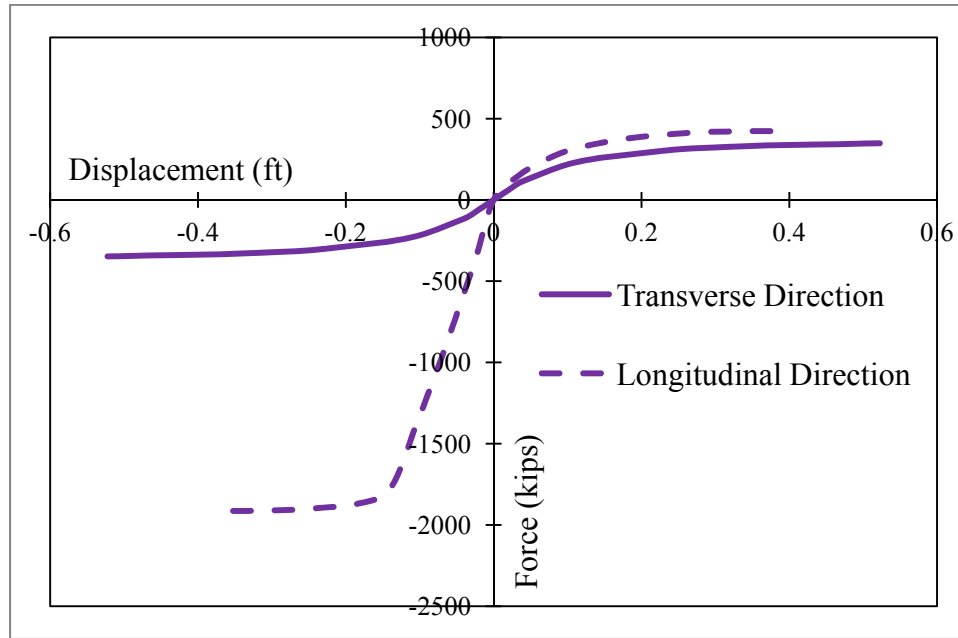
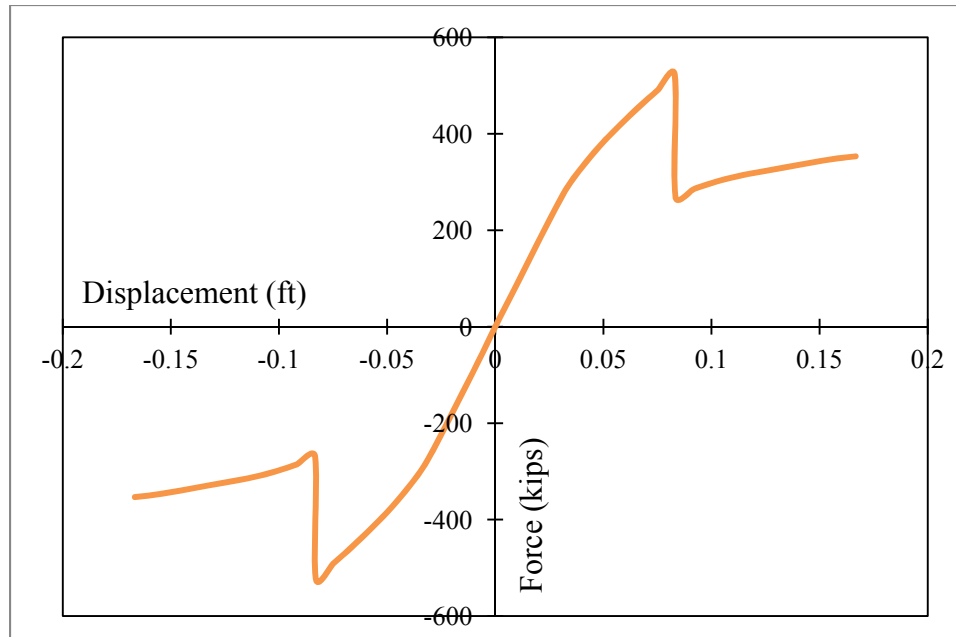


Figure 13. Force-Displacement Curve for Nonlinear Springs at the Forrester Rd-I69 Abutments.



*Figure 14.* Force-Displacement Curve for Nonlinear Springs at the Forrester Rd-I69 Footings in Both Directions.

### 3.2 Selected Pushover Analysis Software

#### 3.2.1 SAP2000

SAP2000 is a general-purpose finite element analysis program for static and dynamic analysis of two- and three-dimensional linear and nonlinear structures. The software was developed by Computers and Structures Inc. (CSI) and its version 15.1 (2011) has been used for this study. In SAP2000, the nonlinearity could be modeled by assigning concentrated plastic hinges at the ends of each column element. Three different options were examined to define the plastic hinge property, including two SAP2000 built-in hinge properties and a user defined property based on moment-curvature analysis results. In all cases, the P-M2-M3 degree of freedom was chosen and the plastic hinge was assigned at the half plastic hinge length distance from the rigid end zone. The plastic hinge length,  $L_p$ , was calculated as 1.73 ft following the AASHTO Specifications (2009).

The first SAP2000 built-in hinge property, Auto Hinge, is based on Table 6-8 of FEMA-356 (2000), which describes the modeling parameters and numerical acceptance criteria for the nonlinear behavior of concrete columns in flexure. The second plastic hinge was modeled using the SAP2000 Auto Hinge properties following the Caltrans Bridge Design Specifications (2004). It should be noted that the Caltrans Auto Hinge model can only be assigned to the sections if the Caltrans Section Properties are used. For the same reason, column sections were replaced by the Caltrans section properties when using the second type of hinge.

Finally, the User Defined Hinge properties are defined in SAP2000 based on the CONSEC moment-curvature curves for various axial load values. To input the  $M-\phi$  curves into SAP2000, the moment values should be divided by the value of the yield moment. Also, SAP2000 assumes that no deformation occurs in the plastic hinge before the yield point. Consequently, as illustrated in Figure 15 for  $P = 1,050$  kips, the vertical axis ( $M/M_y$ ) is shifted to the right, to cross the horizontal axis at  $\phi_{yi}$ . Note that, although no performance level is defined beyond the point of the ultimate curvature, two more points are required to define the plastic hinge property. A normalized moment value of 0.2 was selected for the drop point, and twice the value of the ultimate curvature was assumed for the last point.

Appendix A presents a detailed step-by-step modeling and analysis process of the SR21-I69 Bridge with SAP2000.

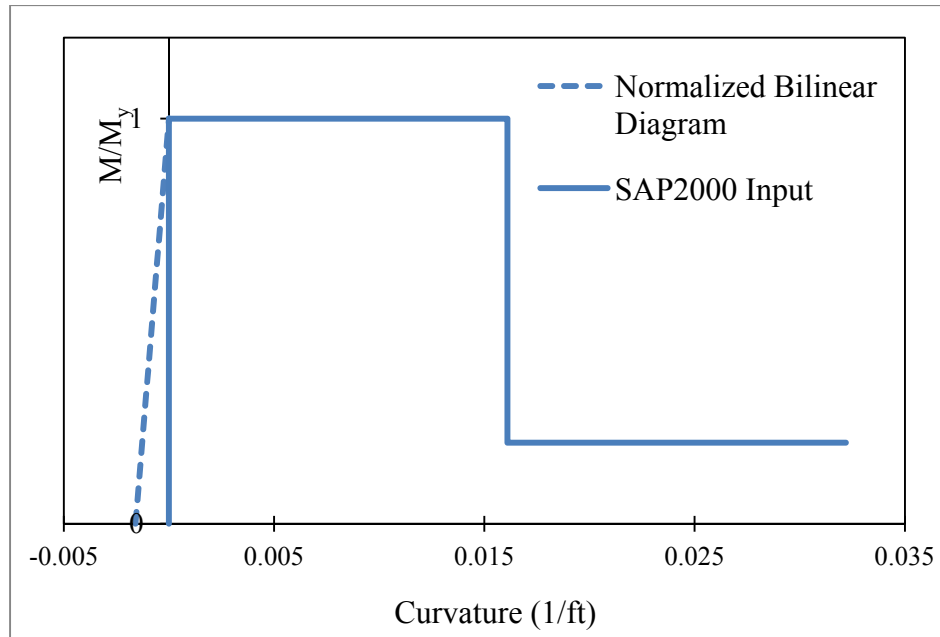


Figure 15. Moment-Curvature Diagrams at P = 1,050 kips.

### 3.2.2 ADINA

ADINA (Automatic Dynamic Incremental Nonlinear Analysis), developed by ADINA R & D Inc., is a finite element program system for comprehensive analyses of structures, fluids, and fluid flows with structural interaction. In this study, version 8.6.4 (2010) of the software was used. ADINA can perform pushover analysis, but unlike SAP2000, there are no specific utilities available in ADINA to aid the user in performing such an analysis.

To model nonlinearity in ADINA, the column elements must be defined as Beam elements in which the stiffness is defined by a moment-curvature rigidity model (Figure 16). With the moment-curvature material model, the cross-section and material behavior are described by several curves. This model accurately captures the dependence of mo-



ment-curvature data on the axial force, as well as the multilinear nature of the yielding behavior.

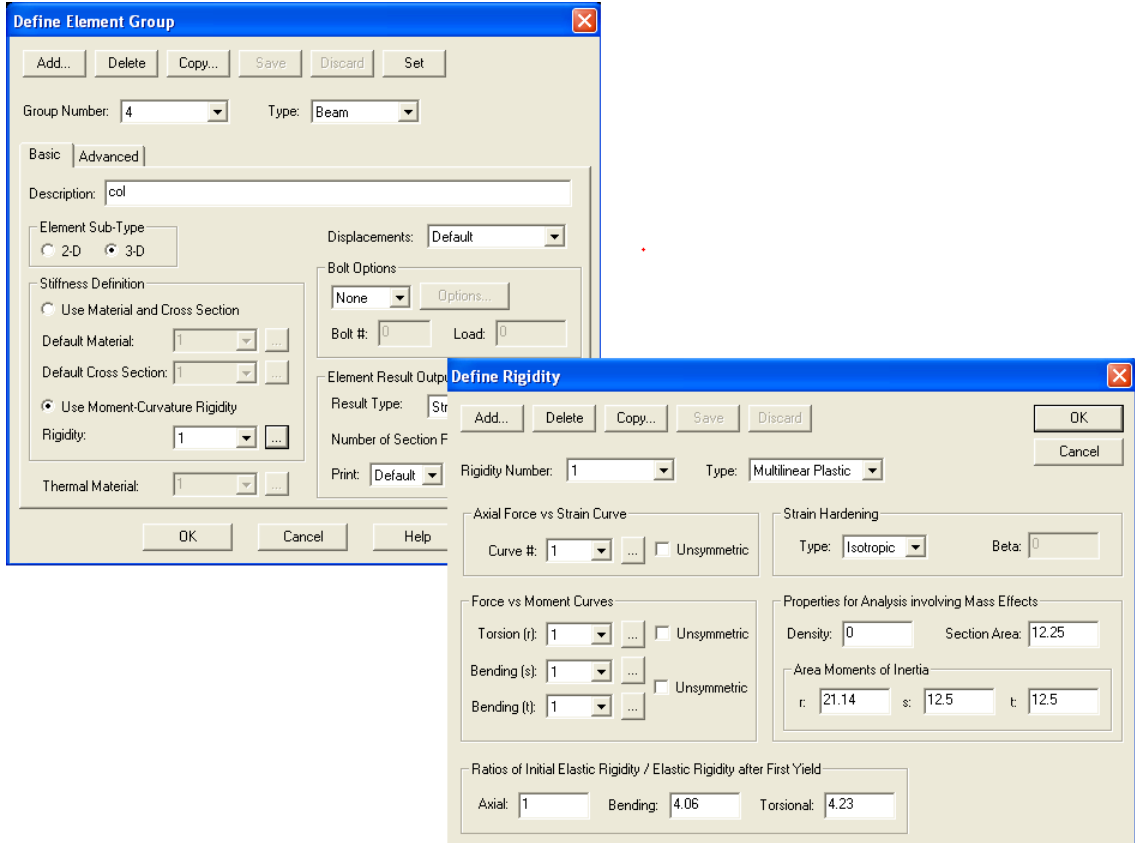


Figure 16. Defining Nonlinear Column Elements in ADINA.

The first step in defining the moment-curvature rigidity model is constructing the axial force-axial strain curve for the columns' section. This was achieved using the stress-strain curves of the three materials existing in the composite section (i.e., reinforcing steel bars, confined concrete, and unconfined concrete). Assuming uniform axial displacement, the stress for each material was determined at many pre-determined strain values. The axial force corresponded to each strain value was then simply calculated as

the summation of stress times cross-sectional area for all three materials. Figure 17 shows the constructed  $P$ - $\varepsilon$  curve for the column elements.

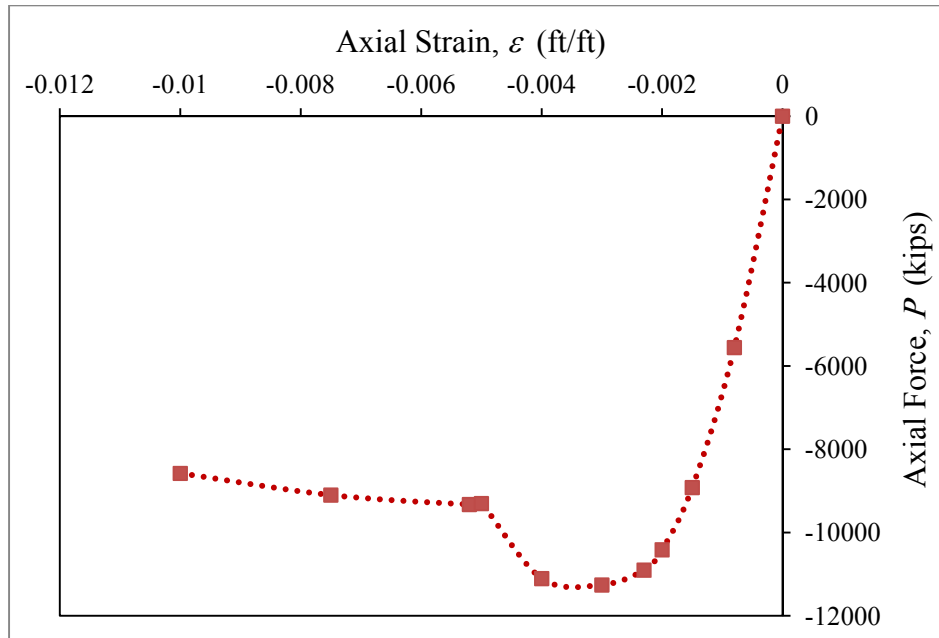


Figure 17. Axial Force-Axial Strain Curve for Column Elements.

The CONSEC moment-curvature curves were used in the second step to define the bending behavior of the section about its strong and weak axes, referred to as the  $s$  and  $t$  axes in ADINA. One constant and one linear time function were defined to be used by gravity loads and the pushover analysis lateral load, respectively.

### 3.2.3 OpenSees

OpenSees, the Open System for Earthquake Engineering Simulation, is an object-oriented, open source software framework created by the NSF-sponsored Pacific Earthquake Engineering (PEER) Center. OpenSees has advanced capabilities for modeling and analyzing the nonlinear response of systems using a wide range of material models, elements, and solution algorithms. A wide range of uniaxial materials and section mod-

els are available for beam-column elements. Users of OpenSees create applications by writing scripts in the *Tcl* programming language. OpenSees Version 2.3.2 (2011) was used in this research project.

*ElasticBeamColumn* elements were used to model super structure and cap beam members, while *NonlinearBeamColumn* elements were utilized for column elements. The latter could be defined based on the number of integration points along the element and the pre-defined section. The nonlinearity of the system was actually taken into account when defining the column section. The *UniaxialMaterial Concrete02* and the *UniaxialMaterial Steel02* were used to define the concrete and reinforcing steel materials of the section, respectively. The column section was discretized into its counterparts, as shown on Figure 18, and was modeled as a *Fiber Section*.

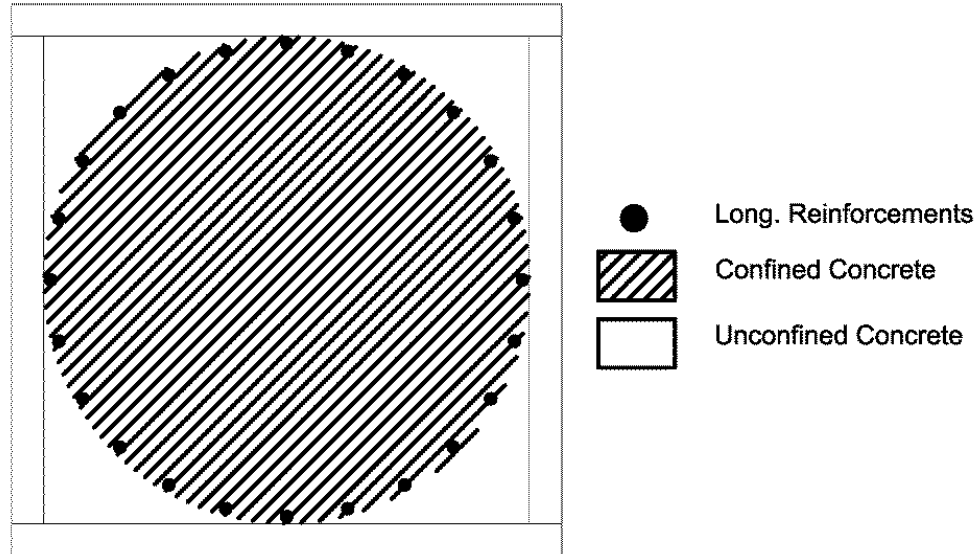


Figure 18. Discretized Column Section for Modeling as Fiber Section in OpenSees.

The Tcl script for creating the SR21-I69 Bridge model in OpenSees is presented below.

```

#units kips/ft/sec
wipe

#-----nodal mass calculaions-----#

set Qsuper 22.44;           #kips/ft sum of external loads+self
weight on super structure
set Qcap1 5.59;           #kips/ft sum of external loads
on cap beam
set Qcap2 [expr 0.15*6.3*4]; #kips/ft self weight on cap
set Qcap [expr $Qcap1+$Qcap2] #total cap load
set Qcol [expr 0.15*3.5*3.5]; #kips/ft self weight on columns
set Pabut 457;           #kips self weight of abutments

set Wsuper [expr $Qsuper*29.6]; #length of each super element
set Wcap1 [expr $Qcap*5.75]; #length of cap element 1
set Wcap2 [expr $Qcap*24]; #length of cap element 2
set Wcap3 [expr $Qcap*12]; #length of cap element 3
set Wcol1 [expr $Qcol*3.125]; #length of col element 1
set Wcol2 [expr $Qcol*19.76]; #length of col element 2

set mabut [expr ($Wsuper/2+$Pabut)/32.2]
set msuper [expr $Wsuper/32.2]
set mcap1 [expr ($Wcap1/2)/32.2]
set mcap2 [expr ($Wcap1/2+$Wcap2/2+$Wcol1/2)/32.2]
set mcap3 [expr ($Wcap2/2+$Wcap3/2+$Wcol1/2)/32.2]
set mcap4 [expr $Wcap3/32.2]
set mcol1 [expr ($Wcol1/2)/32.2]
set mcol2 [expr ($Wcol1/2+$Wcol2/2)/32.2]

puts "0ok"

#-----nodes-----#

model BasicBuilder -ndm 3 -ndf 6

node 11 -36 0 0 -mass $mcol1 $mcol1 $mcol1 0 0 0;
#base level
node 12 -12 0 0 -mass $mcol1 $mcol1 $mcol1 0 0 0
node 13 12 0 0 -mass $mcol1 $mcol1 $mcol1 0 0 0
node 14 36 0 0 -mass $mcol1 $mcol1 $mcol1 0 0 0

```

```

node 21 -36 0 3.125 -mass $mcol2 $mcol2 $mcol2 0 0 0;
      #top of bottom rigid length level
node 22 -12 0 3.125 -mass $mcol2 $mcol2 $mcol2 0 0 0
node 23 12 0 3.125 -mass $mcol2 $mcol2 $mcol2 0 0 0
node 24 36 0 3.125 -mass $mcol2 $mcol2 $mcol2 0 0 0

node 31 -36 0 22.885 -mass $mcol2 $mcol2 $mcol2 0 0 0;      #bot-
tom of top rigid length level
node 32 -12 0 22.885 -mass $mcol2 $mcol2 $mcol2 0 0 0
node 33 12 0 22.885 -mass $mcol2 $mcol2 $mcol2 0 0 0
node 34 36 0 22.885 -mass $mcol2 $mcol2 $mcol2 0 0 0

node 41 -41.75 0 26.01 -mass $mcap1 $mcap1 $mcap1 0 0 0;
      #cap level
node 42 -36 0 26.01 -mass $mcap2 $mcap2 $mcap2 0 0 0
node 43 -12 0 26.01 -mass $mcap3 $mcap3 $mcap3 0 0 0
node 44 0 0 26.01 -mass $mcap4 $mcap4 $mcap4 0 0 0
node 45 12 0 26.01 -mass $mcap3 $mcap3 $mcap3 0 0 0
node 46 36 0 26.01 -mass $mcap2 $mcap2 $mcap2 0 0 0
node 47 41.75 0 26.01 -mass $mcap1 $mcap1 $mcap1 0 0 0

node 501 0 148 34.71 -mass $mabut $mabut $mabut 0 0 0;      #super
level
node 502 0 118.4 34.71 -mass $msuper $msuper $msuper 0 0 0
node 503 0 88.8 34.71 -mass $msuper $msuper $msuper 0 0 0
node 504 0 59.2 34.71 -mass $msuper $msuper $msuper 0 0 0
node 505 0 29.6 34.71 -mass $msuper $msuper $msuper 0 0 0
node 506 0 0 34.71 -mass $msuper $msuper $msuper 0 0 0
node 507 0 -29.6 34.71 -mass $msuper $msuper $msuper 0 0 0
node 508 0 -59.2 34.71 -mass $msuper $msuper $msuper 0 0 0
node 509 0 -88.8 34.71 -mass $msuper $msuper $msuper 0 0 0
node 510 0 -118.4 34.71 -mass $msuper $msuper $msuper 0 0 0
node 511 0 -148 34.71 -mass $mabut $mabut $mabut 0 0 0

node 5001 0 148 34.71;
      #zero length elements
node 5011 0 -148 34.71

#fixities
fix 501 0 0 1 1 1 1
fix 511 0 0 1 1 1 1
fix 5001 1 1 1 1 1 1
fix 5011 1 1 1 1 1 1
fixZ 0.0 1 1 1 1 1 1

```

puts "1ok"

#-----materials-----#

set conconc 1  
set unconc 2  
set reinforce 3  
set torsionmat 5  
set linspring 6

# nominal concrete compressive strength  
set fc [expr -(5.2)\*144]  
set Ec [expr 144\*1820\*sqrt(5.2)]

# confined concrete; based on Mander, Priestley, and Park (1988)  
set fcc [expr -6.86\*144]  
set epscc [expr 2\*\$fcc/\$Ec]  
set fcu [expr -5.16\*144]  
set epscu -0.0188  
set ftc [expr -0.04\*\$fcc]  
set Etc [expr -\$ftc/\$epscc]

uniaxialMaterial Concrete02 \$conconc \$fcc \$epscc \$fcu \$epscu 0.1 \$ftc  
\$Etc; # Core concrete (confined)

# unconfined concrete  
set fcu \$fc  
set epscu [expr 2\*\$fcu/\$Ec]  
set fuu 0  
set epsuu -0.005  
set ftu [expr -0.04\*\$fcu]  
set Etu [expr -\$ftu/\$epscu]

uniaxialMaterial Concrete02 \$unconc \$fcu \$epscu \$fuu \$epsuu 0.1 \$ftu  
\$Etu; # Cover concrete (unconfined)

#reinforcing steel  
set Fy [expr 68\*144]  
set Es [expr 29000.\*144]

uniaxialMaterial Steel02 [expr \$reinforce+1] \$Fy \$Es 0.025 18.0 0.925  
0.15  
uniaxialMaterial MinMax \$reinforce [expr \$reinforce+1] -min -0.090 -  
max 0.090

```

#torsional behavior
uniaxialMaterial Elastic $torsionmat 100000;
    #big torsional stiffness

#linear spring material
uniaxialMaterial Elastic $linspring 4080;
    #stiffness from TDOT

puts "2ok"

#-----column section-----#

set colsecfiber 1
set colsec 2

set h [expr 3.5/2]
set z1 1.52
set y1 0.0
set z2 1.46
set y2 0.43
set z3 1.28
set y3 0.82
set z4 1.0
set y4 1.15
set z5 0.63
set y5 1.38
set z6 0.22
set y6 1.51

section fiberSec $colsecfiber {

    #core elements
        patch circ $conconc 6 4 0 0 0 1.62 0 360

    #cover elements
        patch rect $unconconc 1 1 -1.75 1.62 1.75 1.75
        patch rect $unconconc 1 1 -1.75 -1.75 1.75 -1.62
        patch rect $unconconc 1 1 -1.75 -1.62 -1.62 1.62
        patch rect $unconconc 1 1 1.62 -1.62 1.75 1.62

        fiber 1.258 1.258 0.5632 $unconconc
        fiber 1.258 -1.258 0.5632 $unconconc
        fiber -1.258 1.258 0.5632 $unconconc
        fiber -1.258 -1.258 0.5632 $unconconc

```

```

        #reinforcing elements
        layer circ $reinforce 22 0.0055 0 0 1.52625 0 360
    }

section Aggregator $colsec $storsionmat T -section $colsecfiber

puts "3ok"

#-----elements-----#

#define geometric transformations
set colgeomtransf 1
set capgeomtransf 2
set supergeomtransf 3

geomTransf Linear $colgeomtransf 0 1 0;      #strong axis is Global
Y
geomTransf Linear $capgeomtransf 0 1 0;      #strong axis is Global
Y
geomTransf Linear $supergeomtransf 1 0 0;    #strong axis is Global
X

#define zerlength elements (linear spring supports)

        element zeroLength 5001 5001 501 -mat $linspring $linspring -dir
1 2
        element zeroLength 5011 5011 511 -mat $linspring $linspring -dir
1 2

#define super structure elements (based on TDOT documents and G based
on nu=0.2)
        element elasticBeamColumn 501 501 502 95.7 828770 345320
11.73 540 58128 $supergeomtransf
        element elasticBeamColumn 502 502 503 95.7 828770 345320
11.73 540 58128 $supergeomtransf
        element elasticBeamColumn 503 503 504 95.7 828770 345320
11.73 540 58128 $supergeomtransf
        element elasticBeamColumn 504 504 505 95.7 828770 345320
11.73 540 58128 $supergeomtransf
        element elasticBeamColumn 505 505 506 95.7 828770 345320
11.73 540 58128 $supergeomtransf
        element elasticBeamColumn 506 506 507 95.7 828770 345320
11.73 540 58128 $supergeomtransf

```



```

        element elasticBeamColumn 507 507 508 95.7 828770 345320
11.73 540 58128 $supergeomtransf
        element elasticBeamColumn 508 508 509 95.7 828770 345320
11.73 540 58128 $supergeomtransf
        element elasticBeamColumn 509 509 510 95.7 828770 345320
11.73 540 58128 $supergeomtransf
        element elasticBeamColumn 510 510 511 95.7 828770 345320
11.73 540 58128 $supergeomtransf

```

```

#define cap bema elements (based on TDOT documents and G based on
nu=0.2)

```

```

        element elasticBeamColumn 41 41 42 25.2 597634 249014 81.38
83.35 33.6 $scageomtransf
        element elasticBeamColumn 42 42 43 25.2 597634 249014 81.38
83.35 33.6 $scageomtransf
        element elasticBeamColumn 43 43 44 25.2 597634 249014 81.38
83.35 33.6 $scageomtransf
        element elasticBeamColumn 44 44 45 25.2 597634 249014 81.38
83.35 33.6 $scageomtransf
        element elasticBeamColumn 45 45 46 25.2 597634 249014 81.38
83.35 33.6 $scageomtransf
        element elasticBeamColumn 46 46 47 25.2 597634 249014 81.38
83.35 33.6 $scageomtransf

```

```

#define column elements

```

```

set np 5;      # number of Gauss integration points for nonlinear curva-
ture distribution

```

```

        element nonlinearBeamColumn 11 21 31 $np $colsec
$colgeomtransf
        element nonlinearBeamColumn 12 22 32 $np $colsec
$colgeomtransf
        element nonlinearBeamColumn 13 23 33 $np $colsec
$colgeomtransf
        element nonlinearBeamColumn 14 24 34 $np $colsec
$colgeomtransf

```

```

#rigid links

```

```

        rigidLink beam 42 31
        rigidLink beam 43 32
        rigidLink beam 45 33
        rigidLink beam 46 34

```

```

        rigidLink beam 11 21
        rigidLink beam 12 22

```

```
rigidLink beam 13 23
rigidLink beam 14 24

puts "4ok"

#-----constraints-----#

equalDOF 506 44 1 2 3 4 5 6

puts "5ok"

#-----model ready for modal analysis-----#

puts "Model Done!"
```

### 3.3 Modal Analysis

Prior to the seismic analysis, SAP2000 was used to perform an eigenvalue analysis, resulting in the dominant mode(s) in the transverse direction that capture at least 90% of the total modal mass participating ratio in that direction. Table 1 summarizes the natural periods and associated modal participating mass ratios of the dominant transverse mode(s) for all four cases.

In all cases, the damping in the bridge was characterized by an assumed 5% modal damping for each mode of vibration. For the modal analysis of the nonlinear spring support case, the effective support spring stiffness was used for the initial stiffness of each nonlinear spring.

Table 1  
*Summary of Fundamental Natural Periods and the Associated Modal Mass Participating Ratios for Transverse Direction*

<b>Case Study</b>	<b>Support Model</b>	<b>Mode Number</b>	<b>Period (sec)</b>	<b>Modal Participating Mass Ratio (%)</b>
SR 21 – I 69 Bridge	Basic	2	0.84	99.7
	Nonlinear Springs	1	0.7	78.9
		6	0.3	12.6
Forrester Rd – I69 Bridge	Basic	1	0.75	99.8
	Nonlinear Springs	1	0.61	96.1

## 4 NONLINEAR STATIC (PUSHOVER) ANALYSIS

### 4.1 General Considerations

This chapter discusses various aspects of the pushover analysis. In this study, the pushover curves were obtained by first analyzing the bridge under the effect of gravity loads and then pushing the bridge in the transverse direction. The pushover analysis was defined as a displacement control case, based on the transverse displacement at the control node located at the intersection of the cap beam and the superstructure. The analysis was stopped when the monitored displacement reached 0.75 ft.

The gradually increasing lateral force was defined as an invariant force distribution  $s = m\phi$ , where  $m$  is the structural mass matrix and  $\phi$  is the fundamental transverse mode shape. In this research, the lateral load pattern was applied to the superstructure joints only.

The pushover analysis was performed for the Basic Support Model of both case studies using the computer programs SAP2000, ADINA, and OpenSees. When using SAP2000, the effect of choosing each of the available plastic hinge properties was also investigated for both bridges. The Nonlinear Springs Support Models were studied by performing the pushover analysis using the user-defined hinge property in SAP2000. For the SR21-I69 Bridge with Nonlinear Springs Support configuration only, a multi-modal pushover analysis was performed using SAP2000, since its higher transverse modes are significantly effective (see Table 1). Prior to performing any of the analysis procedures mentioned in the earlier chapters, SAP2000 with the user-defined hinge property was used to check whether the progressive stiffness degradation has any influence on the structural performances of either bridge model.

## 4.2 SAP2000

The inelastic behavior was assumed to occur in concentrated plastic hinges assigned at the ends of each column element when SAP2000 was used. Three different options were examined to define the plastic hinge property. A user-defined hinge property based on the moment-curvature analysis results of the section was first employed. The need to consider the progressive stiffness degradation in the pushover analysis was first examined for all cases. As shown in Figures 19 and 20 for the SR21-I69 Bridge, since the first “sawtooth” is formed after the expected maximum performance displacement, which was assumed based on the TDOT seismic design results as  $\Delta_{P,max} = 0.5$  ft., the stiffness degradation was not affecting the structural responses. The same situation was observed for the Forrester Rd-I69 Bridge.

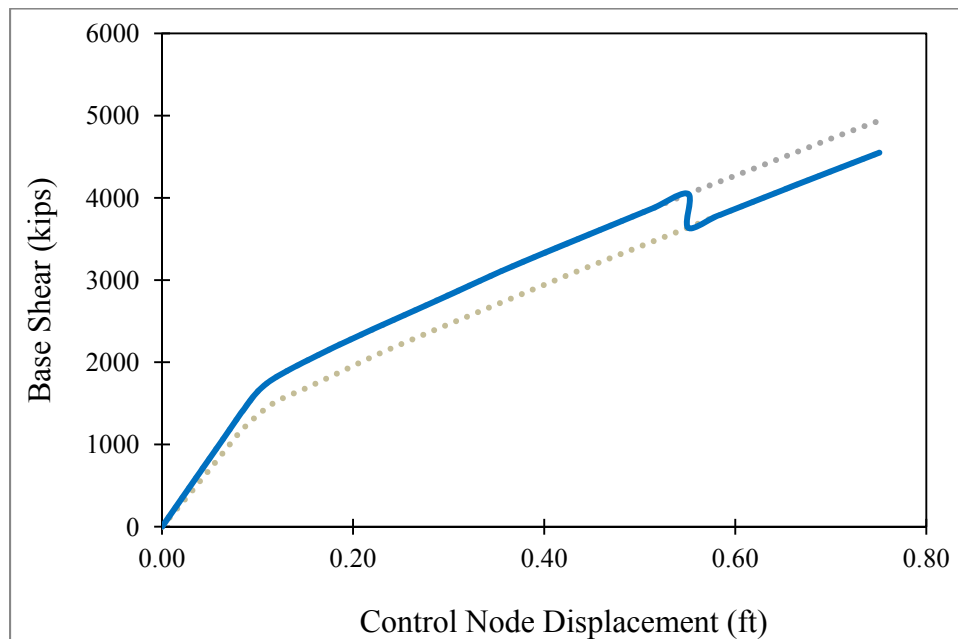


*Figure 19.* Pushover Curve with Stiffness Degradation for the SR21-I69 Bridge with the Basic Support Configuration.

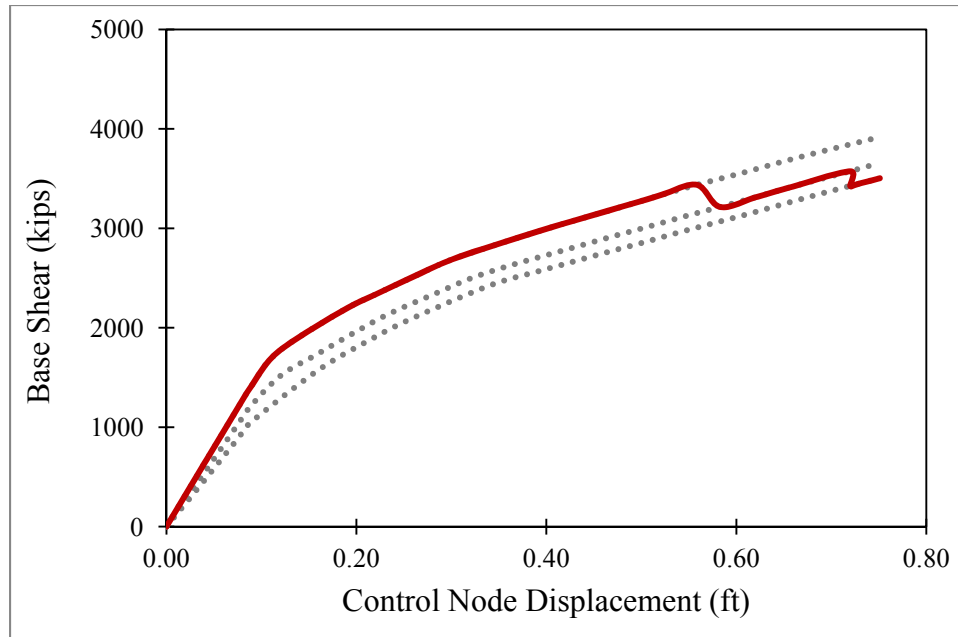


*Figure 20.* Pushover Curve with Stiffness Degradation for the SR21-I69 Bridge with the Nonlinear Springs Support Configuration.

For the Basic Support Models only, the other two SAP2000 built-in plastic hinge properties, discussed earlier, were used and the pushover analysis was performed for each bridge system. Figures 21 and 22 display the pushover curves when employing each plastic hinge property for the SR21-I69 and the Forrester Rd-I69 Bridges, respectively.

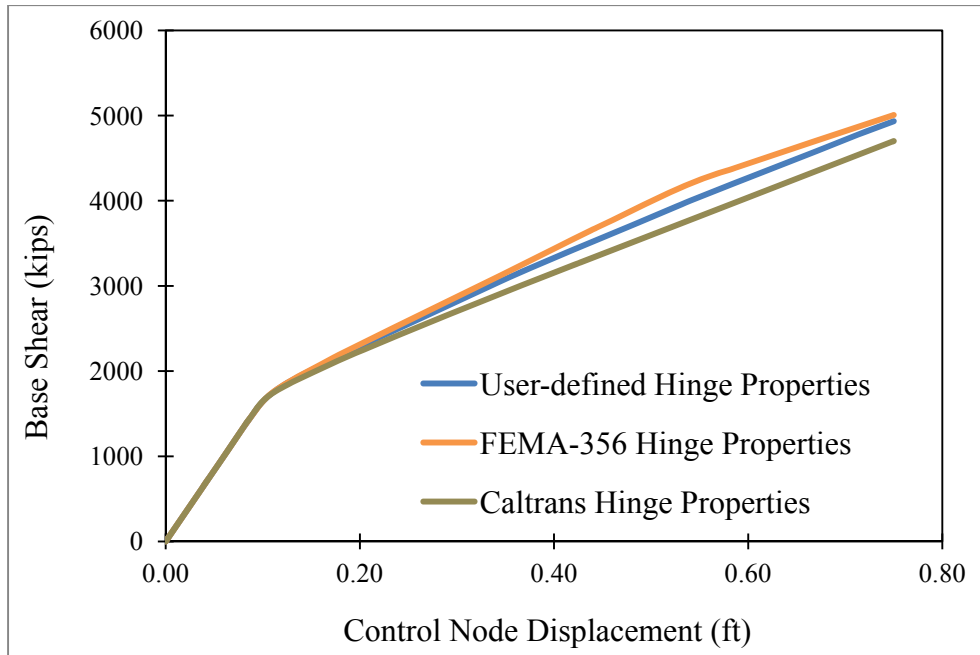


Figure 21. Pushover Curves with Different Plastic hinge Properties for the SR21-I69 Bridge with the Basic Support Configuration.

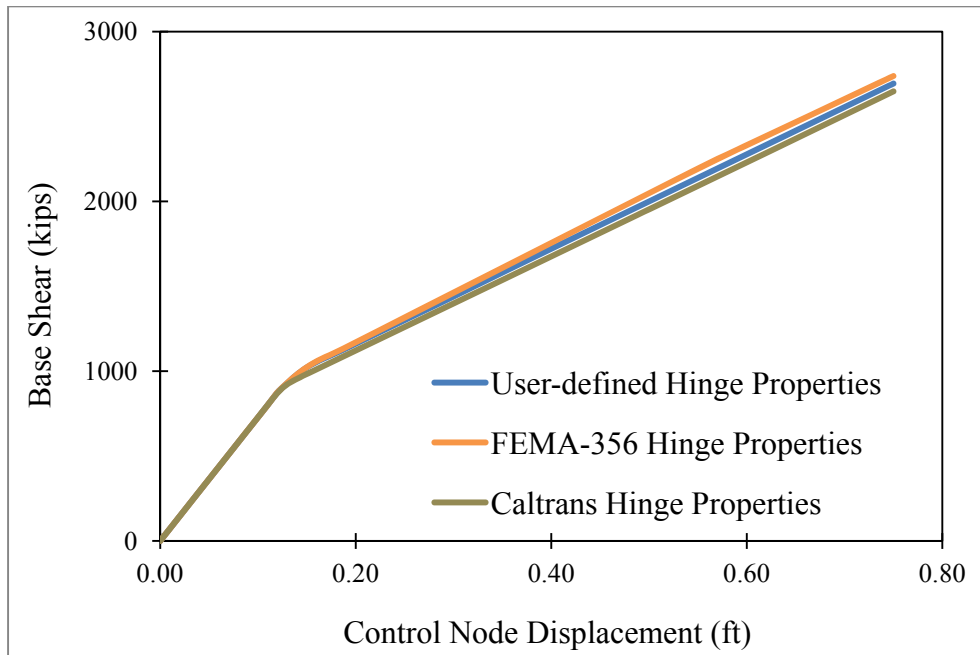


Figure 22. Pushover Curves with Different Plastic Hinge Properties for the Forrester Rd-I69 Bridge with the Basic Support Configuration.

The next pushover analysis was performed to determine the Forrester Rd-I69 Bridge's response when modeled with the Nonlinear Springs Support configuration using the user-defined plastic hinge properties. Figure 23 shows the results.

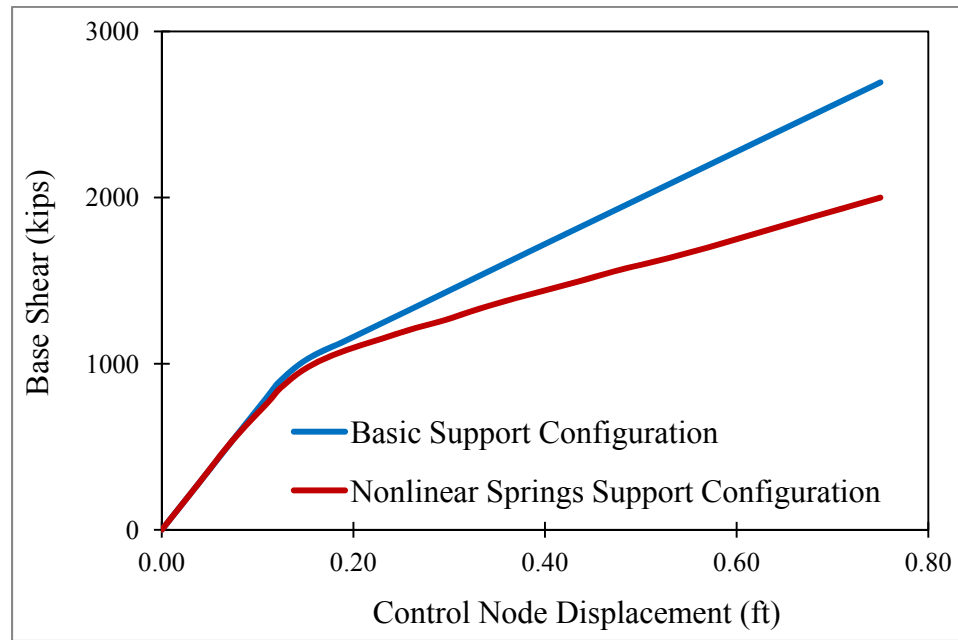


Figure 23. Pushover Curves with the User-Defined Plastic Hinge Property for the Forrester Rd-I69 Bridge with Different Support Configurations.

Finally, for the SR21-I69 Bridge with the Nonlinear Springs Support configuration modeled with user-defined hinge properties, multi-modal pushover analysis was performed following the MPA procedure (Chopra & Goel, 2002). Figure 24 shows the results for both single-mode and multi-modal pushover methods.



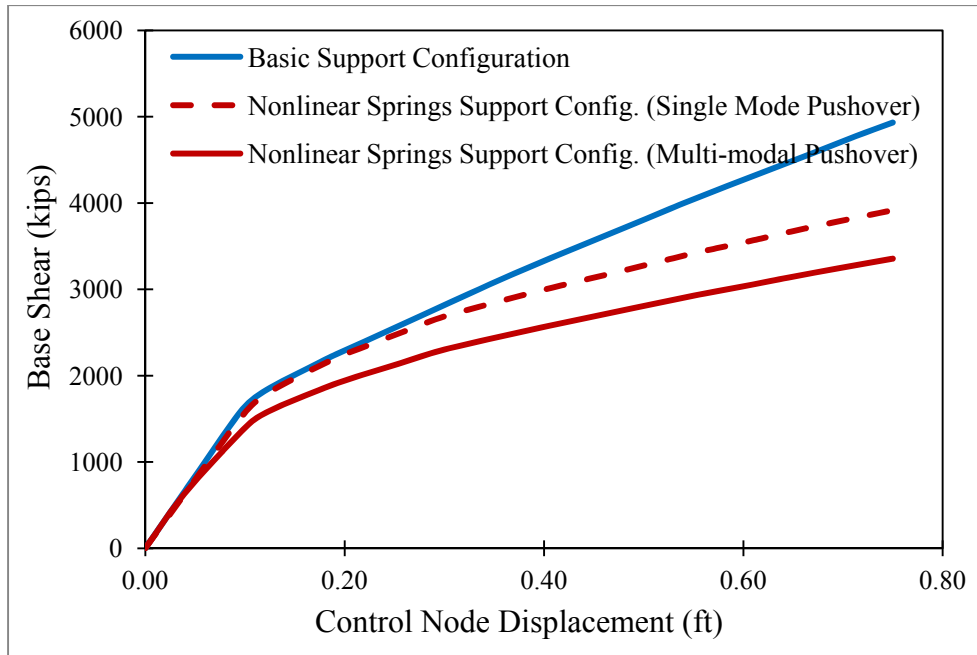
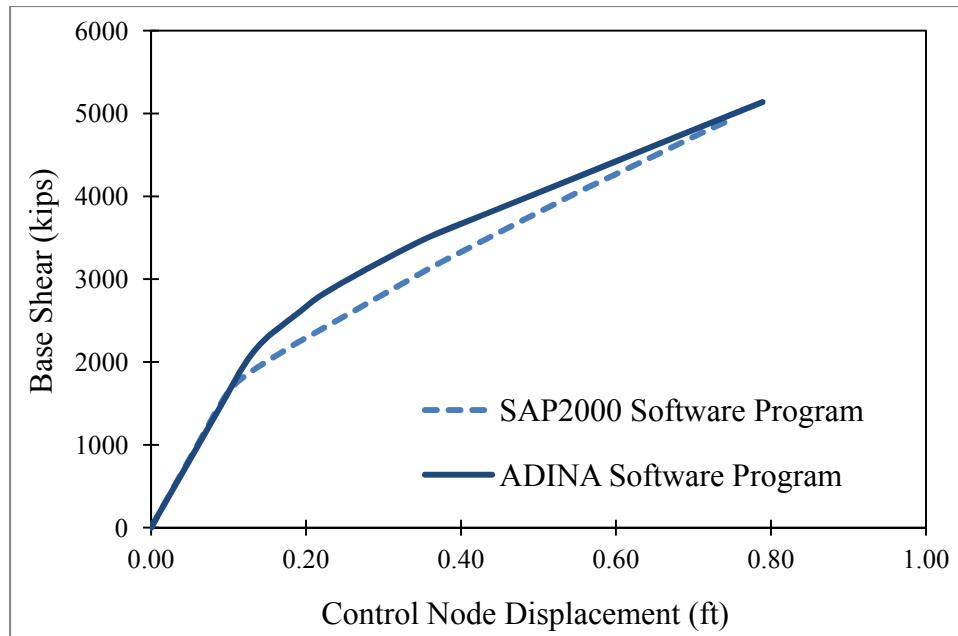


Figure 24. Pushover Curves with the User-defined Plastic Hinge Property for the SR 21-I69 Bridge with Different Support Configurations and Analysis Methods.

### 4.3 ADINA

The most common way to define nonlinearity in ADINA is through nonlinear beam elements, for which the material could be modeled by defining *Axial Force vs. Strain Curve*; *Force vs. Moment Curves*; *Twist vs. Moment (Torsion) Curves*; and *Curvature vs. Moment (Bending) Curves*. To construct the axial force vs. axial strain curve for column elements, the stress-strain behavior model of the materials (Mander et al., 1988) is used to determine the values of stress and force for many specific values of strain (Figure 17). ADINA requires the  $P-\epsilon$  curve's values to be in increasing order, and its segments' slopes to be in decreasing order. Therefore, only the first part of the curve, up to its absolute maximum value, was used.

One constant and one linear time function were defined to be followed by gravity loads and pushover analysis lateral load, respectively. Finally, by defining the lateral load pattern (the same pattern as used in SAP2000), pushover analysis was performed for the Basic Support Models in ADINA. Figures 25 and 26 display both pushover curves obtained from the ADINA and the SAP2000 programs.



*Figure 25.* Pushover Curves for the SR 21-I69 Bridge with the Basic Support Configuration Using the SAP2000 Computer Program with the User-defined Plastic Hinge Property and the ADINA Computer Program.

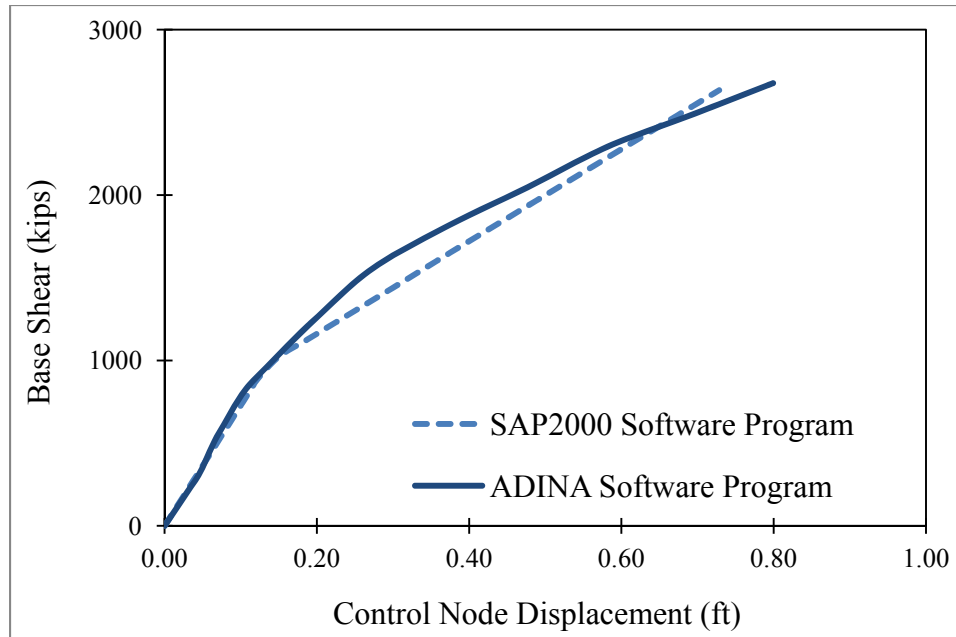


Figure 26. Pushover Curves for the Forrester Rd-I69 Bridge with the Basic Support Configuration Using the SAP2000 Computer Program with the User-defined Plastic Hinge Property and the ADINA Computer Program.

#### 4.4 OpenSees

The model was first subjected to gravity loads. Then, the gravity load effects of the system were saved by using the *loadConst* command, and the pushover lateral load was applied to the structure in an incremental fashion. The control node displacement and the support reactions were reported by pre-defined *recorders*. Sometimes in the non-linear analysis, the regular *Newton* algorithm may not converge at some steps. Therefore, many extra lines were added to check for convergence at each step and, in the case of failure, temporarily switch to the *Newton with initial Stiffness* algorithm. The full Tcl script for performing gravity and pushover analyses of the SR21-I69 Bridge in OpenSees is presented below.

```

#-----GRAVITY ANALYSIS-----#

file mkdir sr21basic
recorder Node -file sr21basic/controldisp.out -time -node 506 -dof
1 disp
recorder Node -file sr21basic/reactions.out -time -node 5001 5011
21 22 23 24 -dof 1 reaction

#gravity load

pattern Plain 1 Linear {
load 501 0 0 $Pabut 0 0 0
load 511 0 0 $Pabut 0 0 0
eleLoad -ele 501 502 503 504 505 506 507 508 509 510 -type -
beamUniform -$Qsuper 0
eleLoad -ele 41 42 43 44 45 46 -type -beamUniform -$Qcap 0
eleLoad -ele 11 12 13 14 -type -beamUniform 0 0 $Qcol
}

#analysis

constraints Lagrange
numberer RCM
system BandGeneral
test EnergyIncr 1e-8 6
algorithm Newton
integrator LoadControl 0.1
analysis Static

analyze 10

puts "GRAVITY DONE!"

#-----PUSHOVER ANALYSIS-----#

#reset time
loadConst -time 0

#lateral load proportional to the dominant mode shape (from modal analy-
sis)

pattern Plain 2 Linear {
load 501 1358 0 0 0 0 0
load 502 1210 0 0 0 0 0
load 503 1306 0 0 0 0 0

```

```

        load 504 1335 0 0 0 0
        load 505 1286 0 0 0 0
        load 506 1237 0 0 0 0
        load 507 1286 0 0 0 0
        load 508 1335 0 0 0 0
        load 509 1306 0 0 0 0
        load 510 1210 0 0 0 0
        load 511 1358 0 0 0 0
    }

set IDctrlNode 506
set IDctrlDOF 1
set Tol 1.e-8
set maxNumIter 6
set TestType EnergyIncr

set algorithmType Newton

set Dmax 1
set Dincr 0.01

integrator DisplacementControl $IDctrlNode $IDctrlDOF $Dincr

set Nsteps [expr int($Dmax/$Dincr)]; # number of pushover analysis
steps
set ok [analyze $Nsteps]; # this will return zero if no conver-
gence problems were encountered

# ----- in case of convergence problems-----
-----#

if {$ok != 0} {
# change some analysis parameters to achieve convergence
# performance is slower inside this loop
    set ok 0;
    set controlDisp 0.0; # start from zero
    set D0 0.0; # start from zero
    set Dstep [expr ($controlDisp-$D0)/($Dmax-$D0)]
    while {$Dstep < 1.0 && $ok == 0} {
        set controlDisp [nodeDisp $IDctrlNode $IDctrlDOF ]
        set Dstep [expr ($controlDisp-$D0)/($Dmax-$D0)]
        set ok [analyze 1 ]
        if {$ok != 0} {
            puts "Trying Newton with Initial Tangent .."
            test NormDispIncr $Tol 2000 0
            algorithm Newton -initial
        }
    }
}

```

```

        set ok [analyze 1 ]
        test $TestType $Tol $maxNumIter 0
        algorithm $algorithmType
    }
    if {$ok != 0} {
        puts "Trying Broyden .."
        algorithm Broyden 8
        set ok [analyze 1 ]
        algorithm $algorithmType
    }
    if {$ok != 0} {
        puts "Trying NewtonWithLineSearch .."
        algorithm NewtonLineSearch .8
        set ok [analyze 1 ]
        algorithm $algorithmType
    }
}
}; # end if ok !0

puts "PUSHOVER DONE!"

```

The pushover curves obtained for the Basic Support Models using the OpenSees software program are shown in Figures 27 and 28. They have been compared with the SAP2000 results on the same figure.

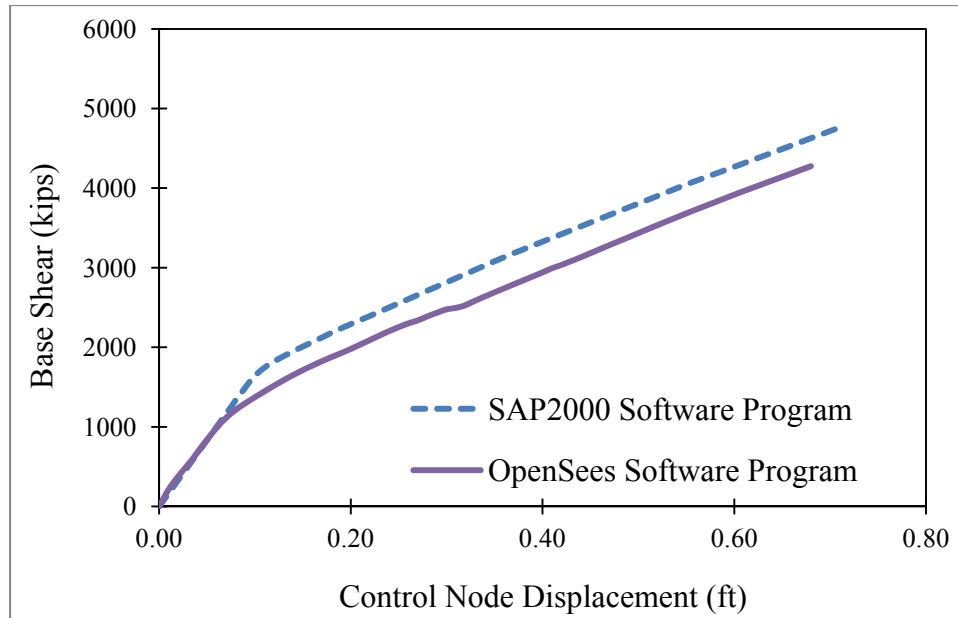


Figure 27. Pushover Curves for the SR 21-I69 Bridge with the Basic Support Configuration Using the SAP2000 Computer Program with the User-defined Plastic Hinge Property and the OpenSees Computer Program.

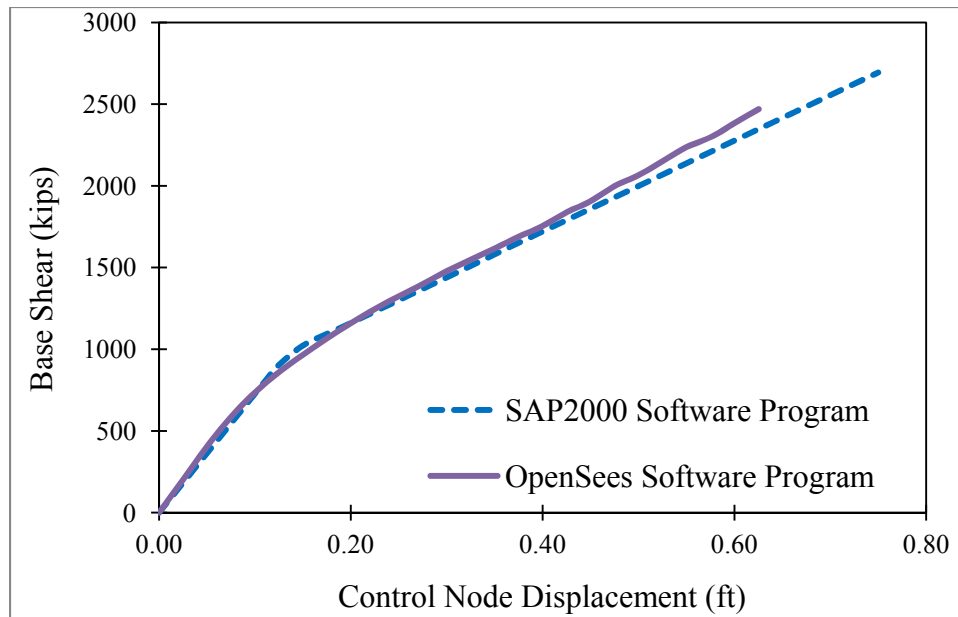


Figure 28. Pushover Curves for the Forrester Rd-I69 Bridge with the Basic Support Configuration Using the SAP2000 Computer Program with the User-defined Plastic Hinge Property and the OpenSees Computer Program.

## 4.5 Capacity Diagrams

All achieved pushover curves were converted to capacity diagrams using conversion factors presented in Equations 4.1 and 4.2 below. These factors represent the fundamental mode shape of the bridge in the desired direction and convert the base shear ( $V_b$ ) vs. control node displacement ( $u_N$ ) curve to a spectral acceleration ( $S_a$ ) vs. spectral displacement ( $S_d$ ) capacity curve for the fundamental mode:

$$S_a = \frac{V_b}{M_1^*} \quad (4.1)$$

$$S_d = \frac{u_N}{\Gamma_1 \varphi_{N1}} \quad (4.2)$$

where  $M_1^*$  is the effective modal mass of the fundamental mode,  $\varphi_{N1}$  is the modal amplitude of the control node in the fundamental mode, and  $\Gamma_1$  is the modal participation factor of the fundamental mode:

$$\Gamma_1 = \frac{\sum_{j=1}^N m_j \phi_{j1}}{\sum_{j=1}^N m_j \phi_{j1}^2} \quad (4.3)$$

$$M_1^* = \frac{\left( \sum_{j=1}^N m_j \phi_{j1} \right)^2}{\sum_{j=1}^N m_j \phi_{j1}^2} \quad (4.4)$$

where  $m_j$  is the lumped mass at the  $j$ -th node,  $\phi_{j1}$  is the  $j$ -th node modal amplitude in the fundamental mode, and  $N$  is the number of nodes. The middle node of the superstructure



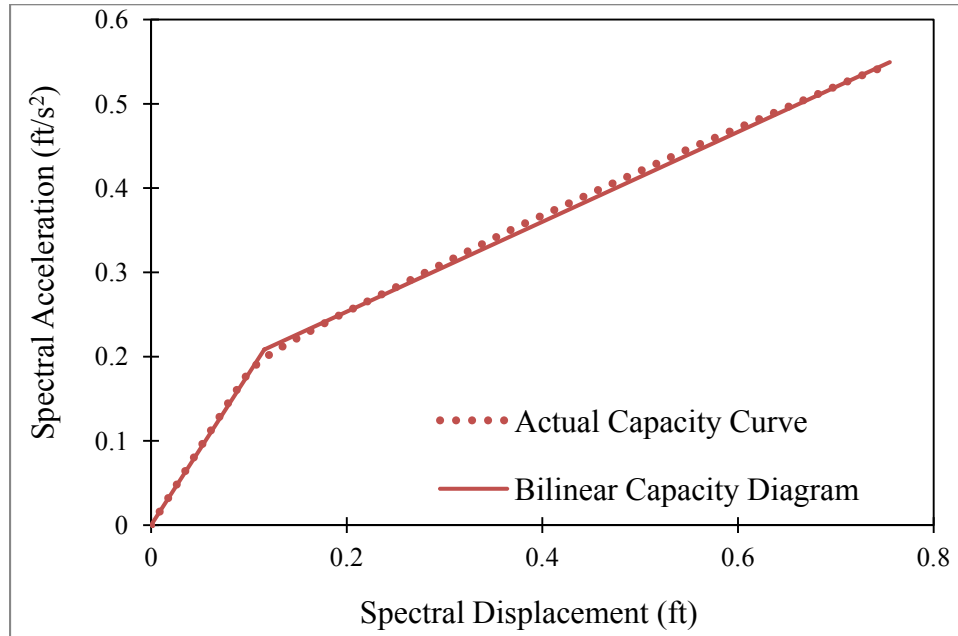
was taken as the control node. Using the modal analysis results and Equations 4.1 through 4.4, the conversion factors were obtained and summarized in Table 2.

Table 2  
*Capacity Curve Conversion Factors*

Case Study	Support Model	$M_1^*$ (kips- s <sup>2</sup> /ft)	$\Gamma_1 \phi_{N1}$ (ft/ft)
SR21-I69 Bridge	Basic	9017.2	0.9928
	Nonlinear Springs	7140.0	1.2138
Forrester Rd-I69 Bridge	Basic	3349.0	0.9885
	Nonlinear Springs	3224.4	0.9836

In every displacement-based method, it is necessary to determine the ductility of the structure at different points along the capacity curve. This property could be achieved by replacing the actual capacity curve by its bilinear representation, on which the yielding spectral displacement,  $(S_d)_y$ , is clearly determined. A simple way to construct the bilinear capacity spectrum is to draw the first line just by extending the pre-yielding part of the capacity curve. The second line, starting from the last point on the capacity curve, is drawn such that the generated areas above and below the capacity curve are equal. The intersection of these lines is then defined as the yield point of the bilinear capacity diagram. Figure 29 shows a sample bilinear representation of its corresponding actual capacity curves, and Figures 30 and 30 display all of the bilinear capacity diagrams for the

SR21-I69 and the Forrester Rd-I69 bridges, respectively, while the yielding spectral displacement,  $(S_d)_y$ , values for each case are tabulated in Table 3.



*Figure 29.* Actual and Bilinear Capacity Diagrams for the SR21-I69 Bridge with the Basic Support Configuration Achieved from SAP2000 Results with the User-defined Hinge.

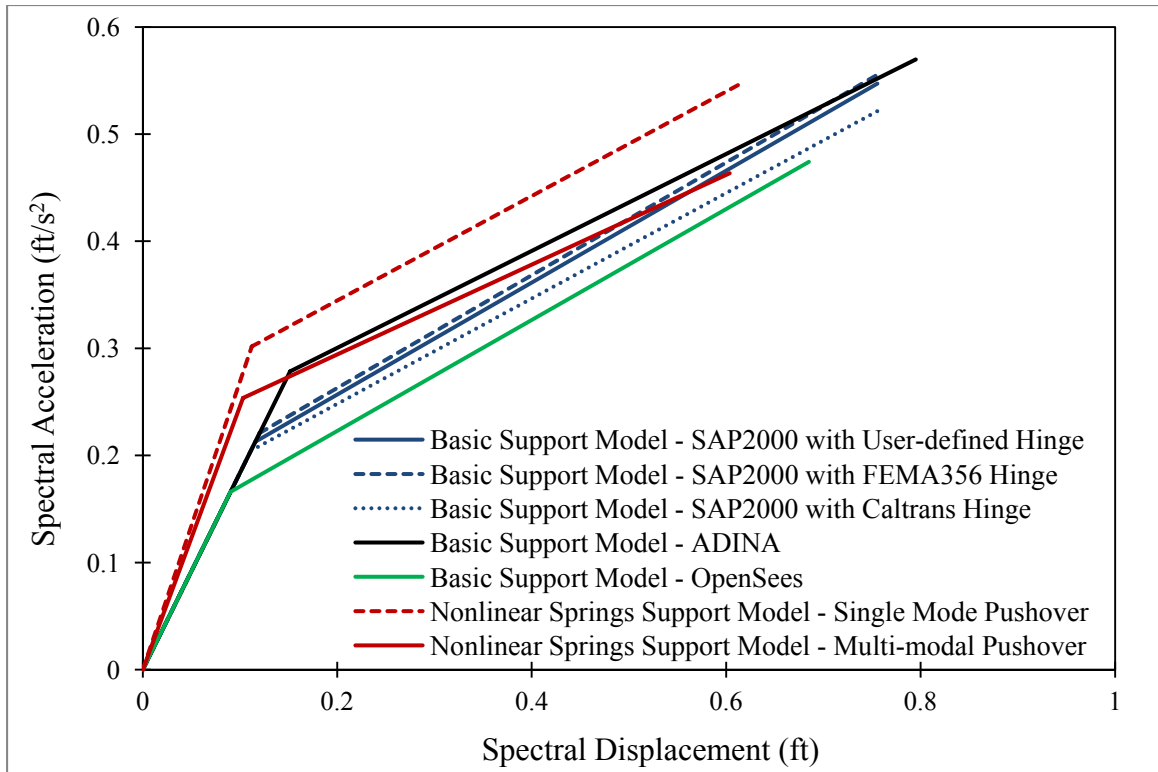


*Figure 30.* Bilinear Capacity Diagrams for the SR21-I69 Bridge with Various Modeling Properties Achieved from Different Computer Programs.

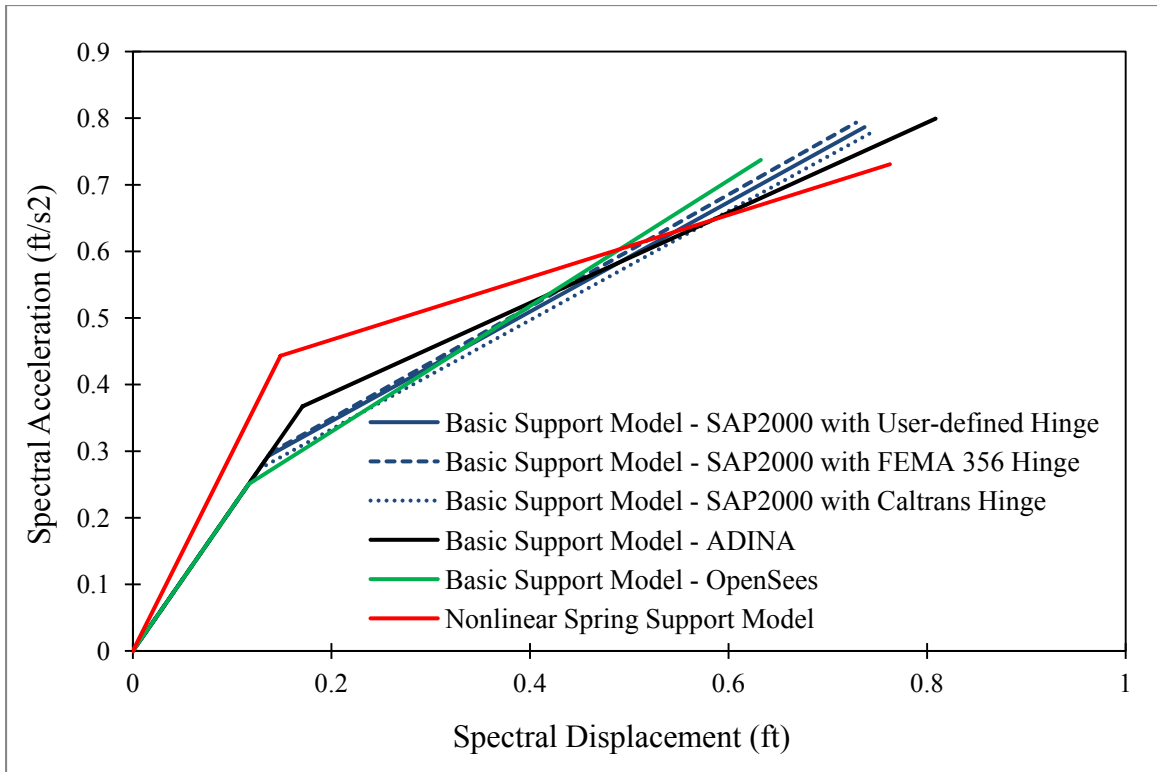


*Figure 31.* Bilinear Capacity Diagrams for the Forrester Rd-I69 Bridge with Various Modeling Properties Achieved from Different Computer Programs.

Table 3  
*Bilinear Capacity Diagram Properties*

Case Study	Support Model	Analysis Option	$(S_d)_y$ (ft)	
SR21-I69 Bridge	Basic	SAP2000: User-defined Hinge	0.1158	
		SAP2000: FEMA-356 Hinge	0.1201	
		SAP2000: Caltrans Hinge	0.1112	
	Nonlinear Springs		ADINA	0.1514
			OpenSees	0.0903
			Single Mode Pushover	0.1121
			Multi-modal Pushover	0.1030
Forrester Rd-I69 Bridge	Basic	SAP2000: User-defined Hinge	0.1362	
		SAP2000: FEMA-356 Hinge	0.1383	
		SAP2000: Caltrans Hinge	0.1271	
	Nonlinear Springs		ADINA	0.1710
			OpenSees	0.1166
			Single Mode Pushover	0.1487

## 5 DISPLACEMENT-BASED ANALYSIS PROCEDURES

### 5.1 Seismic Demand

The seismic excitation used in this study was represented by design response spectra. Using the actual location of the bridge, the design response spectrum was obtained from the AASHTO GM program. The spectral acceleration vs. spectral displacement ( $S_a$  vs.  $S_d$ ) format of the design response spectra for both bridges are shown in Figures 32 and 33.

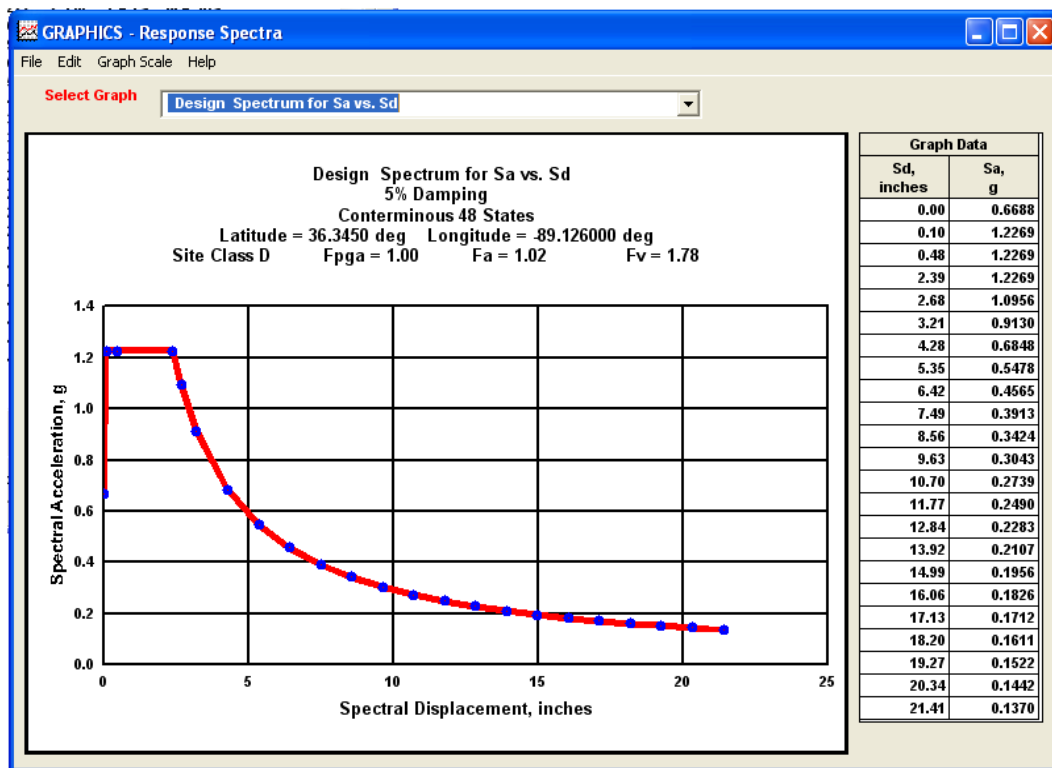


Figure 32. Design Response Spectrum for the SR21-I69 Bridge.

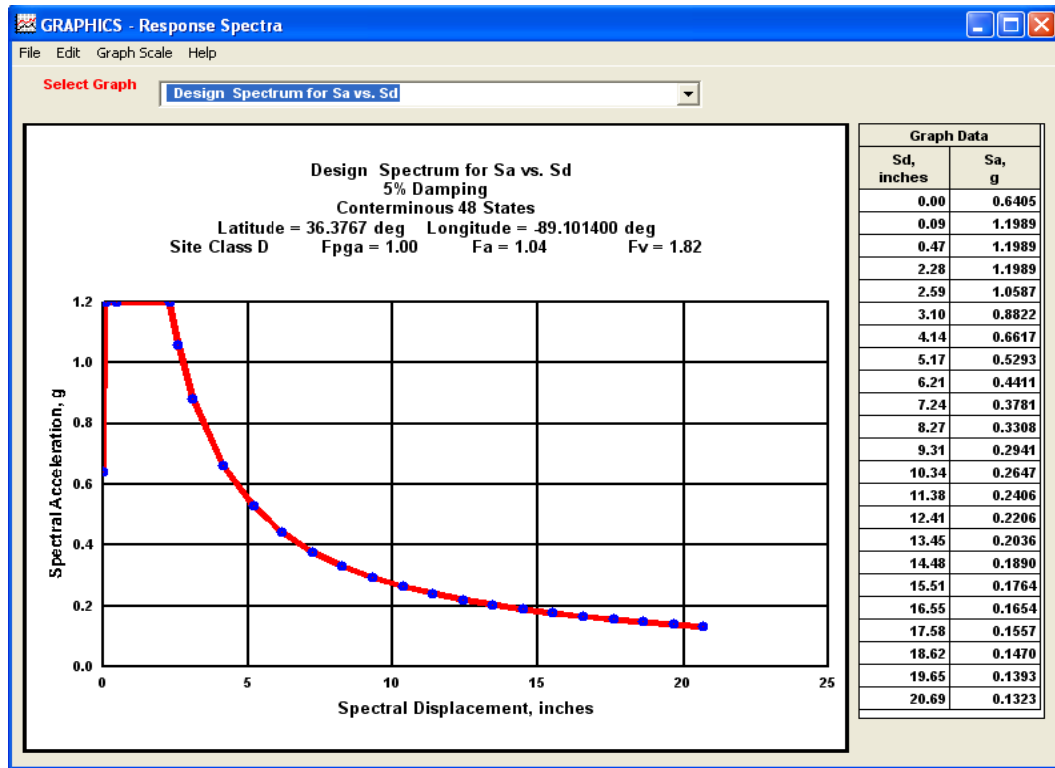


Figure 33. Design Response Spectrum for the Forrester Rd-I69 Bridge.

## 5.2 AASHTO Specifications Procedure

Three different displacement-based methods were used to evaluate the seismic response of the case study bridges. The first procedure is presented by the AASHTO Specifications and was used by the TDOT engineers in the actual design of the bridges. Based on the TDOT design documents, the finite element model of the bridge supported by the Basic Support configuration had been subjected to the design response spectrum in four different combinations: longitudinal direction only, transverse direction only, and two 100%-30% combinations. The CQC modal combination for the first twenty mode shapes had been used to calculate the maximum transverse displacement of the bent frame. The seismic displacement demand,  $\Delta_D$ , in the transverse direction was determined as 0.374 and 0.335 ft for the SR21-I69 and the Forrester Rd-I69 Bridges, respectively. The capac-

ity analysis of the bent frame was then performed using the TDOT developed pushover analysis spreadsheets. The spreadsheets follow the same methodology as the capacity design method presented in the AASHTO Specifications. The same computer program used in this study was used to determine the plastic hinge properties. Finally, the seismic displacement capacity,  $\Delta_C$ , of the bent frame was calculated as 0.386 ft for the SR21-I69 Bridge and 0.48 ft for the Forrester Rd-I69 Bridge. In terms of the displacement ductility,  $\mu_D = \Delta_{max} / \Delta_y$ , the values of 4.202 and 2.997 were obtained. Table 4 summarizes the AASHTO Specifications procedure results.

Table 4  
*Seismic Analysis Results Based on AASHTO Procedure (Adopted from TDOT Documents)*

Case Study	Seismic Displacement Demand, $\Delta_D$ (ft)	Bent Frame Displacement Capacity, $\Delta_C$ (ft)	Displacement Ductility, $\mu_D$
SR21-I69 Bridge with the Basic Support Model	0.374	0.386	4.202
Forrester Rd-I69 Bridge with the Basic Support Model	0.335	0.48	2.997



### 5.3 FEMA-440 Procedure C

The next two displacement-based procedures also use the intersection of the capacity (pushover) curve and the demand diagram to estimate the maximum seismic displacement, which is called the "performance point." They differ in reducing the elastic ( $\mu=1$ ) response spectrum to an inelastic ( $\mu_i$ ) demand diagram. FEMA-440 (2005) presents three procedures as modifications to the CSMs of ATC-40, from which we chose Procedure C for this study. This approach uses the modified acceleration-response spectrum for multiple assumed solutions ( $S_{a_{pi}}, S_{d_{pi}}$ ) and the corresponding ductilities to generate a locus of possible performance points. The actual performance point is located at the intersection of this locus and the capacity curve (FEMA, 2005). Procedure C, like the other procedures in FEMA-440, is an equivalent linearization procedure which adjusts the initial response spectrum to the appropriate level of effective damping,  $\beta_{eff}$ , as follows:

$$(S_a)_{\mu_i} = M_i \times \frac{(S_a)_{\mu=1}}{4} \frac{1}{5.6 - \ln(\beta_{eff})_i} \quad (5.1)$$

$$M_i = \left( \frac{(T_{eff})_i}{(T_{sec})_i} \right)^2 \leq 1.0 \quad (5.2)$$

$$(T_{sec})_i = \frac{T_0}{\sqrt{\frac{1 + \alpha(\mu_i - 1)}{\mu_i}}} \quad (5.3)$$

where,  $\mu_i$  is the assumed ductility,  $M_i$  is the acceleration modification factor,  $(T_{sec})_i$  is the secant period for the assumed ductility,  $T_0$  is the natural period of the system,  $\alpha$  is the post-elastic stiffness from the bilinear capacity curve, and  $(\beta_{eff})_i$  and  $(T_{eff})_i$  are the effective damping and the effective period for the assumed ductility, respectively. The parameters  $(\beta_{eff})_i$  and  $(T_{eff})_i$  are defined as follows:

for  $1.0 < \mu_i < 4.0$ :

$$(T_{eff})_i = (0.2(\mu_i - 1)^2 - 0.038(\mu_i - 1)^3 + 1)T_0 \quad (5.4)$$

$$(\beta_{eff})_i = 4.9(\mu_i - 1)^2 - 1.1(\mu_i - 1)^3 + \beta_0 \quad (5.5)$$

for  $4.0 \leq \mu_i \leq 6.5$ :

$$(T_{eff})_i = (0.28 + 0.13(\mu_i - 1) + 1)T_0 \quad (5.6)$$

$$(\beta_{eff})_i = 14 + 0.32(\mu_i - 1) + \beta_0 \quad (5.7)$$

where,  $\beta_0$  is the initial damping ratio of the structure, taken as 5%. By constructing a family of demand curves for selected  $\mu$  values of 2.0, 2.5, 3.0, and 3.5, the spectral displacement of the performance point was determined for each of the Basic Support Models with the SAP2000 user-defined hinge property and the Nonlinear Springs Support Models. Figures 34 and 35 show the procedure for the Basic Support models. The spectral displacement of the performance point could be then converted back to the control node displacement using Equation 4.2.

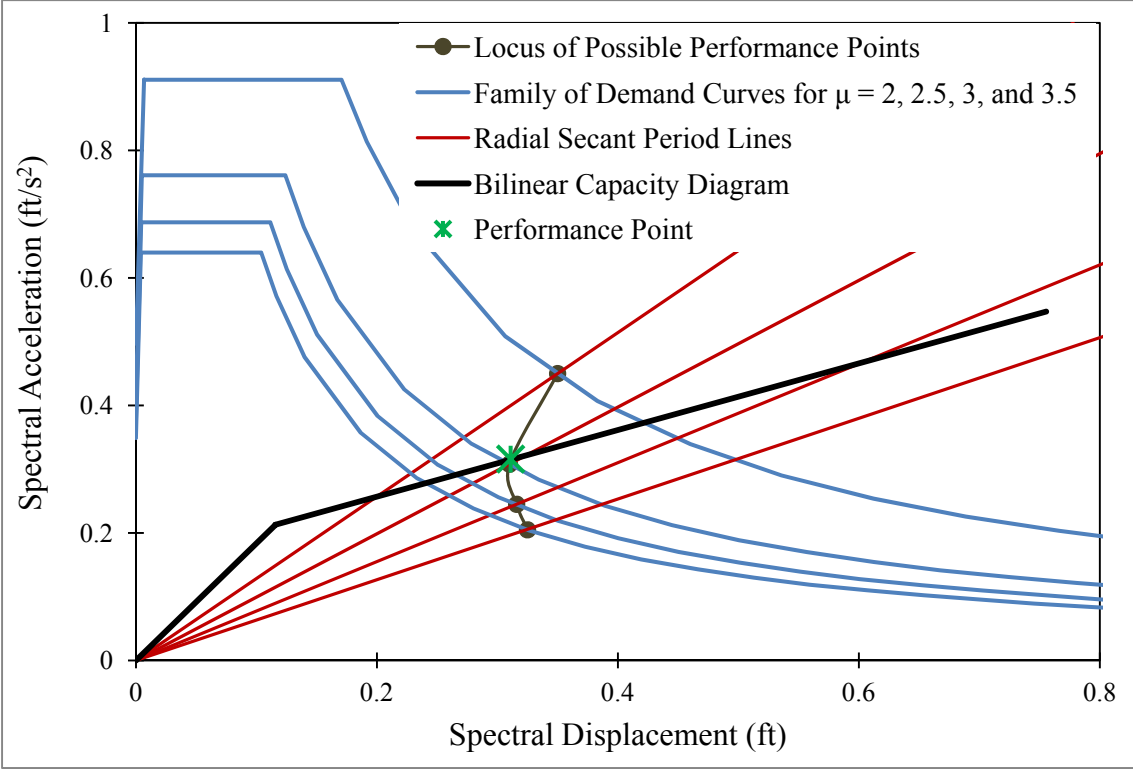


Figure 34. Seismic Analysis of the Basic Support Model of the SR21-I69 Bridge with the SAP2000 User-Defined Hinge Property Using FEMA-440 Procedure C.

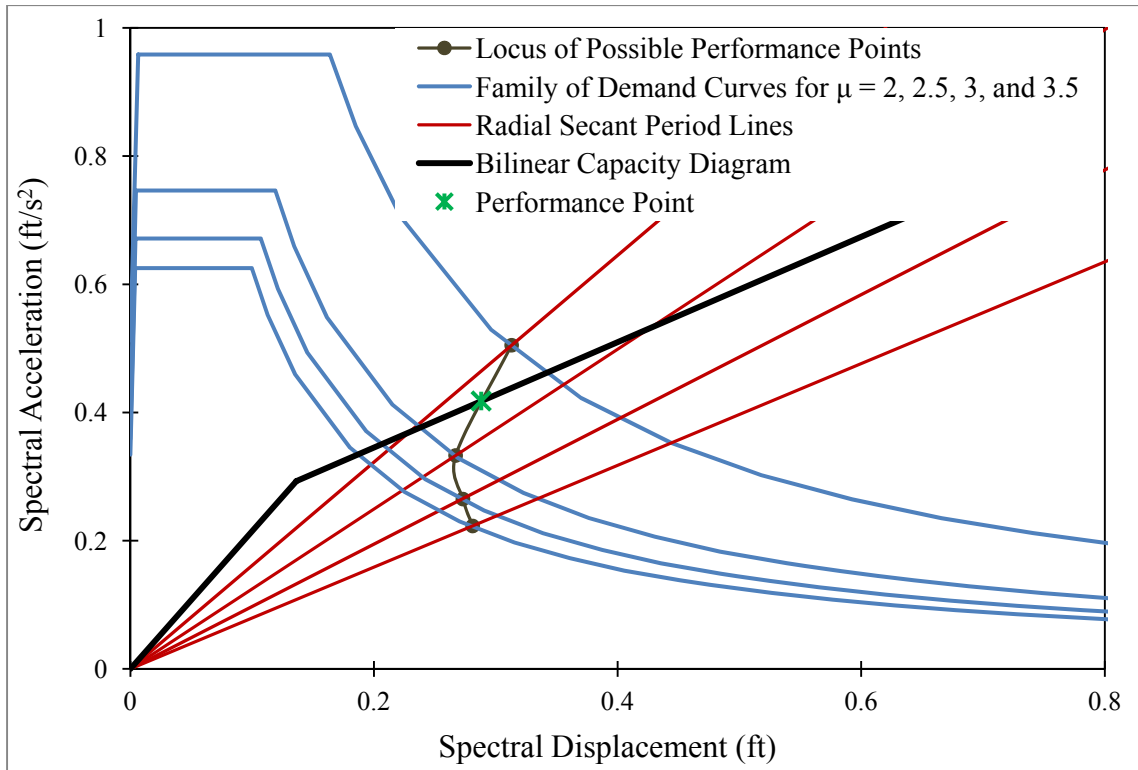


Figure 35. Seismic Analysis of the Basic Support Model of the Forrester Rd-I69 Bridge with the SAP2000 User-Defined Hinge Property Using FEMA-440 Procedure C.

The displacement ductility of the system was calculated by dividing the maximum displacement by the yielding displacement (Table 3) for each case. Table 5 summarizes the results of the seismic design of the SR21-I69 and the Forrester Rd-I69 Bridges using FEMA-440 Procedure C.

Table 5  
*Seismic Analysis Results Based on FEMA-440 Procedure C*

Case Study	Performance Point's Spectral Displacement, ( $S_d$ ) <sub>p</sub>	Seismic Displacement Demand, $\Delta_D$ (ft)	Displacement Ductility, $\mu_D$
SR21-I69 Bridge with the Basic Support Model	<b>0.311</b>	<b>0.309</b>	<b>2.686</b>
SR21-I69 Bridge with the Non-linear Springs Support Model (Single Mode Pushover)	<b>0.252</b>	<b>0.25</b>	<b>2.23</b>
SR21-I69 Bridge with the Non-linear Springs Support Model (Multi-modal Pushover)	<b>0.251</b>	<b>0.249</b>	<b>2.417</b>
Forrester Rd-I69 Bridge with the Basic Support Model	<b>0.288</b>	<b>0.285</b>	<b>2.114</b>
Forrester Rd-I69 Bridge with the Nonlinear Springs Support Model	<b>0.217</b>	<b>0.213</b>	<b>1.459</b>

## 5.4 Capacity-demand-diagram Method

The third displacement-based seismic design procedure used in this study called the capacity-demand-diagram method and was presented by Chopra and Goel (1999). This procedure determines the demand by analyzing the inelastic system instead of the equivalent linear systems in the CSMs of ATC-40. A family of constant-ductility demand spectra is constructed by reducing the elastic design spectrum by appropriate ductility-dependant factors,  $R_y$ :

$$(S_a)_{\mu_i} = (S_a)_{\mu=1} / (R_y)_{\mu_i} \quad (5.8)$$

Various  $R_y$ - $\mu$ - $T$  equations have been presented by Chopra (2007). In this study, we used the Newmark-Hall equations as follows:

$$(R_y)_{\mu_i} = \begin{cases} 1 & T < T_a \\ (2\mu_i - 1)^{\frac{\beta}{2}} & T_a < T < T_b \\ \sqrt{2\mu_i - 1} & T_b < T < T'_c \\ \frac{T}{T_c} \mu_i & T'_c < T < T_c \\ \mu_i & T > T_c \end{cases} \quad (5.9)$$

$$\beta = \ln(T/T_a) / \ln(T_b/T_a) \quad (5.10)$$

$$T'_c = T_c \sqrt{2\mu_i - 1} / \mu_i \quad (5.11)$$

where,  $T_a = 1/33 \text{ sec.}$ ,  $T_b = 0.125 \text{ sec.}$ , and  $T_c$  is the period of the last point in the constant acceleration region of the design spectrum, equal to 0.446 seconds for the SR21-I69 Bridge and 0.442 for the Forrester Rd-I69 Bridge. For selected values of  $\mu = 1.75, 2.0, 2.25,$  and  $2.5$ , the demand curves were plotted on the same chart as the bilinear capacity

spectrum for each combination of support configuration and hinge property of both bridges. At one relevant intersection point, the ductility factor calculated from the ratio of the displacement of the point to the yielding displacement matches the ductility value associated with the intersecting demand curve, which determines the performance point of the structure. Figure 36 shows the capacity-demand-diagram procedure for the SR21-I69 Bridge with the Basic Support configuration and the SAP2000 user-defined hinge property.

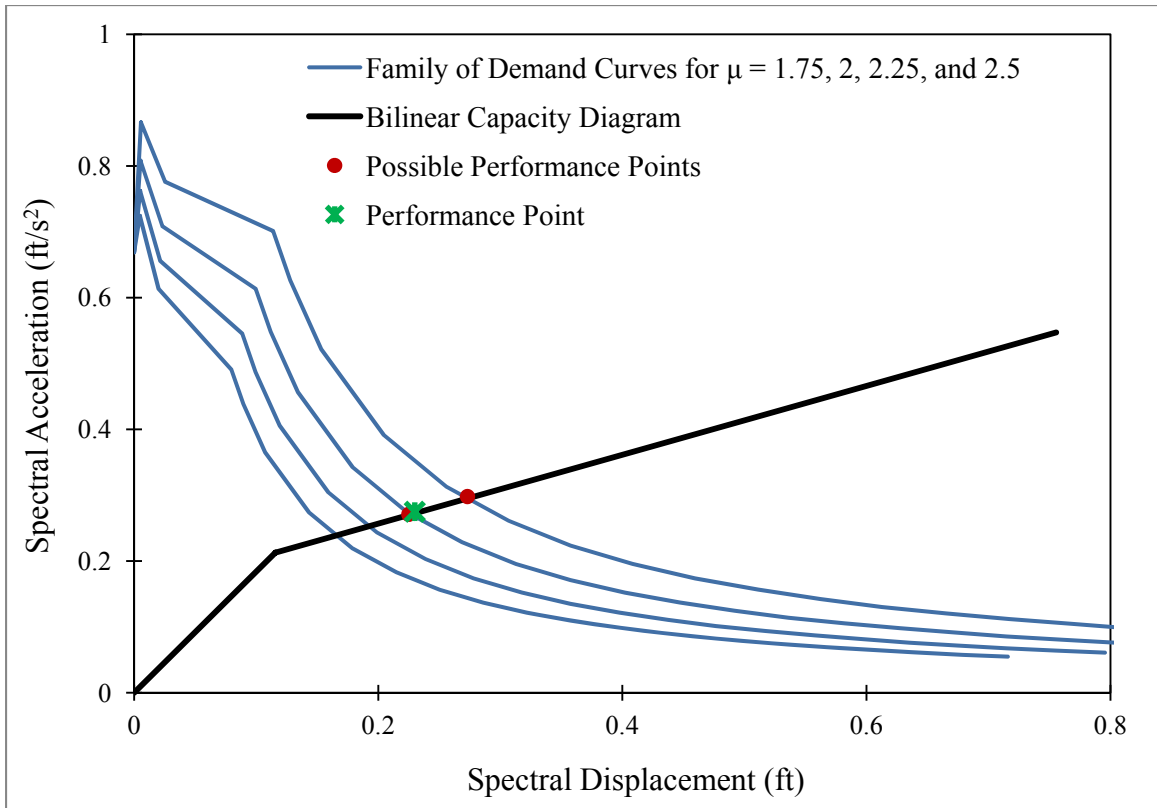
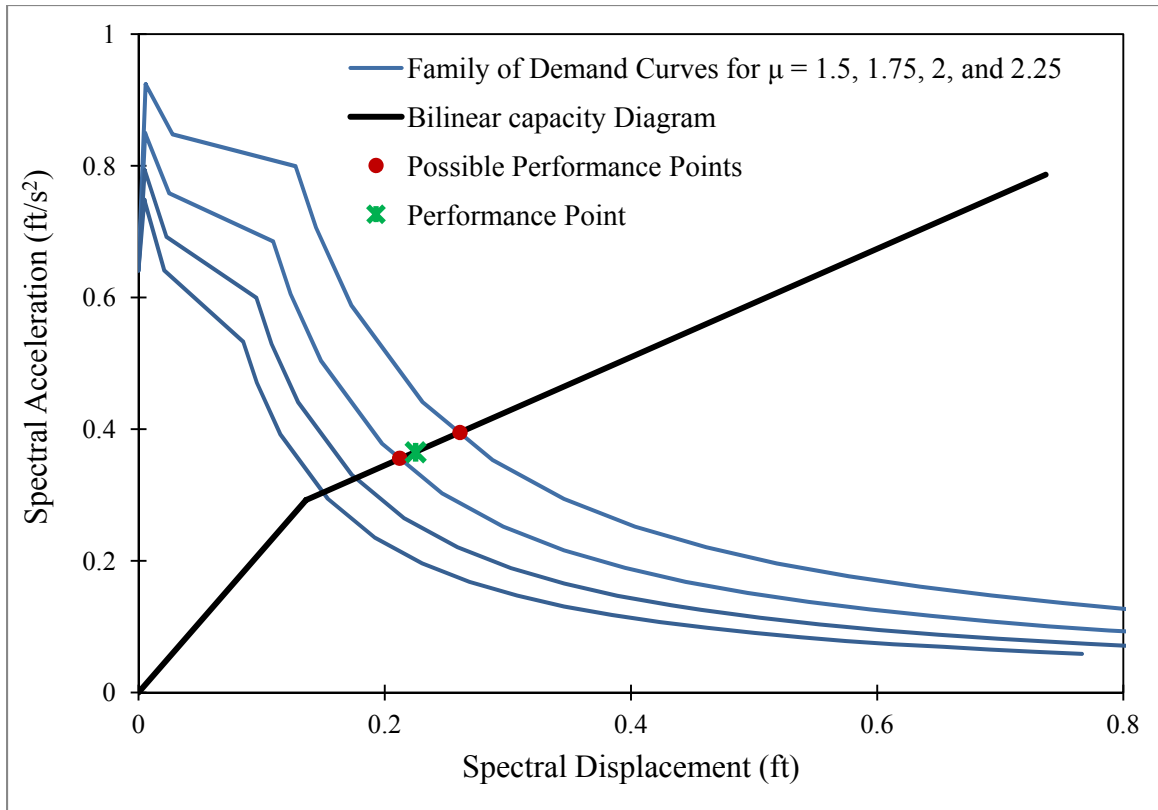


Figure 36. Seismic Analysis of the Basic Support Model of the SR21-I69 Bridge with the SAP2000 User-defined Hinge Property Using the Capacity-Demand-Diagram Method.

As shown in Figure 36, each demand curve intersects the bilinear capacity diagram at its relevant point. While the yielding spectral displacement for this case is equal to 0.1158 ft (Table 3), the  $S_d$  coordinate of the intersection of the point ( $\mu=1.75$ ) demand curve and the capacity diagram is 0.275 ft, which results in a displacement ductility value of 2.375. On the other hand, the ( $\mu=2.0$ ) demand curve intersects the capacity spectrum at  $S_d = 0.227$  ft, and  $\mu_D=1.96$ . None of these intersection points' ductility matches with the ductility value of the corresponding demand curve. A linear interpolation determined the performance point's ductility and the spectral displacement as 1.985 and 0.23 ft, respectively.

Figure 37 displays the same seismic analysis method for the Forrester Rd-I69 Bridge with Basic Support configuration and the SAP2000 user-defined hinge property and the results of the capacity-demand-diagram seismic design method for various cases are tabulated in Table 6.





*Figure 37.* Seismic Analysis of the Basic Support Model of the Forrester-I69 Bridge with the SAP2000 User-Defined Hinge Property Using the Capacity-Demand-Diagram Method.

Table 6  
*Seismic Analysis Results Based on the Capacity-demand-diagram Method.*

Case Study	Support Model	Analysis Option	Performance Point's Spectral Displacement, ( $S_d/p$ )	Seismic Displacement Demand, $\Delta_D$ (ft)	Displacement Ductility, $\mu_D$
SR21-I69 Bridge	Basic	SAP2000: User-defined Hinge	0.23	0.228	1.985
		SAP2000: FEMA-356 Hinge	0.23	0.228	1.912
		SAP2000: Caltrans Hinge	0.228	0.226	2.051
		ADINA	0.259	0.257	1.71
		OpenSees	0.207	0.206	2.297
	Nonlinear Springs	Single Mode Pushover	0.208	0.206	1.838
		Multi-modal Pushover	0.207	0.205	1.99
Forrester Rd-I69 Bridge	Basic	SAP2000: User-defined Hinge	0.227	0.225	1.671
		SAP2000: FEMA-356 Hinge	0.228	0.226	1.654
		SAP2000: Caltrans Hinge	0.22	0.217	1.733
		ADINA	0.253	0.25	1.48
		OpenSees	0.21	0.208	1.805
	Nonlinear Springs	Single Mode Pushover	0.221	0.218	1.488

## 6 DISCUSSIONS AND CONCLUSIONS

### 6.1 Discussions

*Methods of Performing Displacement-based Seismic Analysis:* Three methods for performing displacement-based seismic analysis were studied in this research: the AASHTO Guide Specifications for the LRFD Seismic Bridge Design method, FEMA-440 Procedure C, and the Capacity-demand-diagram method. The AASHTO Specifications method is the common procedure in bridge design practice and, like almost all code procedures, was expected to show the most conservative results. FEMA-440 Procedure C is the most comprehensive equivalent linearization method in earthquake engineering and is mostly being utilized for building structures. The capacity-demand-diagram method follows the more realistic concept of inelastic demand diagrams and has been primarily used within research studies.

*Influence of Support Conditions:* The dynamic behavior of a bridge could be influenced by the support conditions. Two different support conditions were examined in this research: the Basic Support Configuration based on the common code suggestions for using fixed support for pier columns and linear springs for abutments, and the Nonlinear Springs Support Configuration obtained from the analysis of the actual soil-foundation properties. For the bridges analyzed in this study, the support conditions were expected to affect the eigenvalue analysis results, while, since the seismic excitations were applied in the transverse direction only, changes in the seismic response of the bridges when using different support conditions were anticipated to be not significant.

*Consideration of Higher Mode Effects:* It is generally accepted that a sufficient number of modes have been considered when at least 90% of the mass is participating in

those modes or when the fundamental period of vibration is greater than about one second. Therefore, in this study, the higher mode effects were only considered for the Nonlinear Springs Support Model of the SR21-I69 Bridge. Even for that unique case, the fundamental transverse mode was capturing almost 79% of the total mass participation, thus a single mode analysis was also performed for better understanding of the higher mode effects.

*Nonlinear Static (Pushover) Analysis:* This study includes a detailed explanation of performing pushover analysis to generate pushover curves using different software programs. All pushover analyses performed herein were displacement controlled and were stopped when the control node's transverse displacement reaches 0.75 ft. The lateral loading pattern used to push the bridge structures was selected as the fundamental-mode-proportional. The need to consider stiffness degradation within the expected deformation range was also checked. SAP2000 has the ability to assign various types of concentrated plastic hinge along an element. For this study, two SAP2000 built-in plastic hinge properties as well as one user-defined property, based on the results of the moment-curvature analysis for the columns' section, were employed. ADINA models the material's nonlinearity through the definition of Moment Curvature Rigidity for beam-column elements. In spite of not having a specific utility for performing pushover analysis, ADINA was selected for evaluation as a popular computer program for performing static and dynamic analysis of structural systems. The most accurate nonlinear analysis could be expected to be performed by OpenSees, which can model distributed nonlinearity through defining fiber sections for nonlinear beam-column elements. The unavailability

of a graphical interface and the need for some extra script lines for performing pushover analysis might reduce the popularity of OpenSees among practicing engineers.

*Capacity Curves:* The pushover curves in the base shear vs. control node's displacement format (MDOF domain) were converted to the spectral acceleration vs. spectral displacement format (SDOF domain) using the common conversion factors in all capacity analysis procedures. These conversion factors are obtained based on the fundamental mode shape properties. The actual capacity curves were then replaced by their idealized bilinear diagrams in order to determine the yielding point. Regarding the current literature, various available methods for constructing the bilinear capacity diagram have shown very slight differences in the displacement-based analysis results.

*Demand Curves:* In this research, the generation of seismic demand curves was initiated from the 5% damped design response spectrum. In the case of following FEMA-440 Procedure C, like other capacity spectrum methods, the demand is represented by the elastic response spectra for a range of various equivalent damping ratios. For the use of the capacity-demand-diagram method, like other constant ductility procedures, the demand is represented by the inelastic response spectra for a range of ductility levels.

*Software Evaluation:* Based on a complete evaluation of the selected software programs and experience in utilizing the computer programs for the displacement-based analysis, Table 7 shows the qualitative evaluation of the software programs.

Table 7  
*Qualitative Evaluation of Selected Software Programs*

Feature	SAP2000	ADINA	OpenSees
Pushover Analysis Utility	*		
Graphical Input	*	*	
Graphical Output	*	*	
Different Foundation Conditions Modeling	*	*	*
Concentrated Plasticity	*		
Distributed Plasticity		*	*
P-delta Effects in Pushover Analysis	*	*	*

## 6.2 Conclusions

- Based on this study, it can be concluded that the current AASHTO Specifications displacement-based seismic design method is more conservative than the other two evaluated methods proposed by Chopra and Goel (1999) and FEMA-440 (2005) in terms of the seismic displacement demand (maximum displacement). The AASHTO Specifications procedure also overestimates the displacement ductility of the system. Figure 38 compares the seismic response of both case studies obtained from different displacement-based analysis methods. It should be noted

that since the AASHTO Specifications procedure has been applied to the bridge models with the Basic Support configuration and the concentrated user-defined plastic hinges, its results were only compared to the similar cases in the other two displacement-based procedures.

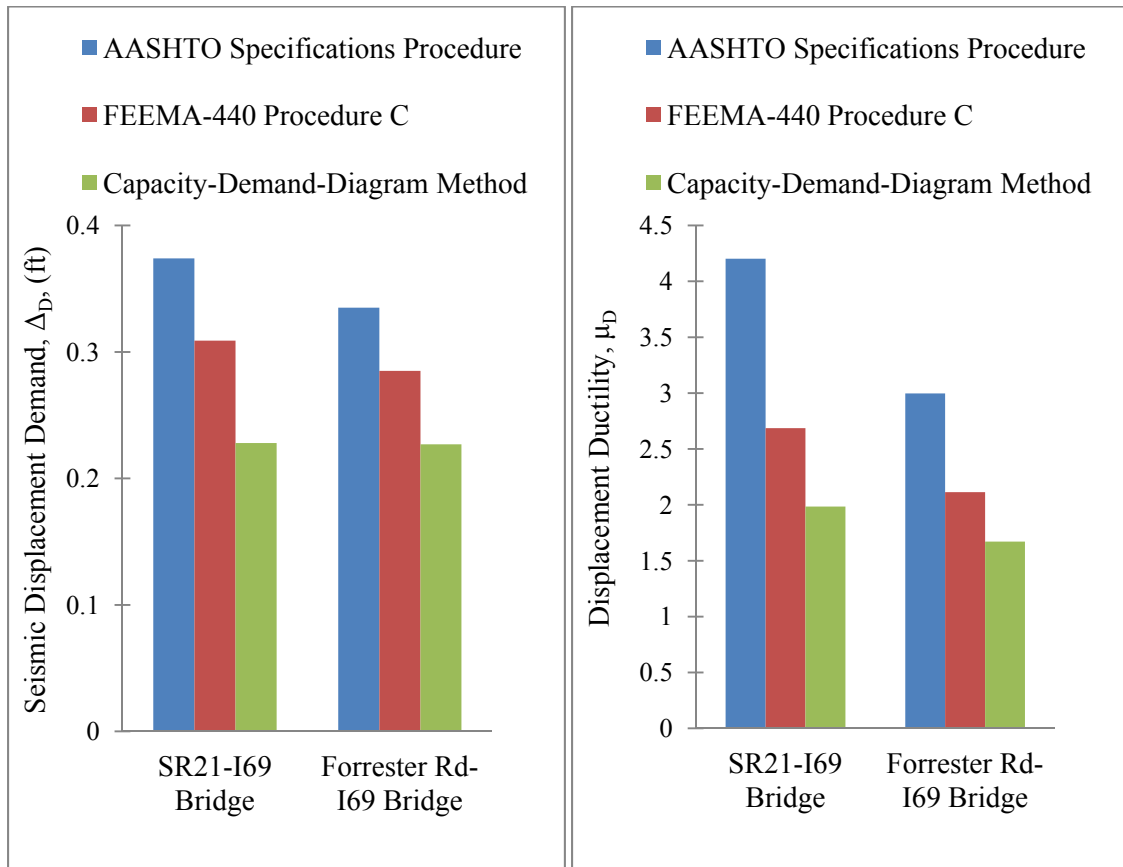
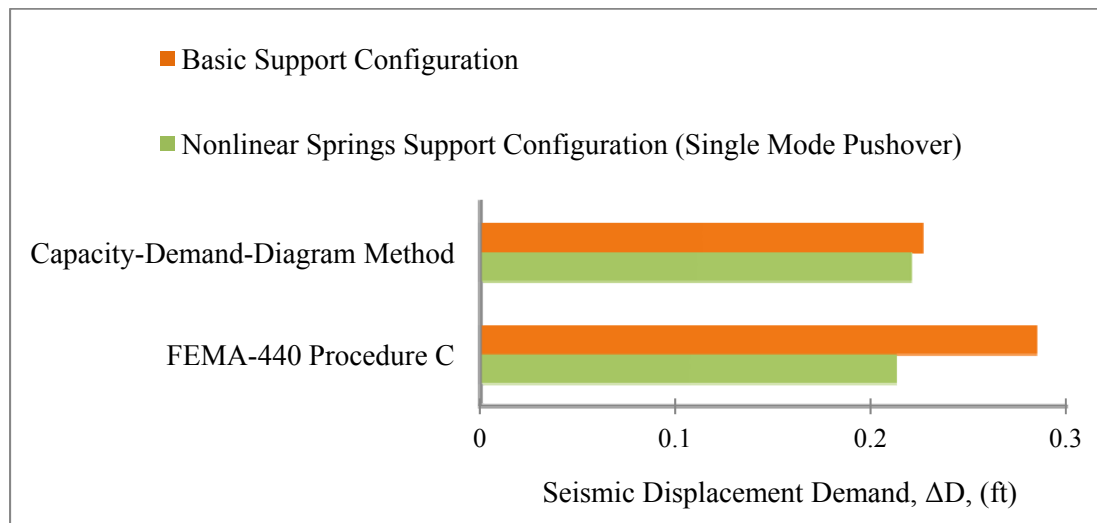


Figure 38. Seismic Response of the Bridges with the Basic Support Configuration and the User-Defined Hinge Property Using Different Displacement-based Methods.

- Generally, as shown on Figures 39 to 42, using the Basic Support configuration results in more conservative values for the seismic response of both bridges when compared to the same variable obtained from the Nonlinear Springs Support models. Although the Nonlinear Spring Support configuration more precisely

represents the actual condition of the system, using the Basic Support configuration does not make significant changes in seismic response values (especially when using the Capacity-demand-diagram method) and could be considered as a relatively accurate way to model the bridge, while needing much lower effort. In addition, using the multi-modal pushover procedure makes slight changes in the seismic design results of the SR21-I69 Bridge with the Nonlinear Springs Support configuration when compared with the results of single mode pushover procedure (Figures 41 and 42).



*Figure 39.* Seismic Displacement Demand of the Forrester Rd-I69 Bridge with Different Support Models and Various Analysis Methods.



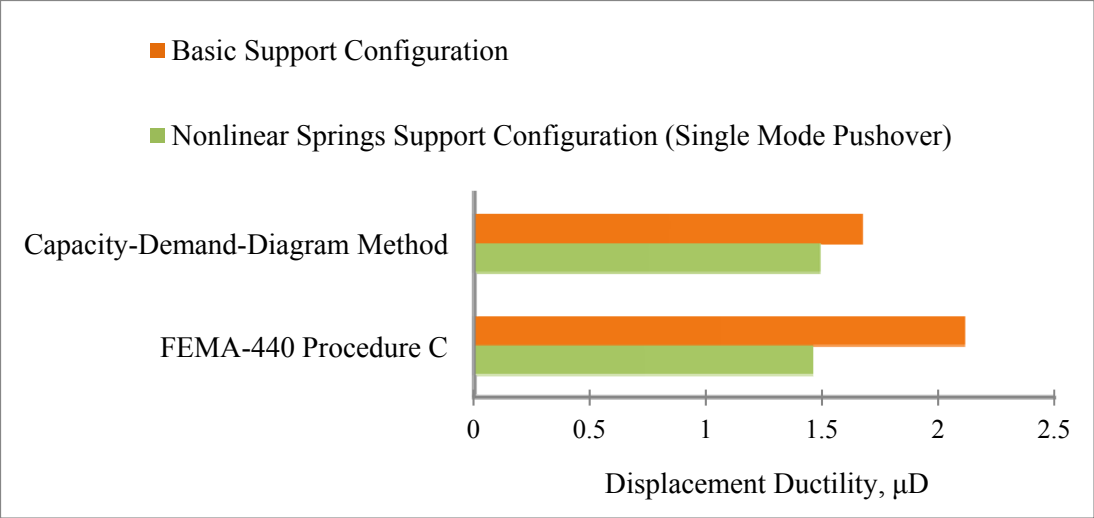


Figure 40. Displacement Ductility of the Forrester Rd-I69 Bridge with Different Support Models and Various Analysis Methods.

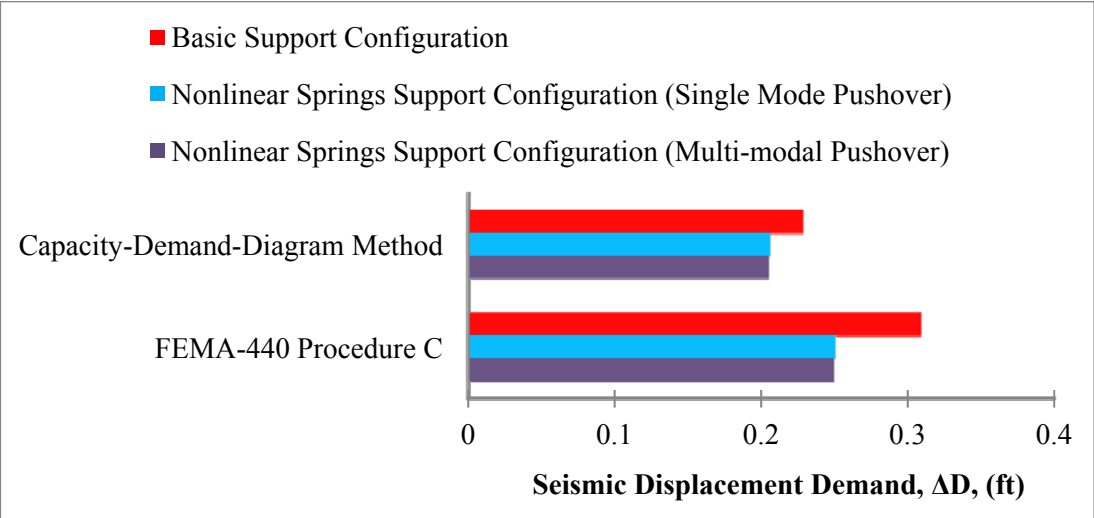


Figure 41. Seismic Displacement Demand of the SR21-I69 Bridge with Different Support Models and Various Analysis Methods.

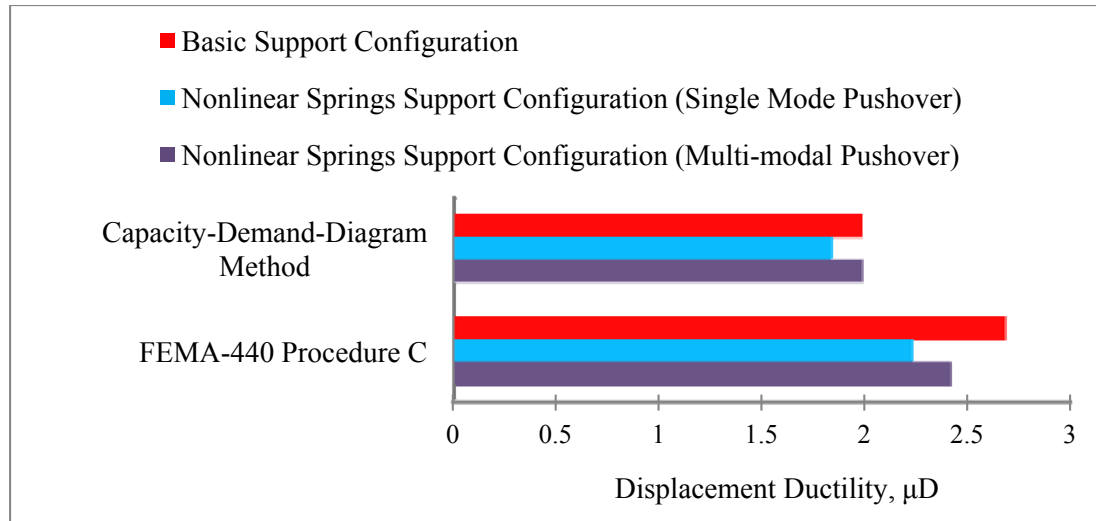


Figure 42. Displacement Ductility of the SR21-I69 Bridge with Different Support Models and Various Analysis Methods.

- Analyzing both the SR21-I69 and Forrester Rd-I69 Bridges using the capacity-demand-diagram method showed lower values for both the seismic displacement demand and the displacement capacity, compared with the results of FEMA-440 Procedure C. The capacity-demand-diagram could be used as an alternative to the AASHTO Specifications procedure due to the more accurate concepts behind the procedure, in addition to its more straight-forward nature, over FEMA-440 Procedure C.
- When performing pushover analysis with the SAP2000 computer program, various options are available for the plastic hinge property. Taking the user defined hinge properties as the most accurate ones, the results of this study, presented in Figure 43, showed that using the SAP2000 built-in hinge properties results in almost the same seismic response characteristics while requiring much less model-

ing effort. Note that all presented results are achieved from the Basic Support models using the Capacity-demand-diagram method.

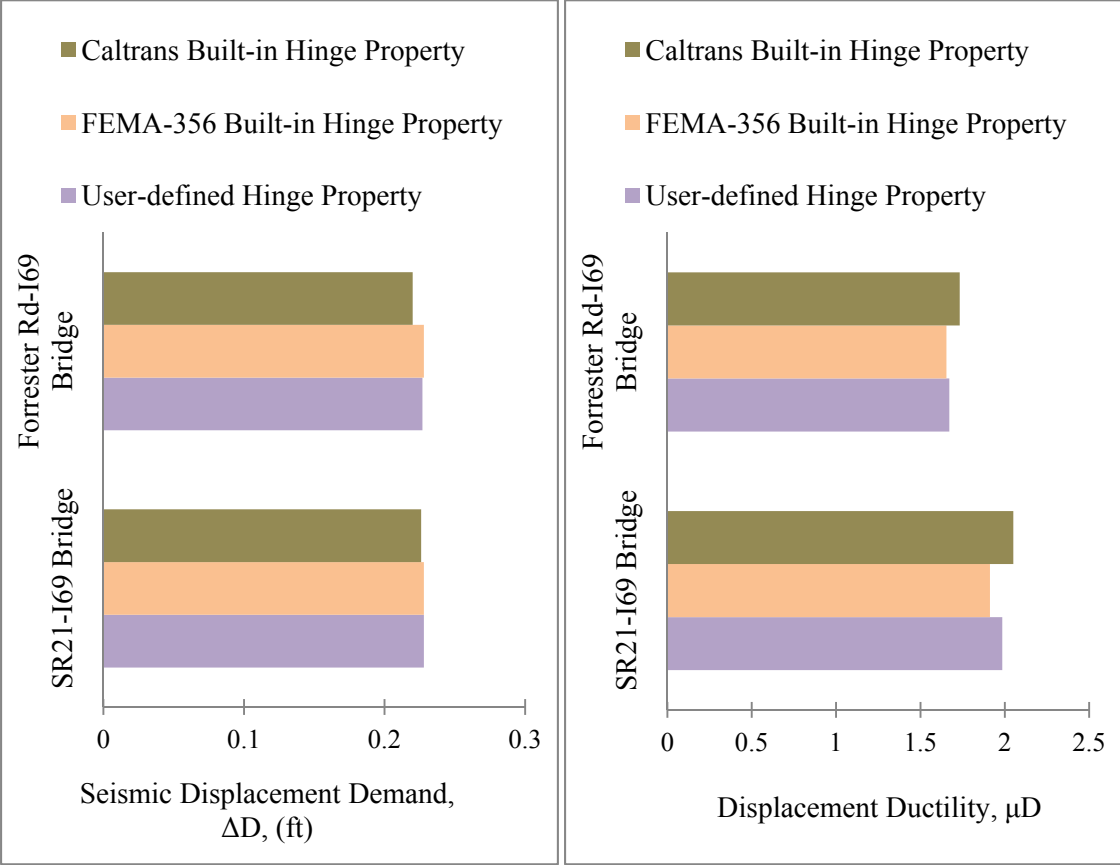


Figure 43. Seismic Response of the Bridges with the Basic Support Configuration and Different Hinge Properties Using the Capacity-Demand-Diagram Method.

- Pushover analysis can be performed using a variety of software programs. Figure 44 shows the seismic displacement demand and the displacement ductility resulting from the seismic analysis of both case studies using the Capacity-demand-diagram method, when different computer software packages have been used to perform the pushover analysis of the Basic Support models. In this figure, the SAP2000 results are achieved by assigning the user-defined plastic hinges.

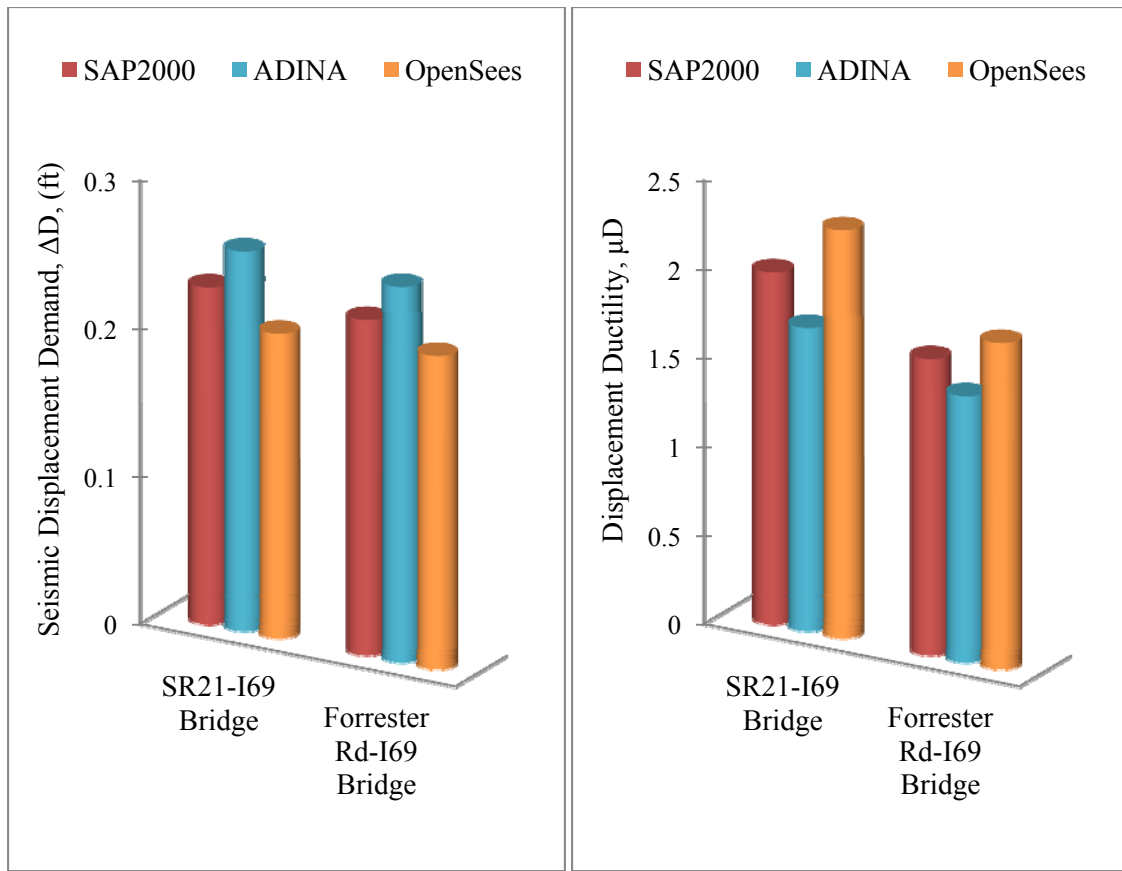


Figure 44. Seismic Response of the Bridges with the Basic Support Configuration Using Different Computer Programs.

- The OpenSees program provides the most accurate option to model the nonlinearity for the bridge structures among the three selected computer programs. Consequently, the OpenSees results could be considered as the most accurate ones when compared to the results of SAP2000 and ADINA. Figure 44 indicates that SAP2000 produces closer results to those obtained from OpenSees. Additionally, SAP2000 is the only computer program that is particularly well-suited to perform pushover analysis. Furthermore, SAP2000 is largely graphical in nature, allowing for straightforward data input and interpretation of results. Thus, SAP2000 is re-

garded as the most efficient software program to be used in practical displacement-based seismic analysis.

## REFERENCES

- Abeysinghe, R. S., Gavaice, E., Rosignoli, M., & Tzaveas, T. (2002). Pushover analysis of inelastic seismic behavior of Greveniotikos Bridge. *ASCE Journal of Bridge Engineering*, 7(2), 115-126.
- ADINA (Version 8.6.4). (2010). ADINA R & D Inc., Watertown, MA.
- Akkar, S. D., & Miranda, E. (2005). Statistical evaluation of approximate methods for estimating maximum deformation demands on existing structures. *ASCE Journal of Structural Engineering*, 131(1), 160-72.
- Albanesi, T., Biondi, S., & Petrangeli, M. (2002). Pushover analysis: An energy-based approach. *Proc. of the Twelfth European Conference on Earthquake Engineering*, London, UK, Paper No. 605.
- American Association of State Highway and Transportation Officials. (2009). *AASHTO Guide Specifications for LRFD Seismic Bridge Design* (1<sup>st</sup> Ed.). Washington, DC: AASHTO Highways Subcommittee on Bridges and Structures.
- Antoniou, S., & Pinho, R. (2009). Displacement-based adaptive pushover. *Proc. of the ECCOMAS Thematic Conference on Computational Methods in Structural Dynamics and Earthquake Engineering COMPDYN 2009*, Rhodes, Greece, 22-24 June.
- Antoniou, S., & Pinho, R. (2004a). Advantages and limitations of adaptive and non-adaptive force-based pushover procedures. *Journal of Earthquake Engineering*, 8(4), 497-522.

- Antoniou, S., & Pinho, R. (2004b). Development and verification of a displacement-based adaptive pushover procedure. *Journal of Earthquake Engineering*, 8 (5), 643-661.
- Applied Technology Council. (1997). *Seismic design criteria for bridges and other highway structures: Current and future (ATC-18)*. Redwood City, CA.
- Applied Technology Council. (1996). *Seismic evaluation and retrofit of concrete buildings (ATC-40)*. Redwood City, CA.
- Aydinoglu, M. N. (2003). An incremental response spectrum analysis procedure based on inelastic spectral deformation for multi-mode seismic performance evaluation. *Bulletin of Earthquake Engineering*, 1, 3-36.
- Bertero, V. V. (1995). Tri-service manual method. *Vision 2000*, Part 2, Appendix J, Structural Engineers Association of California, Sacramento, CA.
- Bracci, J. M., Kunnath, S. K., & Reinhorn, A. M. (1997). Seismic performance and retrofit evaluation of reinforced concrete structures. *ASCE Journal of Structural Engineering*, 123 (1), 3-10.
- California Department of transportation, Caltran. (2010). *Seismic Design Criteria: Version 1.6*. Sacramento, CA (Available online at <http://www.dot.ca.gov>).
- California Department of transportation, Caltran. (2004). *Caltrans bridge Design Specifications*. Sacramento, CA: Caltrans.
- Calvi, G. M., & Kingsley, G. R. (1995). Displacement-based seismic design of multi-degree-of-freedom bridge structures. *Earthquake Engineering and Structural Dynamics*, 24, 1247-1266.

- Chandler, A. M., & Mendis, P. A. (2000). Performance of reinforced concrete frames using force and displacement based seismic assessment methods. *Engineering Structures*, 22, 352-363.
- Chopra, A. K. (2007). *Dynamics of structures: Theory and applications to earthquake engineering*, 3<sup>rd</sup> Ed. Englewood Cliffs, NJ: Prentice-Hall.
- Chopra, A. K., & Goel, R. K. (1999). Capacity-demand-diagram methods based on inelastic design spectra. *Earthquake Spectra*, 15(4), 637-656.
- Chopra, A. K., & Goel, R. K. (2000). Evaluation of NSP to estimate seismic deformation: SDF systems. *ASCE Journal of Structural Engineering*, 126(4), 482-490.
- Chopra, A. K., & Goel, R. K. (2001). Direct displacement-based design: Use of inelastic vs. elastic design spectra. *Earthquake Spectra*, 17(1), 47-64.
- Chopra, A. K., & Goel, R. K. (2002). A modal pushover analysis procedure for estimating seismic demands for buildings. *Earthquake Engineering and Structural Dynamics*, 31, 561-582.
- Elnashai, A. S. (2001). Advanced inelastic static (pushover) analysis for earthquake applications. *Structural Engineering and Mechanics*, 12 (1), 51-69.
- Fajfar, P. (1999). Capacity spectrum method based on inelastic demand spectra. *Earthquake Engineering and Structural Dynamics*, 28, 979-993.
- Federal Emergency Management Agency. (2005). *Improvement of nonlinear static seismic analysis procedures (FEMA-440)*. Washington, DC.
- Federal Emergency Management Agency. (2000). *Prestandard and commentary for the seismic rehabilitation of buildings (FEMA-356)*. Washington, DC.



- Freeman, S. A., Nicoletti, J. P., & Tyrell, J. V. (1975). Evaluation of existing buildings for seismic risk: A case study of Puget Sound naval shipyard, Bremerton, Washington. *First National Conference on Earthquake Engineering*, Berkeley, CA: EERI.
- Gencturk, B., & Elnashai, A. S. (2008). Development and application of an advanced capacity spectrum method. *Engineering Structures*, 30 (11), 3345-3354.
- Gupta, B., & Kunnath, S. K. (2000). Adaptive spectra-based procedure for seismic evaluation of structures. *Earthquake Spectra*, 16 (2), 367-391.
- Hernandez-Montes, E., Kwon, O., & Aschheim, M. (2004). An energy-based formulation for first and multiple-mode nonlinear static (pushover) analysis. *Journal of Earthquake Engineering*, 8 (1), 69-88.
- Kim, H., Min, K. W., Chung, L., Park, M., & Lee, S. H. (2005). Evaluation of capacity spectrum method for estimating the peak inelastic responses. *Journal of Earthquake Engineering*, 9 (5), 695-718.
- Kim, S., & D'Amore, E. (1999). Pushover analysis procedure in earthquake engineering. *Earthquake Spectra*, 15 (3), 417-434.
- Kowalsky, M. J., Priestley, M. J. N., & Macrae, G. A. (1995). Displacement-based design of RC bridge columns in seismic regions. *Earthquake Engineering and Structural Dynamics*, 24, 1623-1643.
- Kowalsky, M. J., & Priestley, M. J. N. (1995). Displacement-based methodology for design and assessment of reinforced concrete bridges. *The Earthquake Engineering Online Archive (Nisee e-library)*. Retrieved from <http://nisee.berkeley.edu/elibrary/Text/200803275>.

- Krawinkler, H. (1995). New trends in seismic design methodology. *Proc. of Tenth European Conference on Earthquake Engineering, Vol. 2*, Vienna, Balkema, Rotterdam.
- Krawinkler, H., & Seneviratna, G. D. P. K. (1998). Pros and cons of a pushover analysis of seismic performance evaluation. *Engineering Structures*, 20 (4-6), 452-464.
- Krawinkler, H., & Nassar, A. A. (1992). Seismic design based on ductility and cumulative damage demands and capacities. *Nonlinear Seismic Analysis and Design of Reinforced Concrete Building*, New York, NY: Elsevier Applied Science.
- Kunnath, S. K. (2004). Identification of modal combination for nonlinear static analysis of building structures. *Computer-Aided Civil and Infrastructure Engineering*, 19, 246-259.
- Leyendecker, E. V., Frankel, A. D., & Rukstales, K. S. (2009). AASHTO GM (Version 2.1) [Software]. Washington, DC: AASHTO.
- Lin, Y. Y., & Chang, K. C. (2003). An improved capacity spectrum method for ATC-40. *Earthquake Engineering and Structural Dynamics*, 32, 2013-2025.
- Lin, Y. Y., Chang, K. C. & Wang, Y. L. (2004). Comparison of displacement coefficient method and capacity spectrum method with experimental results of RC columns. *Earthquake Engineering and Structural Dynamics*, 33, 35-48.
- Lin, Y. Y., & Miranda, E. (2004). Non-iterative capacity spectrum method based on equivalent linearization for estimating inelastic deformation demands of buildings. *Structural Engineering/ Earthquake Engineering*, 21 (2), 113-119.
- Mander, J. B., Priestley, M. J. N., & Park, R. (1988). Theoretical stress-strain model for confined concrete. *ASCE Journal of Structural Engineering*, 114 (8), 1804-1826.

- Matthews, Robert. (2005). CONSEC (Version 1.4) [Software]. Orange, CA.
- Moghadam, A. H., & Tso, W. K. (2002). A pushover procedure for tall buildings. *Proc. of the Twelfth European Conference on Earthquake Engineering*, London, UK, Paper No. 395.
- Newmark, N. M., & Hall, W. J. (1982). *Earthquake Spectra and Design*. Berkeley, CA: Earthquake Engineering Research Institute.
- OpenSees - Open System for Earthquake Engineering Simulation (Version 2.3.2). (2011). University of California Berkeley, Pacific Earthquake Engineering Center. (Available online at <http://OpenSees.berkeley.edu>)
- Paret, T. F., Sasaki, K. K., Eilbeck, D. H., & Freeman, S. A. (1996). Approximate inelastic procedures to identify failure mechanisms from higher modes effect. *Proc. of the Eleventh World Conference on Earthquake Engineering*, Acapulco, Mexico, Paper No. 966.
- Pinho, R., Antoniou, S., Casarotti, C., & Lopez, M. (2005). A displacement-based adaptive pushover for assessment of buildings and bridges. *NATO International Workshop on Advances in Earthquake Engineering for Urban Risk Reduction*, Istanbul, Turkey, 30<sup>th</sup> May-1<sup>st</sup> June.
- Rahnama M, & Krawinkler H. (1993). Effects of soft soil and hysteresis model on seismic demands. *JABEEC Report no. 108*, Stanford, (CA): The John A. Blume Earthquake Engineering Center, Stanford University.
- Reinhorn, A. M. (1997). Inelastic analysis techniques in seismic evaluations. *Seismic Design Methodologies for the Next Generation of codes*, Balkema, Rotterdam, 277-287.

- Requena, M., & Ayala, G. (2000). Evaluation of a simplified method for the determination of the nonlinear seismic response of RC frames. *Proc. of the twelfth Conference on Earthquake Engineering*, Auckland, New Zealand, Paper No. 2109.
- Sasaki, K. K., Freeman, S. A., & Paret, T. F. (1998). Multi-modal pushover procedure (MMP) – A method to identify the effects of higher modes in a pushover analysis. *Proc. of the Sixth US National Conference on Earthquake Engineering*, EERI, Oakland, CA.
- SAP2000 (Version 15.1). (2011). Computers and Structures, Berkeley, CA: CSI.
- Shattarat, N. K., Syman, M. D., McLean, D. I., & Cofer, W. F. (2008). Evaluation of nonlinear static analysis methods and software tools for seismic analysis of highway bridges. *Engineering Structures*, 30, 1335-1345.
- Symans, M. D., Shattarat, N. K., McLean, D. I., & Cofer, W. F. (2003). Evaluation of displacement-based methods and computer software for seismic analysis of highway bridges. Washington State Department of Transportation, Research report WA-RD 553.1, Pullman, WA.
- Vamvatsikos, D., & Cornell, C. A. (2002). Incremental dynamic analysis. *Earthquake Engineering and Structural Dynamics*, 31 (3), 491-514.
- Vasheghani-Farahani, R., Zhao, Q. & Burdette, E. G. (2010). Seismic Analysis of Integral Abutment Bridge in Tennessee, Including Soil-Structure interaction. *Transportation Research record*, 2201 (2), 70-79.
- Vidic, T., Fajfar, P., & Fischinger, M. (1994). Consistent inelastic design spectra: strength and displacement. *Earthquake Engineering and Structural Dynamics*, 23 (5), 502-521.

Yu, Y., Symans, M. D., McLean, D. I., and Cofer, W. f. (1999). Evaluation of analysis methods for assessing seismic response. *Transportation Research Record*, 1688, 163-172

## Appendix A

Appendix A presents a step-by-step modeling and analysis process of the SR21-I69 Bridge in SAP2000. As discussed in Chapter 3, the material, section, and loading properties of the computer model were adopted from TDOT's design documents. Figure 45 shows the general 3D view of the SAP2000 model for the Basic support model.

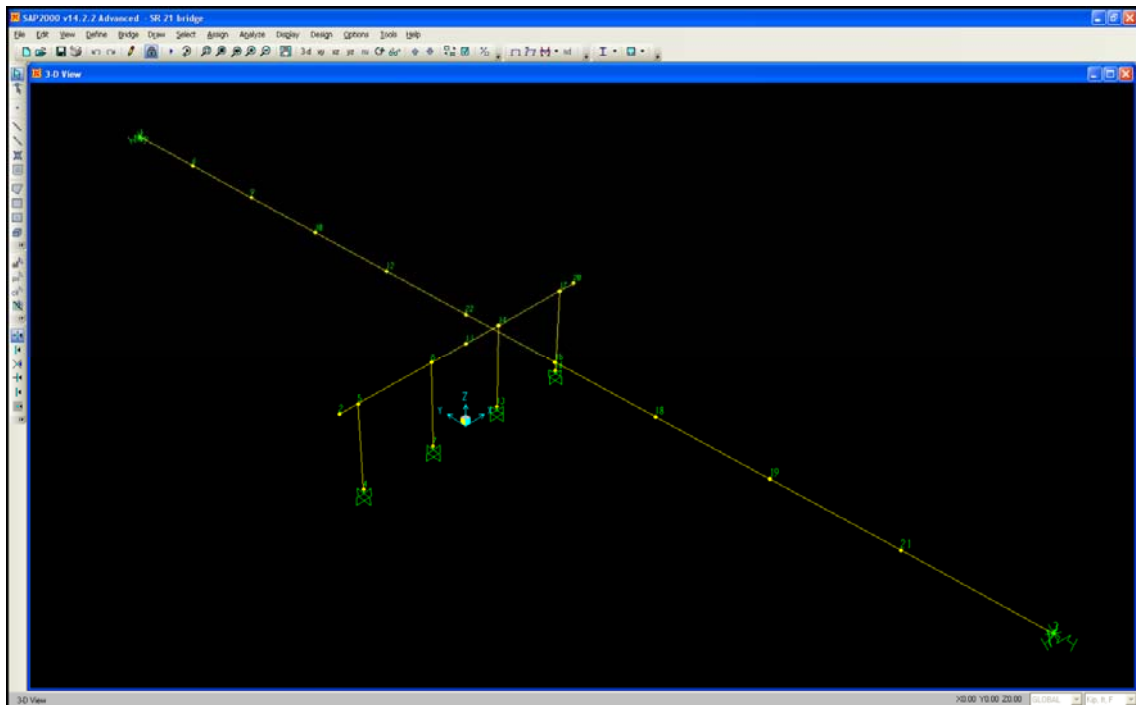


*Figure 45.* General 3D View of the Computer Model of the SR21-I69 Bridge with Basic Support Configuration in SAP2000.

In the case of using Basic support configuration, a *Joint Spring* was used to model the linear spring at each abutment. Figure 46 displays the Joint Spring element properties used to model the Basic support configuration.

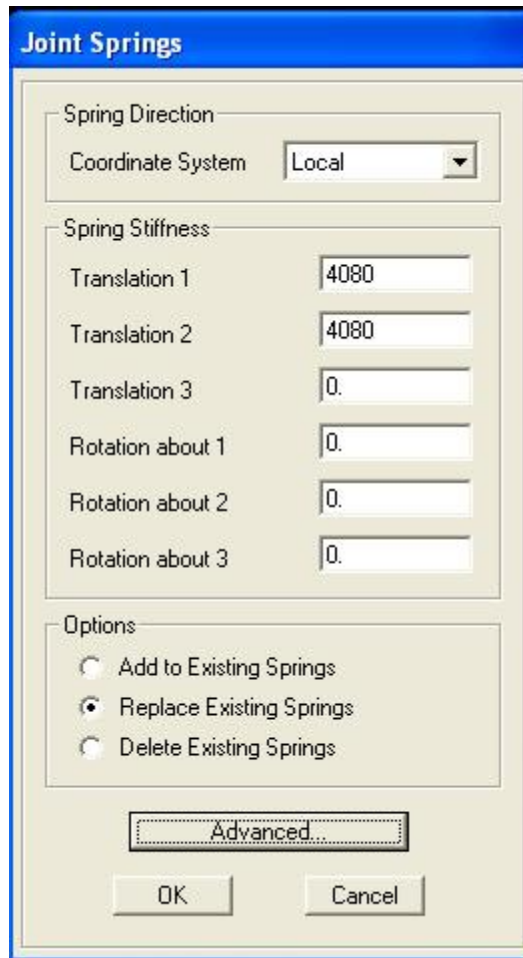


Figure 46. Joint Spring Element Properties Used for Modeling the Linear Springs at Abutments in the Basic Support Configuration.

When modeling the Nonlinear Springs support configuration, *MultiLinear Elastic Link/Support* elements were used at abutments and column footings. As shown in Figure 47, these elements were defined in longitudinal and transverse directions only. SAP2000 assumes the links as fixed in any undefined direction. Using the *Modify/Show* button, the force-deformation behavior of the links can be defined at each direction (see Figure 48). In order to perform modal analysis, an effective stiffness value should be also defined for

the link elements. This value was calculated as the slope of the first segment of the force-deformation curve at each direction.

**Link/Support Property Data**

Link/Support Type: MultiLinear Elastic

Property Name: exterior

Property Notes:

Total Mass and Weight

Mass: 0.0

Weight: 0.0

Rotational Inertia 1: 0.0

Rotational Inertia 2: 0.0

Rotational Inertia 3: 0.0

Factors For Line, Area and Solid Springs

Property is Defined for This Length In a Line Spring: 1.0

Property is Defined for This Area In Area and Solid Springs: 1.0

Directional Properties

Direction	Fixed	NonLinear	Properties
<input type="checkbox"/> U1	<input type="checkbox"/>	<input type="checkbox"/>	Modify/Show for U1...
<input checked="" type="checkbox"/> U2	<input type="checkbox"/>	<input checked="" type="checkbox"/>	Modify/Show for U2...
<input checked="" type="checkbox"/> U3	<input type="checkbox"/>	<input checked="" type="checkbox"/>	Modify/Show for U3...
<input type="checkbox"/> R1	<input type="checkbox"/>	<input type="checkbox"/>	Modify/Show for R1...
<input type="checkbox"/> R2	<input type="checkbox"/>	<input type="checkbox"/>	Modify/Show for R2...
<input type="checkbox"/> R3	<input type="checkbox"/>	<input type="checkbox"/>	Modify/Show for R3...

P-Delta Parameters

Advanced...

OK

Cancel

Fix All

Clear All

Figure 47. Link/Support Element Properties Used for Modeling the Nonlinear Springs in the Nonlinear Springs Support Configuration.



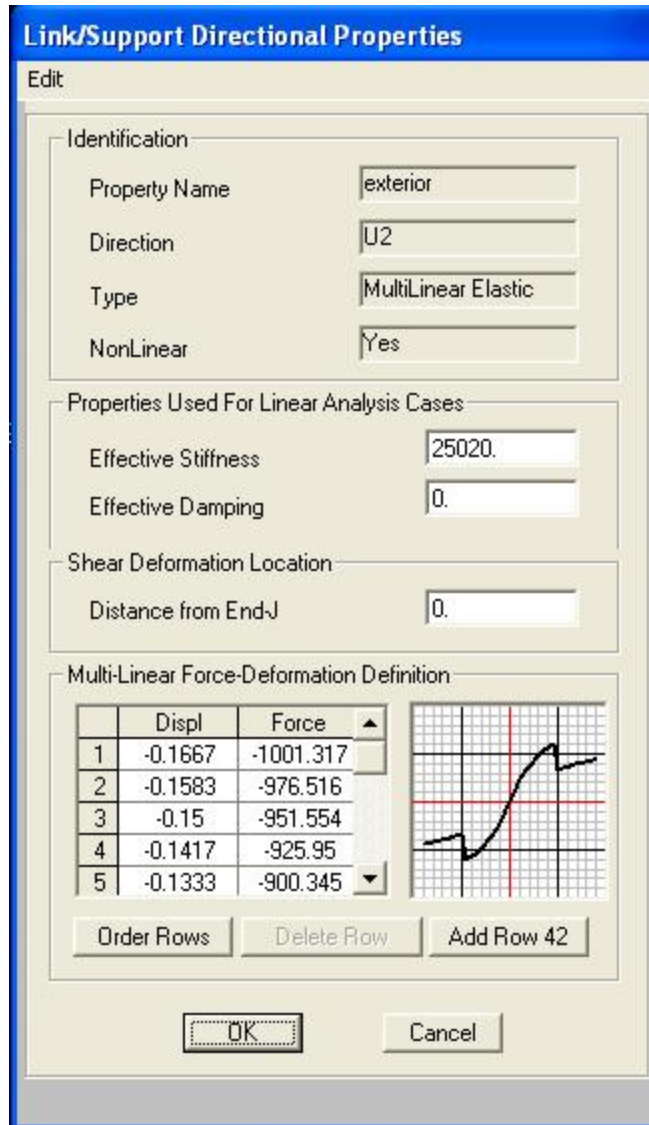


Figure 48. Directional Properties of the Link/Support Elements.

After creating the structural models for both support configurations, the modal analysis was performed for each model, and its results were used to determine the pushover analysis lateral load pattern. Furthermore, the conversion factors (see Table 2) were calculated for each case based on the modal analysis results. Figure 49 shows the mode one deformed shape of the SR21-I69 Bridge with Nonlinear Springs support model.

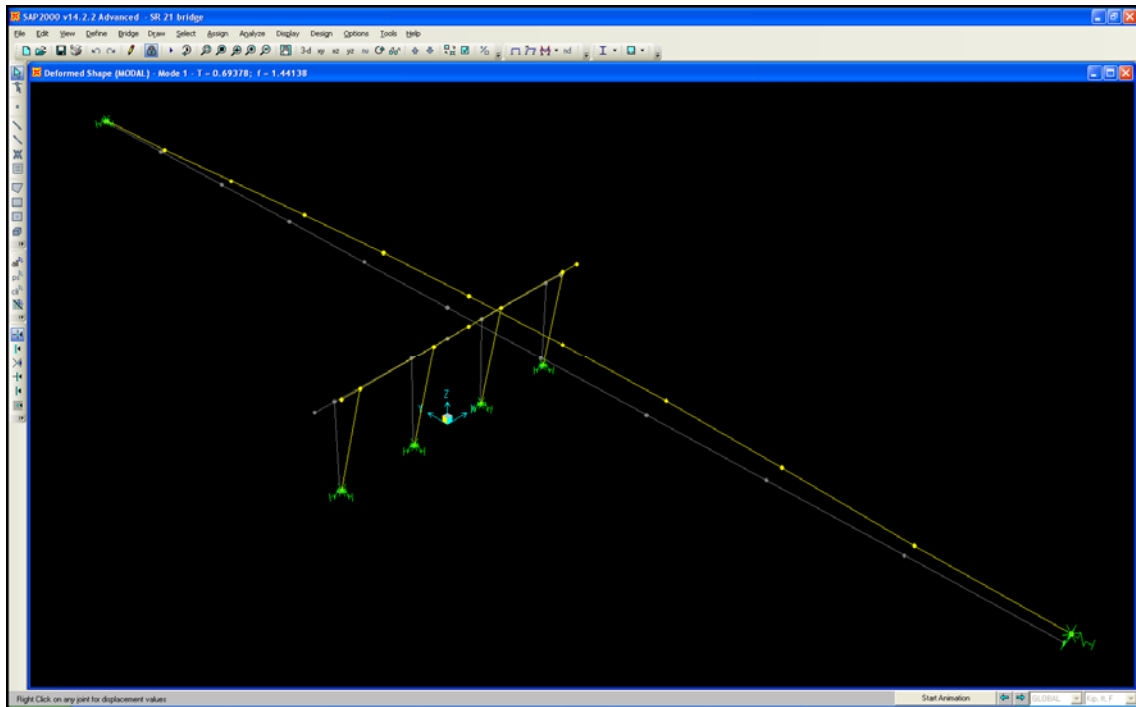


Figure 49. Mode One Deformed Shape of the Nonlinear Springs Model.

The next step was modeling the nonlinearity of the structural systems through assigning plastic hinges at the both ends of each column element. Before that, the user-defined hinge properties were created following the *Define: Section Properties: Hinge Properties* tab. By adding a new P-M2-M3 hinge properties for concrete material, the general properties of the plastic hinge were defined on the hinge property data window, as displayed in Figure 50. Using the *Modify/Show Moment curvature Curve Data* button, the moment-curvature diagrams data were assigned to their corresponding axial forces. Figure 51 shows the moment-curvature data window for  $P = 1,050$  kips.

**Frame Hinge Property Data for user 23 - Interacting P-M2-M3**

**Hinge Specification Type**

Moment - Rotation  
 Moment - Curvature  
 Hinge Length   
 Relative Length

**Scale Factor for Curvature (SF)**

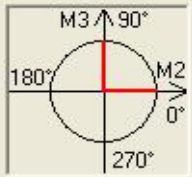
SF is Equal to Yield Curvature (Steel Objects Only)  
 User SF

**Load Carrying Capacity Beyond Point E**

Drops To Zero  Is Extrapolated

**Symmetry Condition**

Moment Curvature Dependence is Circular  
 Moment Curvature Dependence is Doubly Symmetric about M2 and M3  
 Moment Curvature Dependence has No Symmetry



**Requirements for Specified Symmetry Condition**

- Specify curves at angles of 0° and 90°.
- If desired, specify additional intermediate curves where:  $0^\circ < \text{curve angle} < 90^\circ$ .

**Axial Forces for Moment Curvature Curves**

Number of Axial Forces

**Curve Angles for Moment Curvature Curves**

Number of Angles

Figure 50. User-Defined hinge Properties Data Window.

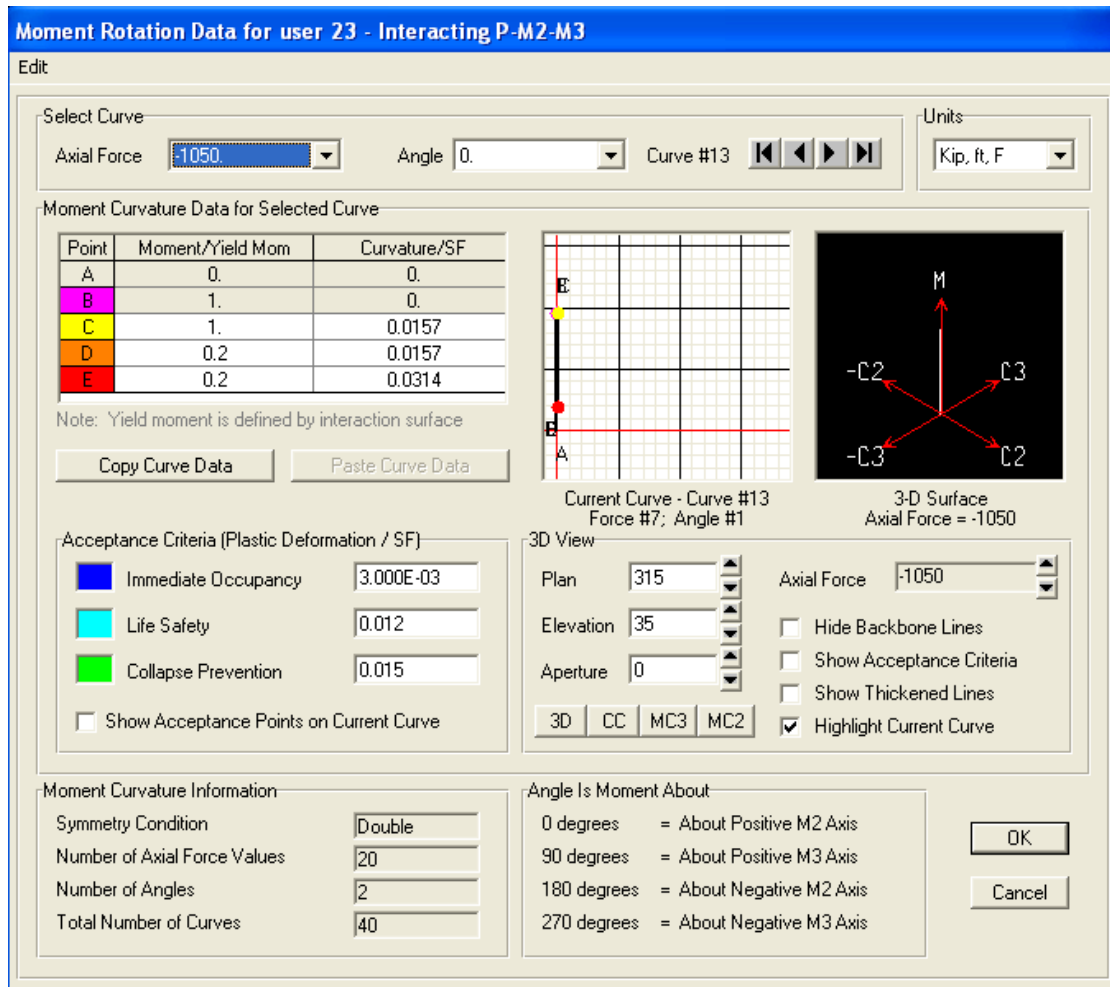
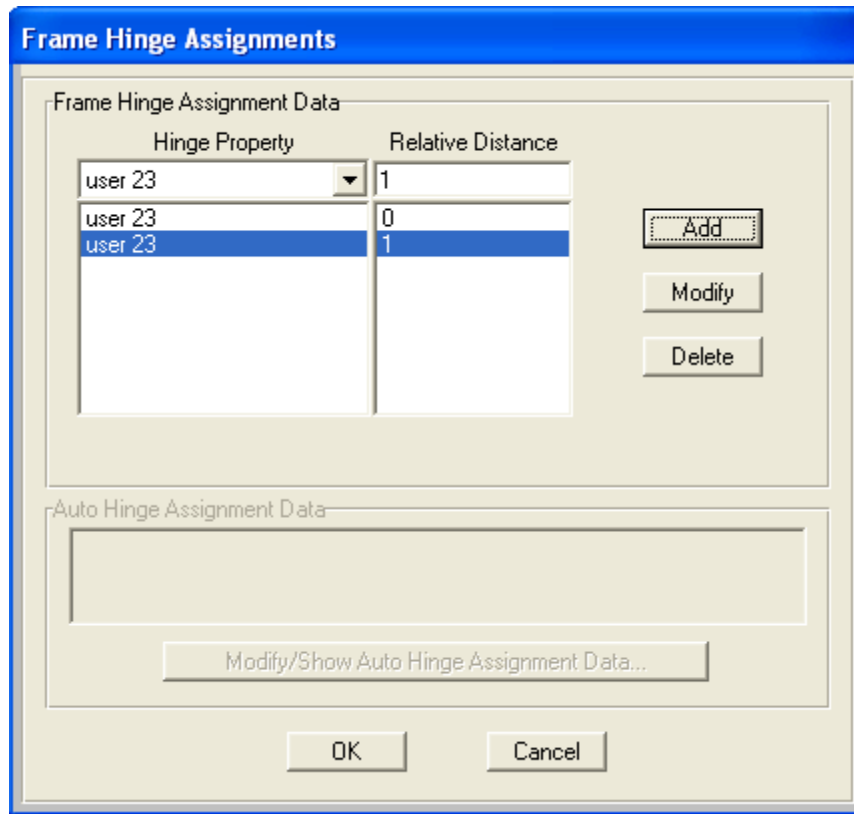


Figure 51. Moment-Curvature Curve Data Window Corresponding to P = 1,050 kips.

All column elements were then selected and user-defined plastic hinges were placed at both ends of each (relative distances 0.0 and 1.0) following the *Assign: Frame: Hinges* tab (Figure 52).



*Figure 52.* Assigning User-Defined Plastic Hinges to the Both Ends of the Columns.

In a duplicated copy of the structural model, the first auto hinge property was selected based on the FEMA-356 tables and was assigned to the both ends of all columns (see figure 53).

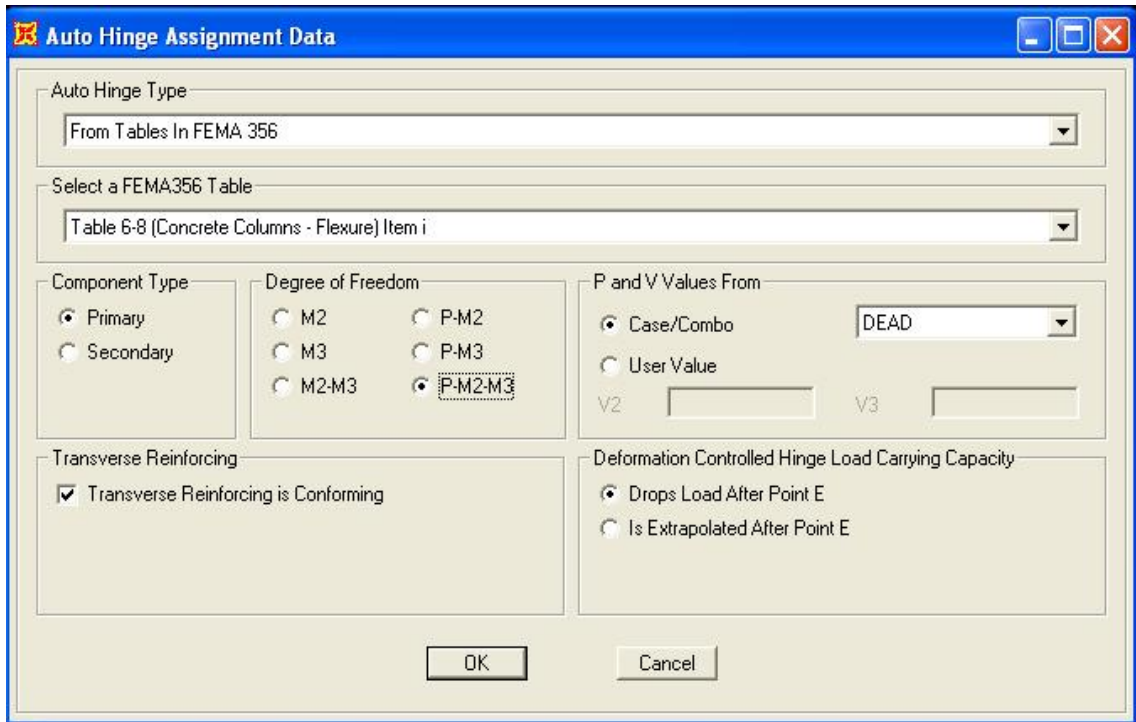


Figure 53. SAP2000 Auto Hinge Property Based on the FEMA-356 Tables.

The second auto hinge property, based on the Caltrans tables, was assigned to the column elements in another saved copy of the model (Figure 54). It should be noted that the Caltrans hinges can be only assigned to the sections defined through the SAP2000 Caltrans Section Library. Therefore, before assigning the hinges, a Caltrans section was defined following the *Define: Section Properties: Frame Sections* tab. Using the *Section Designer* button on the SD section design window, as shown in Figure 55, the Caltrans square section option was selected through the *Draw: Draw Caltrans Shapes: Draw Square* tab (see figure 56). The material properties and reinforcing details of the section were defined in the Caltrans Section Properties window (Figure 57) that can be displayed by right clicking on the square section.

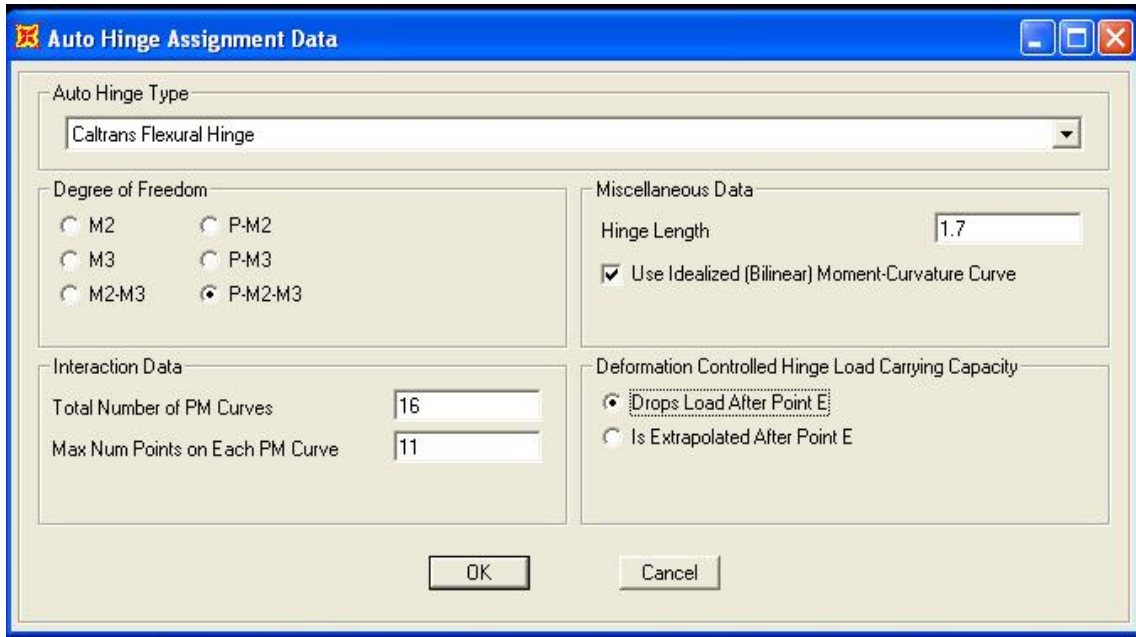


Figure 54. SAP2000 Auto hinge Property Based on the Caltrans Tables.

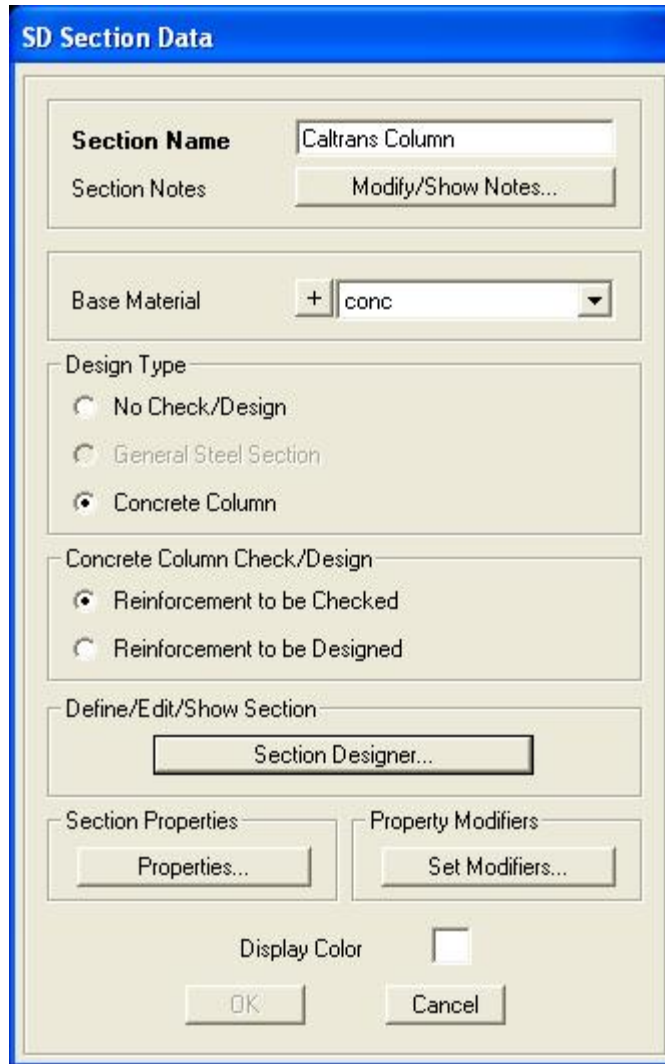


Figure 55. SD Section Data Window.



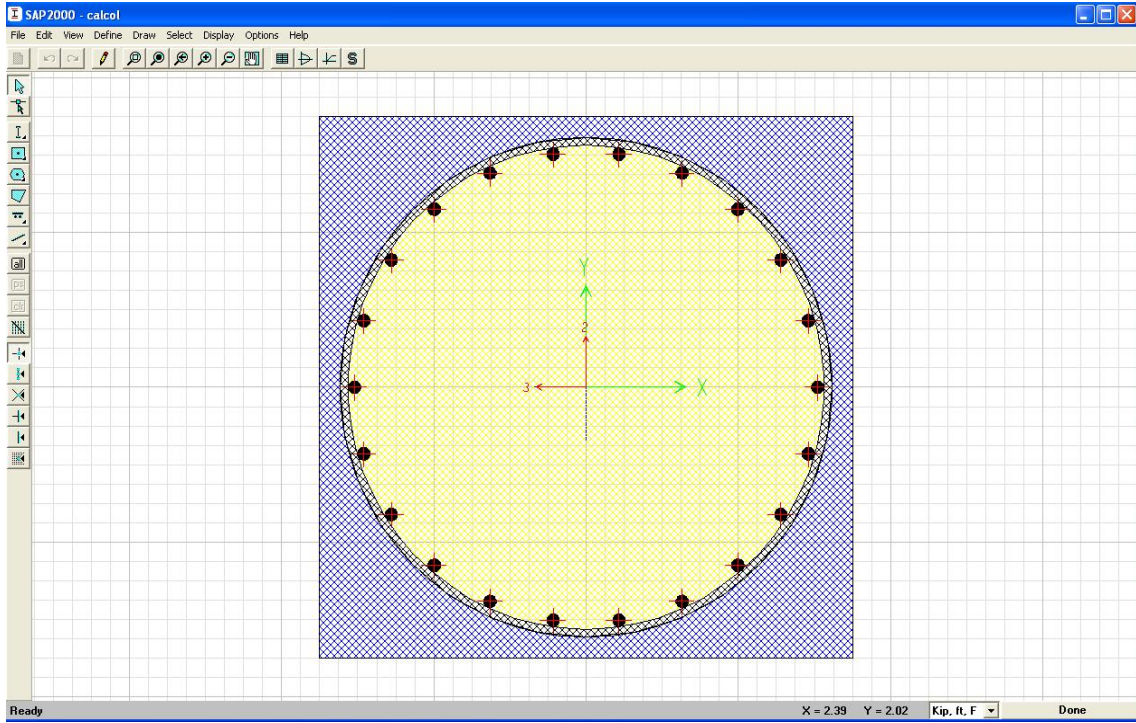


Figure 56. Caltrans Square Section.

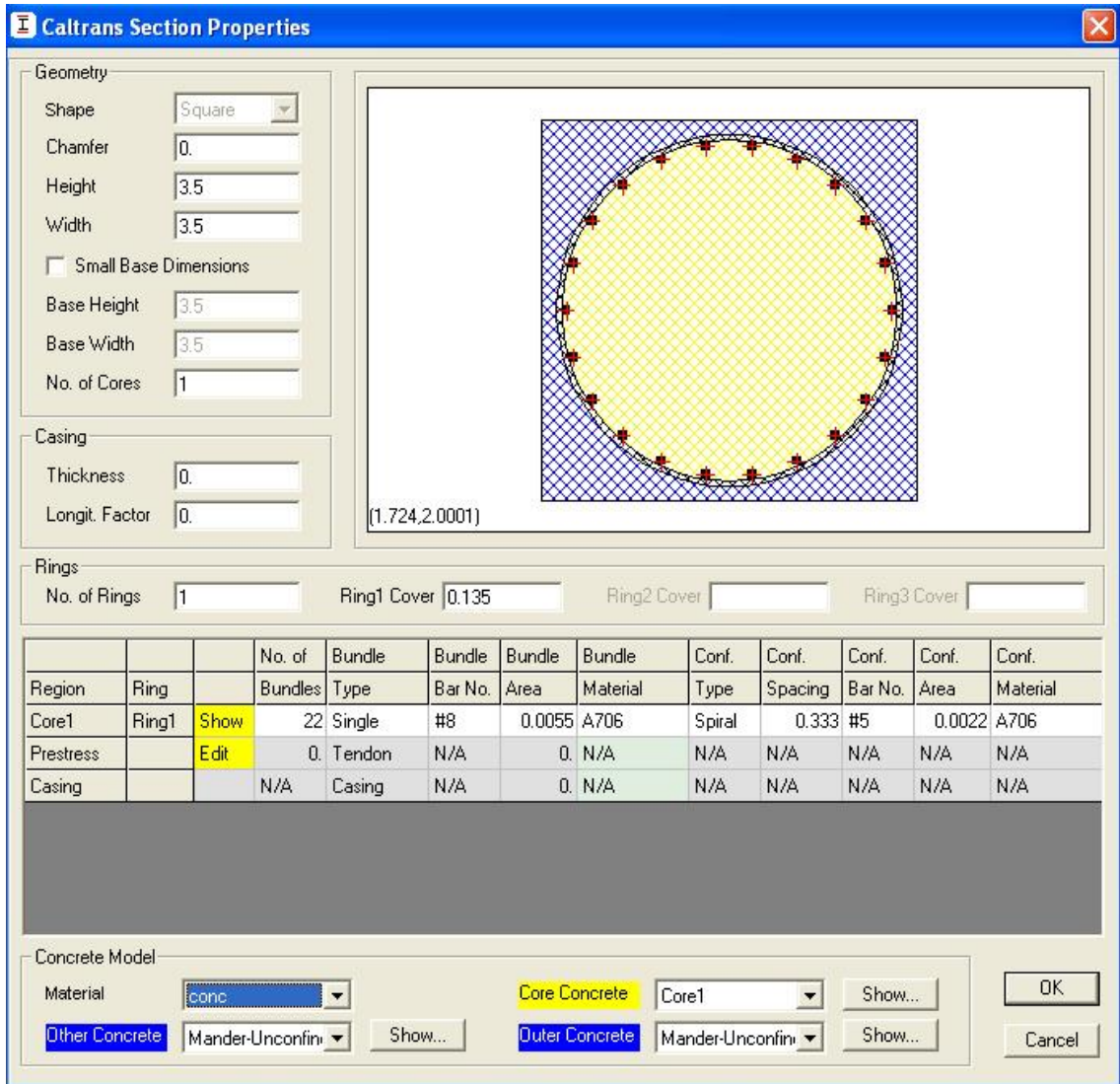


Figure 57. Caltrans Section Properties Window.

Before defining the pushover load case, the analysis type for the dead load case was changed to nonlinear (see Figure 58). This enabled the pushover load case to follow the dead load case in order to consider the gravity load effects during the pushover analysis. As shown in Figure 59, the pushover load case was defined based on the application of the mode shape proportional lateral loading, named Dummy!, to the superstructures

nodes in transverse direction. The load application was set to stop as the control node displacement reaches to 0.75 ft (Figure 60).

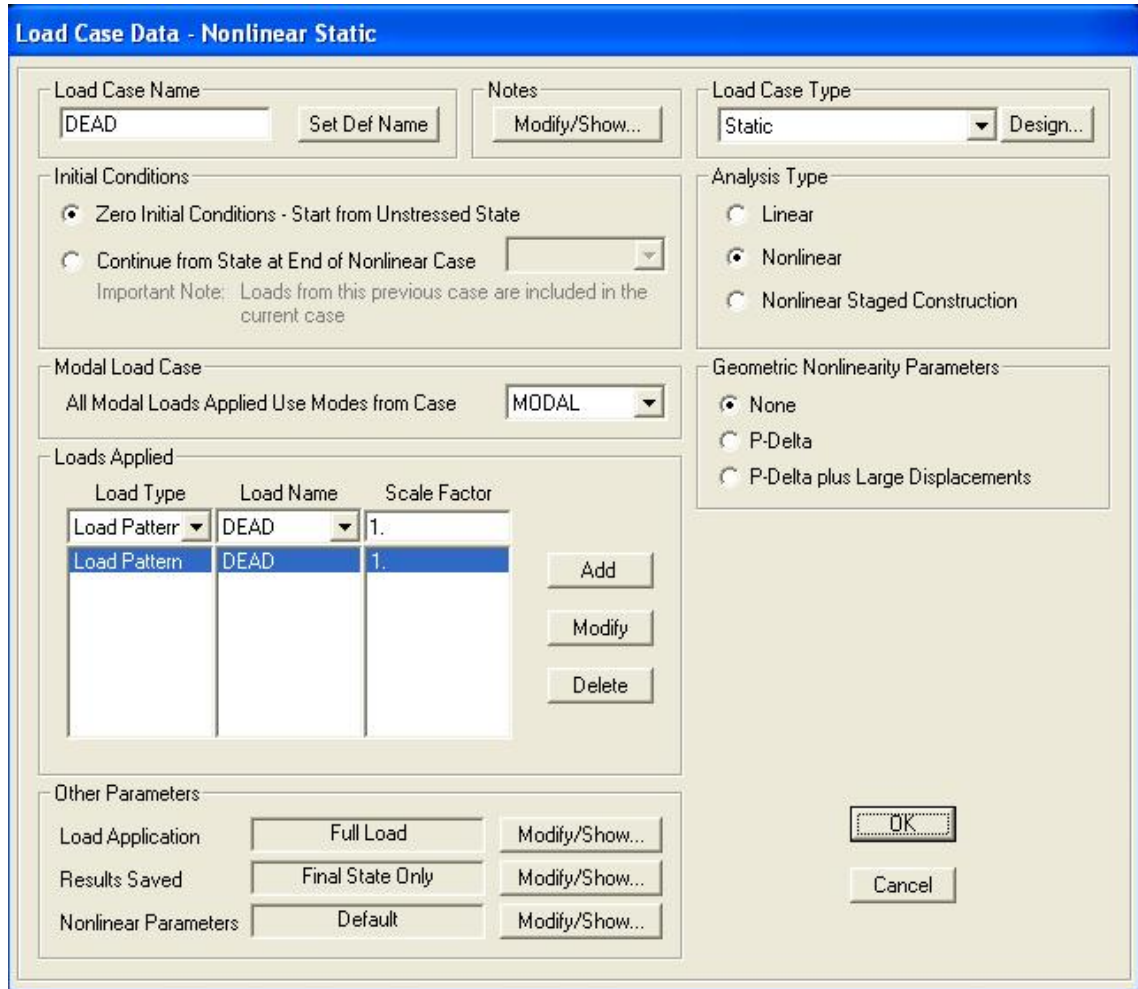


Figure 58. Changing the Analysis Type to Nonlinear for the Dead Load Case.

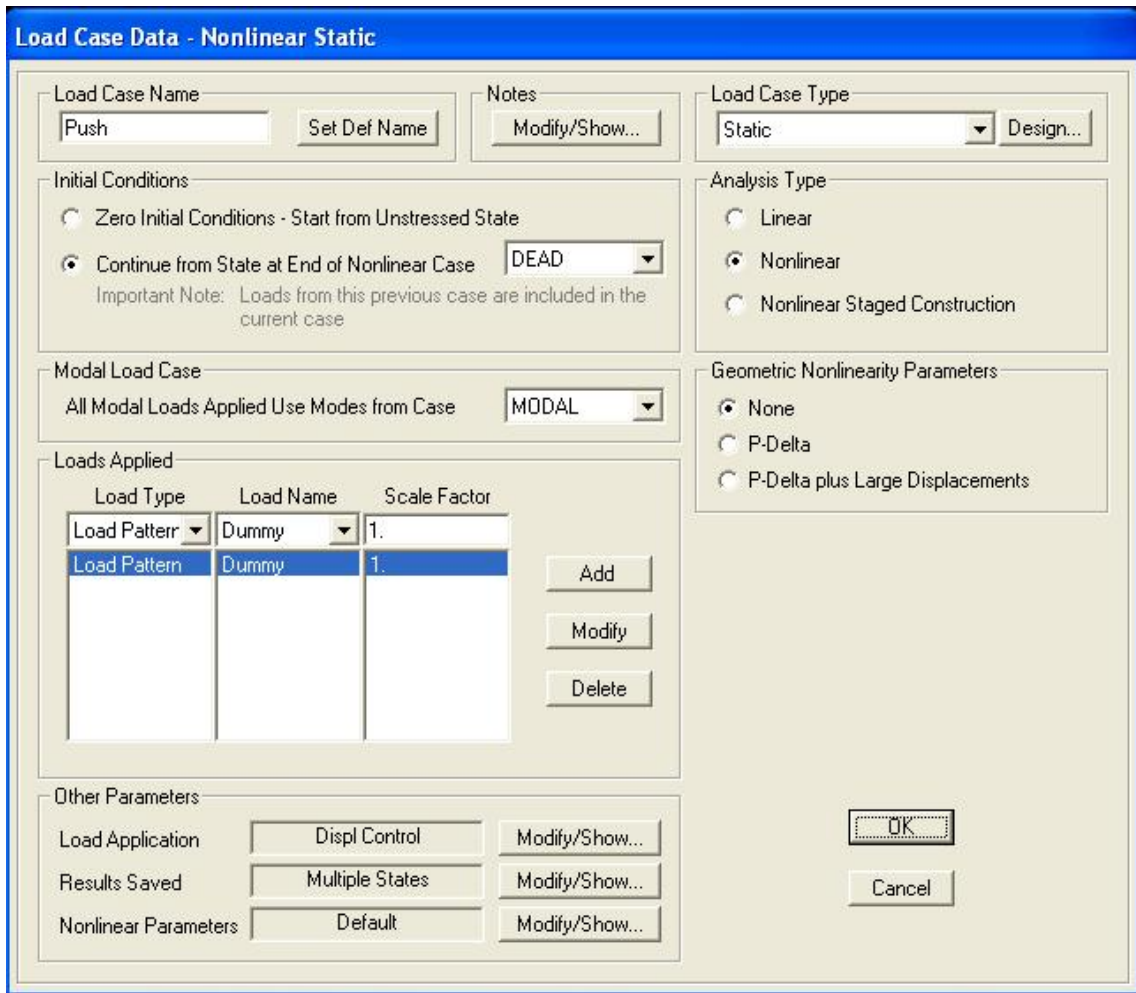


Figure 59. Defining the Pushover Load Case.

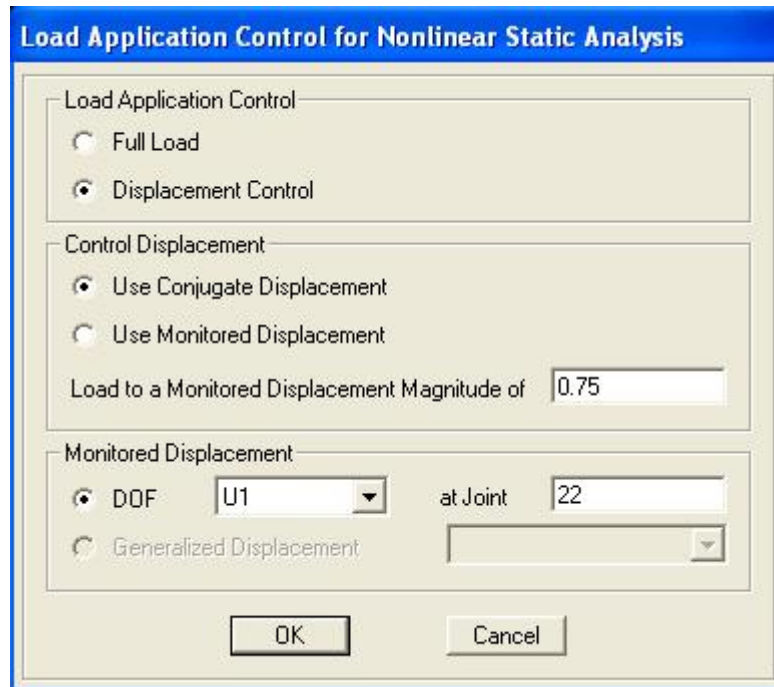


Figure 60. Pushover Analysis Load Application Control Window.

Finally, the pushover analysis was performed for each case and the pushover curves were achieved through the *Display: Show Static Pushover Curve* tab, as shown in Figure 61 for the SR21-I69 Bridge with the Basic model using Caltrans hinge properties.

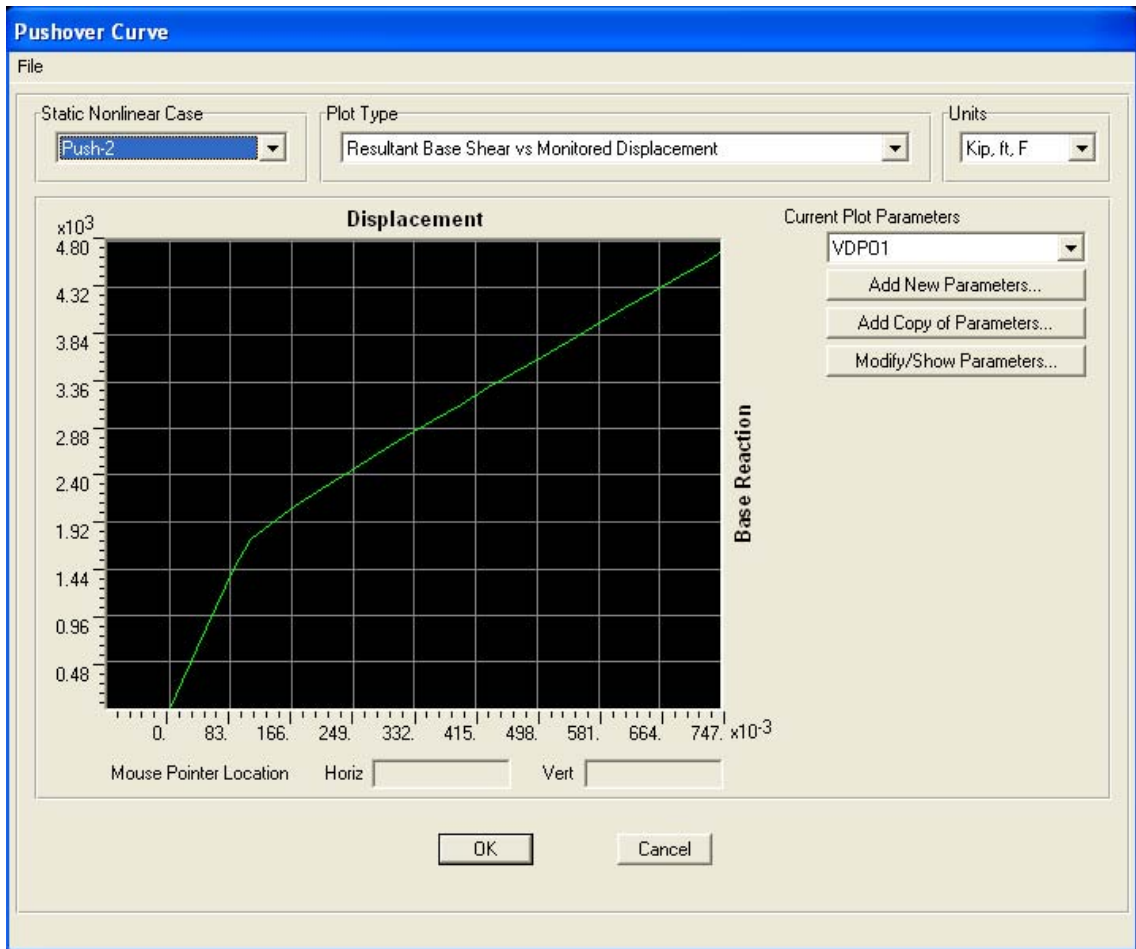


Figure 61. Pushover Curve of the SR21-I69 Bridge with the Basic Support Configuration Using Caltrans Hinge Properties.